Suppression of m^{6}A reader Ythdf2 promotes hematopoietic stem cell expansion

By
Zhenrui Li

Submitted to the graduate degree program in Pathology and Laboratory Medicine and the Graduate Faculty of the University of Kansas in partial fulfillment of the requirements for the degree of Doctor of Philosophy.

Co-Chair: Linheng Li

Co-Chair: Soumen Paul

Wen-xing Ding

Patrick Fields

Timothy Fields

Tatjana Piotrowski

Michael Washburn

Date Defended: 11/19/2018

The dissertation committee for Zhenrui Li certifies that this is the approved version of the following dissertation:

Suppression of m^6A reader Ythdf2 promotes hematopoietic stem cell expansion

Co-Chair: Linheng Li

Co-Chair: Soumen Paul

Date Approved: 12/11/2018

Abstract

Transplantation of hematopoietic stem cells (HSCs) from human umbilical cord blood (hUCB) holds great promise for treating a broad spectrum of hematological disorders including cancer, but the limited number of HSCs in a single hUCB unit restricts its widespread use. Although extensive efforts have developed multiple methods for *ex vivo* expansion of human HSCs by targeting single molecules or pathways, it remains unknown whether simultaneously manipulating a large number of targets essential for stem cell self-renewal could be achievable. Recent studies have emerged that N^6-methyladenosine (m^6A) modulates expression of a group of mRNAs critical for stem cell fate determination by influencing their stability. Among several m^6A readers, Ythdf2 is well recognized to promote the targeted mRNA decay. However, the physiological functions of Ythdf2 on adult stem cells are still elusive. Here we show that conditional knockout (KO) mouse Ythdf2 increased phenotypic and functional HSC numbers, but neither skewed lineage differentiation nor led to hematopoietic malignancies. Furthermore, knockdown (KD) of human YTHDF2 led to over 10-fold increase in *ex vivo* expansion of hUCB HSCs, 5-fold increase in colony-forming units (CFUs), and more than 8-fold increase in functional hUCB HSCs in the secondary serial of limiting dilution transplantation assay. Mechanistically, m^6A mapping of RNAs from mouse hematopoietic stem and progenitor cells (HSPCs) as well as from hUCB HSCs revealed m^6A enrichment on mRNAs encoding transcription factors critical for stem cell self-renewal. These m^6A-marked mRNAs were recognized by Ythdf2 and underwent mRNA decay. In Ythdf2 KO HSPCs and YTHDF2 KD hUCB HSCs, these mRNAs were stabilized, leading to an increase in protein levels and facilitating HSC expansion. Knockdown one of the Ythdf2 key targets, *Tal1* mRNA, partially rescued the phenotype. Therefore, our study for the first time shows the function of Ythdf2 in adult stem cell maintenance and identifies an important role of Ythdf2 in regulating HSC *ex vivo*

expansion via the mechanism of controlling the stability of multiple mRNAs critical for HSC self-renewal, thus having a strong potential for future clinical applications.

Acknowledgments

The research presented in this dissertation was conducted at Linheng Li's laboratory in Stowers Institute for Medical Research in Kansas City, MO.

First and foremost, I am extremely grateful to my mentor Dr. Linheng Li for his continued and unreserved support, advice as well as guidance throughout my graduate studies. His enthusiasm and insight in science always inspire me. I would like to extend my thanks to all past and present lab members, particularly: CiCi He for her trainings, Pengxu Qian for his great collaboration and scientific discussions, Fang Tao, John Perry and Meng Zhao for their great help with big experiments and HSC culture, Mark Hembree for his support as lab manager, and Karen Tannen for her help in manuscript editing.

During my graduate studies, I acquired tremendous help from group of people at research support departments, including members of cytometry, microscopy center, tissue culture facility, lab animal service facility, histology facility, computational biology department, molecular biology facility and media prep facility. I also extend my appreciation to Dr. Chuan He at University of Chicago, for his collaboration and great suggestions. I am also very grateful to Soumen Paul, Wen-xing Ding, Patrick Fields, Timothy Fields, Tatjana Piotrowski and Michael Washburn for serving on my committee and offering their expertise and guidance throughout my graduate studies.

On a personal note, I would like to thank my parents for their love and encouragement throughout my life, and finally for my wife and my daughter, Audrey, who shared with me every great moment.

Table of Contents

Table of Figures

List of Tables

Abbreviations

AGM	aorta/gonad/mesonephros
AML	acute myeloid leukemia
APC	antigen presenting cell
BFU-E	burst forming unit-erythroid
BM	bone marrow
BMP	bone morphogenic protein
bp	base pair
BW	body weight
°C	degrees centigrade
CAR	CXCL12 abundant reticular
CD	cluster of differentiation
CFU	colony forming unit
CFU-G	CFU-granulocyte
CFU-GM	CFU-granulocyte, macrophage
CLIP	UV cross-linking and immunoprecipitation
CLP	common lymphoid progenitor
CMP	common myeloid progenitor
CRU	competitive repopulating unit
CXCL12	chemokine (C-X-C) motif ligand 12
DMEM	Dulbecoo's modified Eagle's medium
DMSO	dimethyl sulfoxide
DNA	deoxyribonucleic acid

E	embryonic (day)
EDTA	diaminoethanetetra-acetic acid
ESC	embryonic stem cell
FBS	fetal bovine serum
FGF	fibroblast growth factor
FGFR1	fibroblast growth factor receptor 1
FLK2	fetal liver kinase 2
FOXO	forkhead box transcription factor
Fzd	frizzled
g	gram
GATA2	GATA-binding factor 2
GEMM	granulocyte, erythroid, macrophage, megakaryocyte
GMP	granulocyte-macrophage progenitor
Gy	Grey (unit)
hh	hedgehog
HSC	hematopoietic stem cell
HSPC	hematopoietic stem/progenitor cell
IACUC	Institutional Animal Care and Use Committee
IFN	interferon
Ig	immunoglobin
kb	kilobase
KO	knockout
KD	knockdown

L	liter
LDA	limiting dilution assay
LSK	Lineage^{-}, Sca-1^{+}, c-Kit^{+}
LT-HSC	long term-hematopoietic stem cell
M	molar
MEP	megakaryocyte-erythrocyte progenitor
Mettl	methyltransferase-like protein
mg	milligram
min	minute
ml	milliliter
mM	millimolar
MOI	multiplicity of infection
MPP	multipotent progenitor
mTOR	mammalian target of rapamycin
Mx1	Myxovirus resistance 1
m^{6}A	*N*^{6}-methyladenosine
PB	peripheral blood
PBS	phosphate buffered saline
PCR	polymerase chain reaction
RNA	ribonucleic acid
RPKM	reads per kilobase million
RPM	revolutions per minute
Ptprc	protein tyrosine phosphatase, receptor type, C

SCF	stem cell factor
SCL	stem cell leukemia
SE	standard error
sec	second
Shh	sonic hedgehog
shRNA	short-hairpin RNA
ST-HSC	short term-hematopoietic stem cell
TAL1	T-cell acute lymphocytic leukemia 1
TGF-β	transforming growth factor-β
TNC	total nucleated cell
TPO	thrombopoietin
UCB	umbilical cord blood
WBC	white blood cell
wt	wild type
YTHDF	YT521-B homology domain family protein
µM	micromolar
µg	microgram

Chapter 1 : Introduction

The origin of the term *Stammzelle* "German for stem cell" which was first used to describe the unicellular ancestor of all multicellular organisms and the fertilized egg that gives rise to all cells of the organism, can be traced back to 1868 in the works of German biologist Ernst Haeckel (Ramalho-Santos & Willenbring, 2007). Even over a century after the existence of the stem cell was proposed, the studies of the development and function of stem cells still attract tremendous efforts of both biologists and clinicians, holding a brilliant potential for clinical applications, such as disease modeling, drug screening and stem cell therapy (Wu & Izpisua Belmonte, 2016).

Stem cells are a population of cells with remarkable ability to replenish themselves through self-renewal and to give rise to downstream differentiated cell lineages (Y. C. Hsu & Fuchs, 2012; Li & Clevers, 2010). The regulation of stem cells is essential to support embryo development and organ formation as well as maintenance of tissue homeostasis. The disruption of stem cell regulation is strongly linked with aging and diseases such as defects in tissue functions and cancer (Hanahan & Weinberg, 2011; Lopez-Otin, Blasco, Partridge, Serrano, & Kroemer, 2013; Shlush et al., 2014).

1. 1 Hematopoietic stem cell

Hematopoiesis is one of the pioneering field that proposed and adapted the concept of "stem cell" to explain the diversity of blood lineages as early as 1908 (Ramalho-Santos & Willenbring, 2007). Over 50 years later, the definitive evidence was first provided by James Till and Ernest McCulloch, showing the regenerative potential of hematopoietic stem cells (HSCs) with clonal *in vivo* repopulation assays, thus establishing the existence of multipotential HSCs (Till & Mc, 1961).

HSCs, one of the best characterized stem cells, are defined by their capacity to give rise to all the blood cell types (Weissman, 2000). The lineage and self-renewal potential of HSCs can be determined by long-term repopulating assays, the most common of which is the competitive repopulation assay. This assay measures the functional potential of the experimental HSCs against a set known number of HSCs (usually from the bone marrow of congenic wild type mice), providing the qualitative or at best semiquantitative information about the experimental HSCs. It is important to note that this method is limited in the ability to distinguish between the number of HSCs or the quality of individual HSCs (Purton & Scadden, 2007). HSCs can also be defined on the immunophenotypic level. Combined with the usage of a wide array of cell surface antibodies and flow sorting, at least two populations of HSCs can be isolated: long-term (LT-) HSCs with quiescence (characterized by high percentage of cells in G_0 phase) and highest self-renewal capacity that function over 16-44 weeks when transplanted into mice; and short-term (ST-) HSCs that enrich actively cycling HSCs and sustain hematopoiesis for around 4-6 weeks (Wilson et al., 2008).

1.1.1 HSCs in development

There are multiple waves of hematopoiesis during development. The initial wave of blood production, known as “primitive hematopoiesis”, happens in the mammalian yolk sac at 7.5-day and 21-day post fertilization in mouse and human, respectively (Figure 1.1). The primary function of primitive hematopoiesis is to produce red blood cells in order to fulfill the high requirement of oxygen during embryo rapid growth. Interestingly, the emergence of multipotent HSCs occurs after primitive hematopoiesis at the aorta-gonad mesonephros (AGM) region during embryonic day 10.5 (E10.5) and E28 in mouse and human, respectively. The primitive hematopoiesis is rapidly replaced by HSC-derived blood production that is termed “definitive”

(Orkin & Zon, 2008; Rowe, Mandelbaum, Zon, & Daley, 2016). It has been shown that HSCs *de novo* arise from endothelial cells in AGM via the endothelial-to-hematopoietic transition (EHT) (Muller, Medvinsky, Strouboulis, Grosveld, & Dzierzak, 1994). After E12.5, mouse definitive HSCs migrate to fetal liver and placenta where HSCs undergo expansion and reach a peak at E16.5. Around E17.5, fetal HSCs seed to bone marrow (BM) and home in an microenvironment or niche during the rest of life time (Mikkola & Orkin, 2006).

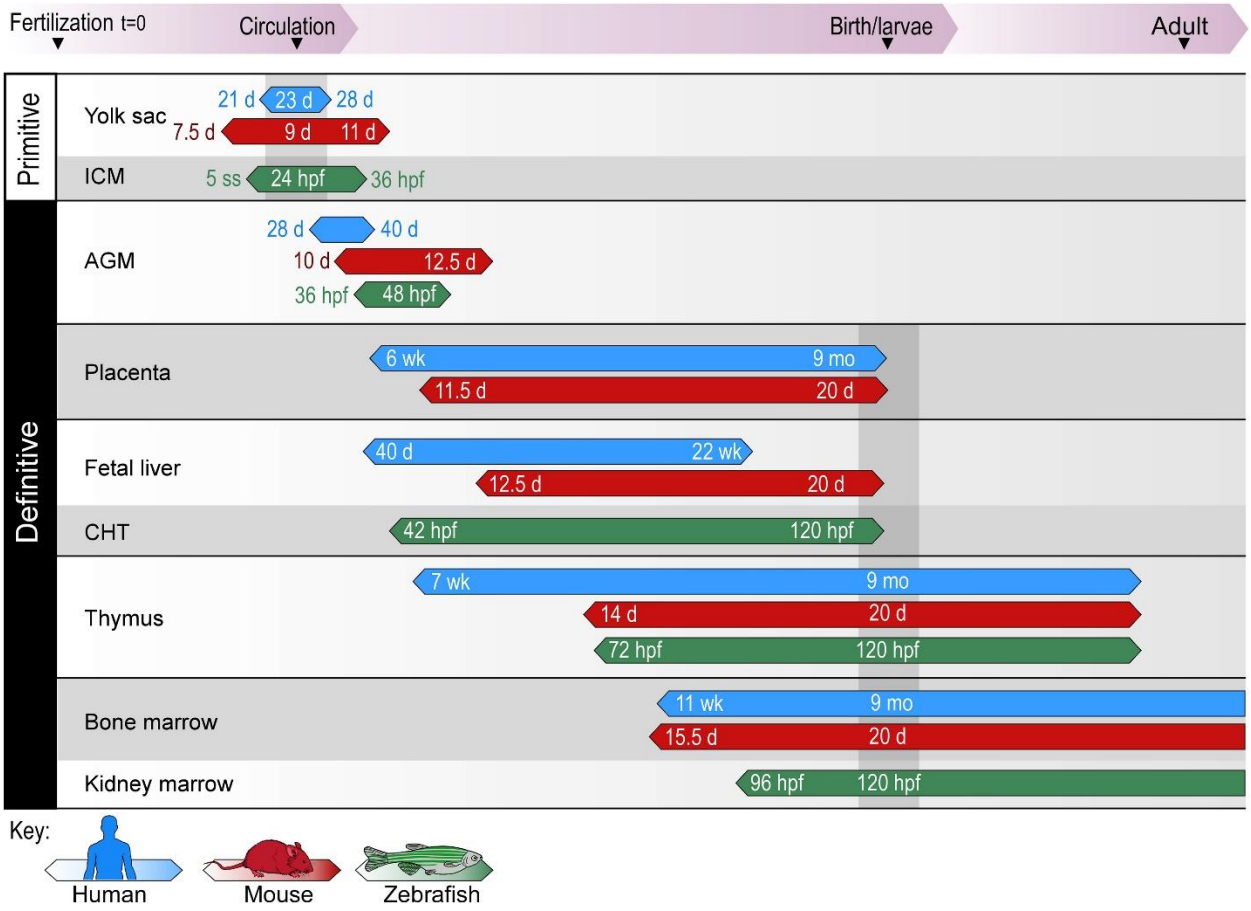

Figure 1.1 Timeline of hematopoietic system development across species.

The development of hematopoiesis during embryonic stages at specific anatomic sites in human (blue), mouse (red) and zebrafish (green). (Adapted from (Rowe et al., 2016))

1.1.2 HSC niches in bone marrow

HSCs have been shown to reside in microenvironment or niches in the bone marrow where a complex milieu of components is responsible for the balance of HSC maintenance and differentiation, including soluble cytokines, intrinsic signaling pathways as well as physical and chemical signals from microenvironment, such as those mediated by adhesion molecules, local oxygen tension, temperature and shear forces (Mendelson & Frenette, 2014; L. D. Wang & Wagers, 2011; Xie & Li, 2007). Linheng Li's Laboratory together with David Scadden's laboratory first reported that phenotypic HSCs can be found adjacent to osteoblasts or N-Cad$^+$ cells on the inner surface of trabecular bone, and subsequent genetic studies have further shown that expansion of trabecular bone, leads to expansion of HSCs (Calvi et al., 2003; J. Zhang et al., 2003). These data provided the first evidence of specific heterologous cells regulating mammalian adult stem cells *in vivo.* In line with this, later studies showed that disruption of endosteal niche results in the development of myeloid disorders (Kode et al., 2014; Raaijmakers et al., 2010).

Following the initial study of N-cad$^+$ cells in the endosteal region, other cell types have been suggested to regulate HSC maintenance and regeneration, such as perivascular cells and endothelial cells. For example, perivascular stromal cells expressing high levels of CXCL12, known as CXCL12-abundant reticular (CAR) cells, are involved in the regulation of HSC functionality in several aspects, including self-renewal, proliferation and trafficking (Sugiyama, Kohara, Noda, & Nagasawa, 2006). Recent studies show that mesenchymal stem cells (MSCs), which possess the capacity to give rise to osteoblasts, adipocytes, and chondroblasts, have considerable influence on HSC maintenance *in vivo* by expressing SCF or CXCL12 (Ding & Morrison, 2013; Mendez-Ferrer et al., 2010; B. O. Zhou, Yue, Murphy, Peyer,

& Morrison, 2014). In addition to the mesenchymal cells, terminally differentiated progeny of HSCs, including megakaryocytes and macrophages, have also been documented to regulate HSC activity directly (Bruns et al., 2014; Chow et al., 2011; Christopher, Rao, Liu, Woloszynek, & Link, 2011; M. Zhao et al., 2014). Previous studies have focused on a population of HSCs identified by signaling lymphocyte activation molecule family markers (SLAM family markers) and show their interactions and relative physical distance to niche cells. However, accumulated evidence reveals a tremendous molecular and functional heterogeneity within SLAM HSCs (Copley, Beer, & Eaves, 2012; Haas, Trumpp, & Milsom, 2018; Schroeder, 2010). More diligent studies on whether and how specified HSC subpopulations are distinctively regulated by different BM niches under homeostasis and stress conditions are required to improve our understanding of HSC maintenance *in vivo*, which may contribute to the discovery of safe technologies to promote functional HSC expansion *in vitro* without inducing cancerous transformations and lineage deficiencies.

1.1.3 Master hematopoietic transcription factors

Transcription factors dictate specific gene expression pattern in a cell to maintain cell identity and perform its unique function. A group of transcription factors has been found to play a pivotal role in the development and maintenance of HSCs. The transcription factors involved in programming endothelial-to-hematopoietic transition have drawn special interests as they may provide clues to *de novo* generation of HSCs from renewable cell types. TAL1/SCL and its associated partner, LMO2, are individually crucial for the development of both primitive and definitive hematopoietic systems (Hoang, Lambert, & Martin, 2016; Stanulovic, Cauchy, Assi, & Hoogenkamp, 2017). Blood cells cannot form in their absence. Similarly, deletion of *Runx1* from VE-cadherin expressing cells abolishes HSC formation at the EHT stage, while knockout of

Runx1 in *Vav1*-expressing cells (potential HSCs) shows no hematopoietic deficiency, indicating that RUNX1 is required for the formation of "definitive" hematopoietic progenitors and HSCs but is dispensable once HSCs are specified (Cai et al., 2011; M. J. Chen, Yokomizo, Zeigler, Dzierzak, & Speck, 2009). In contrast, the expression level of GATA2 plays a crucial role during HSC development and function in adult BM, since haploinsufficiency or overexpression of GATA2 leads to HSC depletion or non-function (de Pater et al., 2013; Guiu et al., 2013; Lim et al., 2012; Ling et al., 2004).

1.2 HSC expansion

Except for the homeostasis condition, HSCs are also responsible for blood reconstitution in response to stress, rendering HSC transplantation a life-saving procedure in the treatment of a broad spectrum of disorders, including hematologic, immune, and genetic diseases (Walasek, van Os, & de Haan, 2012). Although the first successful HSC transplantation using human bone marrow from a related donor was accomplished 50 years ago in a boy with X-linked severe combined immunodeficiency disease (SCID) (Meuwissen, Gatti, Terasaki, Hong, & Good, 1969), associated problems still need to be solved in the future to improve clinical outcomes. One of the problems is that many patients, especially those who possess genetic or epigenetic defects in their blood cells such as leukemia and myeloid disorders, require the transplantation of HSCs derived from genetically nonidentical donors, known as allogeneic transplantation. Despite the current widespread use of this approach (forty percent of one million hematopoietic cell-transplantations performed) (Gratwohl et al., 2015), early studies suggested that allogeneic transplantation was only feasible when donors completely matched the recipient at the human leukocyte antigen (HLA) loci on both copies of chromosome 6 (Armitage, 1994; Thomas et al., 1975). Two main classes of HLA proteins are known to exist: class I (A, B and C) and class II

(DP, DQ and DR). HLA class I molecules are constitutively expressed at variable levels by most cell types, while HLA class II genes are mainly expressed on the surface of hematopoietic cells, especially antigen-presenting cells (APCs), such as B cells, dendritic cells, macrophages and monocytes (Dendrou, Petersen, Rossjohn, & Fugger, 2018; Erlich, Opelz, & Hansen, 2001). However, even when HLA identically matched donors are used, graft-versus-host disease (GVHD), which occurs when immunocompetent T cells in the donated tissue (the graft) recognize the recipient (the host) as foreign, is still a common life-threatening complication, contributing to considerable mortality rate in patients received allogeneic HSC transplantation (Kanakry, Fuchs, & Luznik, 2016; Shlomchik, 2007). Furthermore, though HLA matching is critical to successful allogeneic HSC transplantation, only 20%-30% of patients have HLA-matched sibling donors, meaning the majority of patients requiring HSC transplantation risk a deficit in HSC donors since the number of matched unrelated donors is limited by the extensive polymorphism of HLA genes. Thus, other sources of donor cells have been an urgent demand. If suitable donors are not found, umbilical cord blood (UCB), which can be procured both easily and safely, can be used. UCB has been shown to be a rich source of HSCs. Furthermore, the transplantation of UCB requires less-stringent HLA matching than does the transplantation of adult peripheral blood or marrow, because mismatched cord-blood cells are less likely to cause GVHD, without losing the graft-versus-leukemia effect (Wagner et al., 2002). However, the stem cell number in a single UCB unit is not sufficient for transplantation into an adult patient (Walasek et al., 2012). Significant effort has gone into developing technologies for *ex vivo* expansion of HSCs in order to enable UCB transplants for adults, who comprise the majority of patients.

1.2.1 Extrinsic regulators of HSC self-renewal

The fundamental base of HSC expansion relies on the ability to induce proliferation without compromising stemness, usually known as stem cell self-renewal. The aforementioned HSC niches and microenvironment play a crucial role in regulating HSC fate by secreting cytokines and producing physical and chemical factors to balance self-renewal and differentiation. Early studies about HSC culture have identified various cytokines for their ability to expand and maintain HSCs *in vitro (Miller, Audet, & Eaves, 2002)*. For example, a 20-fold increase in phenotypic HSC expansion was reported in mice when cultured *in vitro* in combination with four cytokines, including SCF, TPO, IGF-2 and FGF-1 (C. C. Zhang & Lodish, 2005). However, clinical trials showed disappointing results with cytokine-expanded cord blood cells (Jaroscak et al., 2003). This may be explained by knowledge gained from cytokine studies indicating the insufficiency of these cytokines, by themselves, to support HSC self-renewal. In fact, they typically induce HSC differentiation, resulting at best in maintenance or modest stem cell amplification, but usually leading to progressive depletion of long-term repopulating cells (Walasek et al., 2012).

Recently, factors that do not necessarily qualify as typical HSC growth factors but rather are involved in hematopoietic development have been shown to also regulate the expansion of HSCs *ex vivo*. These factors either stimulate or antagonize several developmentally conserved pathways, such as wingless-type (Wnt), Notch, sonic hedgehog (Shh), bone morphogenetic protein (BMP)/transforming growth factor β (TGF-β) and fibroblast growth factor (FGF).

Multiple members of the family of secreted Wnt growth factors, as well as their cognate receptors, Frizzled (Fzd), and downstream effectors, including *β*-catenin and the LEF-1 family of transcription factors, have been documented to play a critical role in HSC maintenance both *in*

vivo and *ex vivo (Luis, Ichii, Brugman, Kincade, & Staal, 2012).* Interestingly, the effects of Wnt signaling are dosage and context dependent: low Wnt doses result in expansion of HSCs, whereas high doses cause exhaustion (Luis et al., 2011). Additionally, the effect of Wnt signaling exhibits discrepancy during different development stages: loss of *β*-catenin fails to affect homeostatic hematopoiesis and repopulation capacity of HSCs in adult mice, while loss of *β*-catenin at embryonic stage impairs the expansion of the HSC pool, thereby compromising the long-term repopulation capacity and maintenance of hematopoiesis in adult mice (Cobas et al., 2004; Jeannet et al., 2008; Koch et al., 2008; C. Zhao et al., 2007). Constitutive activation of *β*-catenin alone results in apoptosis of HSCs. However, cooperative activation of both Wnt/β-catenin and PTEN/PI3k/Akt pathways drives phenotypic LT-HSC expansion by inducing proliferation, while simultaneously inhibiting apoptosis and blocking differentiation (Perry et al., 2011). In addition to canonical Wnt signaling, non-canonical Wnt signaling mediated by Fzd8, has been documented to maintain quiescent LT-HSCs by suppressing the $Ca2^{+}$-NFAT- IFNγ pathway and antagonizing canonical Wnt signaling in HSCs. Loss of Fzd8 results in activation of quiescent LT-HSCs and deficiency in repopulation capacity after transplantation (Sugimura et al., 2012).

Both Notch receptors and Notch ligands are expressed on HSCs and their niches, suggesting an interactive regulation of hematopoiesis between stem cells and microenvironment (Butko, Pouget, & Traver, 2016; Mendelson & Frenette, 2014). Studies on the role of the Notch pathway in HSC fate regulation show that an immobilized form of Notch ligand, Delta-1, but not its soluble form, can expand mouse and human HSPCs *ex vivo*. The expanded HSPCs exhibit long-term repopulation ability in immunodeficient recipient mice as shown after secondary transplantation. Intriguingly, the effect of Notch signaling, similar to that of Wnt signaling, was

suggested to be dose-dependent, since HSPC expansion was observed only with lower Delta-1 concentrations (Delaney, Varnum-Finney, Aoyama, Brashem-Stein, & Bernstein, 2005; Varnum-Finney, Brashem-Stein, & Bernstein, 2003; Varnum-Finney et al., 2000). However, clinical trials of transplantation of HSCs expanded via Notch signaling activation indicate that Delta-1 treatment may result in expansion of committed myeloid progenitors occurs without maintenance of the pool of undifferentiated HSCs required for long-term engraftment (Nikiforow & Ritz, 2016).

Shh signaling-mediated human HSPC expansion appears to depend on downstream BMP-4 signaling, as inhibition of BMP-4 abolishes Shh-induced HSC expansion (Bhardwaj et al., 2001). BMP signaling has been shown to play a pivotal role in maintaining mouse HSC quiescence via control of the endosteal niche (J. Zhang et al., 2003). BMPs belongs to the TGF-β superfamily. TGF-β1, another secreted factor, is produced and activated by megakaryocytes and nonmyelinating Schwann cells, respectively, and is involved in maintaining HSC quiescence in the BM (Yamazaki et al., 2011; M. Zhao et al., 2014).

The growing evidence has demonstrated that FGF signaling weighs into HSC regulation both *in vivo* and *ex vivo*. Addition of FGF-1 and FGF-2 in a serum-free medium of unfractionated mouse bone marrow cells supports the expansion of serial-transplantable HSCs (de Haan et al., 2003; Itkin et al., 2012). Loss of FGF receptor 1 (FGFR1,) which is expressed on HSCs, does not affect hematopoiesis homeostasis, but rather results in defects in HSC activation and proliferation in response to 5-fluorouracil (5FU) treatment (M. Zhao et al., 2012). This can be partially, if not entirely, due to loss of FGF signaling activation by FGF-1 secreted from megakaryocytes, which are a major resource for FGF after stress (M. Zhao et al., 2014).

1.2.2 HSC expansion by small molecules

In recent years, much effort has been placed on screening chemical compounds, in addition to cytokines/factors, to expand HSCs *ex vivo*. Retinoid acid (RA), a metabolite of vitamin A (retinol), represents a natural small molecule that has been shown to be involved in hematopoiesis development and regulation of HSC dormancy, as well as treatment for acute promyelocytic leukemia by induction of leukemic cell differentiation (Cabezas-Wallscheid et al., 2017; Degos & Wang, 2001). However, the role of RA in *ex vivo* HSPC expansion is unclear. Furthermore, the effect of RA on balancing HSC self-renewal and differentiation depends on exquisite regulation of RA dosage in the microenvironment (Ghiaur et al., 2013). More investigations are required before applying RA into clinical HSC expansion.

Recent studies have reported the ability to identify novel small molecules with HSC self-renewal stimulatory activity, thus potentially applying to HSC expansion. Taking advantage of high-throughput screening, Boitano *et al*. identified a purine derivative, referred to as StemRegenin 1 (SR1), which was capable of enhancing human $CD34^+$ HSC cell expansion *ex vivo* via antagonizing aryl hydrocarbon receptor (AhR) pathway (Boitano et al., 2010). Though SR1 increases UBC $CD34^+$ cell expansion by 17-fold, it does not support *ex vivo* expansion of mouse HSCs or adult human HSCs. Recently, Kristin Hope's lab reported that overexpression of Musashi-2 is able to expand long-term repopulating human HSCs by attenuating AhR signaling (Rentas et al., 2016). AhR is a member of the Pern-Arnt-Sim (PAS) superfamily of transcription factors that are involved in sensing environmental signals such as toxins (Gutierrez-Vazquez & Quintana, 2018). AhR has been well documented to regulate adaptive immunity, modulating T cell differentiation, especially playing an important role in Treg cell development. Thus, it is

notable to evaluate the efficiency and capacity of immune reconstitution from HSCs expanded with SR1 after transplantation into patients.

Another novel compound, a pyrimidoindole derivative named as UM171 that was identified in a chemical library screen, was shown to expand human CD34+CD45RA–mobilized peripheral blood cells (Fares et al., 2014). Unlike SR1, UM171 does not target AhR pathway. However, the physiological targets of UM171 remain unclear. In the Fed-Batch culture system, UM171 facilitates expansion of hematopoietic progenitors and results in a 13-fold expansion of functional LT-HSCs. However, HSCs expanded with UM171 exhibit a lymphoid-deficient differentiation pattern in transplantation recipient mice.

1.2.3 Intrinsic regulators of HSC self-renewal

Accumulating knowledge has demonstrated the important role of intrinsic factors in regulating HSC self-renewal. One of the first studies of HSC expansion via manipulating of intrinsic factor shows that ectopic expression of transcription factor, Hoxb4, results in 40-fold expansion of repopulating mouse HSCs without inducing leukemia (Amsellem et al., 2003; Antonchuk, Sauvageau, & Humphries, 2002). However, while human $CD34^+$ HSPCs expressing Hoxb4 expand significantly in immunodeficient recipient mice, differentiation of these cells into lymphoid and myeloerythroid lineages is impaired when levels of Hoxb4 are high (Schiedlmeier et al., 2003), suggesting the exquisite balance of stem cell self-renewal and differentiation needs to be taken care before clinical application. Additionally, a retinoid-dependent cis-regulatory element that coordinates regulation of Hoxb expression, has been shown to play a pivotal role in HSC maintenance (Qian et al., 2018). Augmentation of HSC self-renewal can also be achieved by overexpression of chromatin remodelers, such as members of the Polycomb group (PcG) family of proteins, especially zeste (Ez) proteins (Ezh1, Ezh2) and B cell-specific Moloney

murine leukemia virus integration site 1 (Bmi1) (Hidalgo et al., 2012; Iwama et al., 2004; Kamminga et al., 2006; Rizo, Dontje, Vellenga, de Haan, & Schuringa, 2008). Interestingly, loss of Dnmt3a, a *de novo* DNA methyltransferase, immortalizes HSC *in vivo* at the expense of differentiation capacity, rendering very high risk of developing leukemia once mutation occurs (Challen et al., 2011; Jeong et al., 2018; Shlush et al., 2014). In line with this, alterations of epigenetic modifications or mutations of epigenetic regulators have been strongly linked to tumorigenesis and leukemogenesis (Makova & Hardison, 2015; Ntziachristos, Abdel-Wahab, & Aifantis, 2016).

1. 3 RNA m^{6}A modification

RNA modifications have been well documented for over 50 years with the first discovery of pseudouridine in abundant RNAs extracted from yeast (Cohn, 1960). Subsequent studies have further identified over 100 types of RNA nucleotide modifications on various RNA types, including messenger RNA (mRNA), transfer RNA (tRNA), ribosomal RNA (rRNA), transfer-messenger RNA (tmRNA), small nuclear RNA (snRNA), and chromosomal RNA (Cantara et al., 2011). These modifications not only mark and regulate these transcripts, but also diversify and extend information from the simple genetic code in DNA. Here, we focus on the more recent discoveries in mRNA modifications, especially N^6-methyladenosine (m^{6}A) methylation, that have shown a profound effect on biological systems.

1.3.1 m^{6}A writers, erasers and readers

m^{6}A is the most abundant internal modifications in eukaryotic mRNA and was first discovered in the 1970s (Adams & Cory, 1975; Desrosiers, Friderici, & Rottman, 1974; Furuichi et al., 1975; Lavi & Shatkin, 1975; Wei & Moss, 1975). Mammalian mRNA m^{6}A methylation sites were first found in 1984, and measurements from mass spectrophotometry suggested the

amount of m^6A in total RNA was estimated to be 0.1%-0.4% of all adenosine nucleotides in mammals (Horowitz, Horowitz, Nilsen, Munns, & Rottman, 1984). However, due to the low amount of m^6A in mRNA and lack of technologies with high sensitivity, studies to characterize the function of m^6A did not significantly progress until 2012. At that time, techniques using a m^6A specific antibody for methylated RNA immunoprecipitation, followed by high-throughput sequencing, were developed and facilitated the generation of transcriptome-wide maps of m^6A, charting the m^6A epitranscriptome (Dominissini et al., 2012; Meyer et al., 2012).

RNA m^6A modification is catalyzed by a multicomponent methyltransferase complex that was first reported in 1994 (Bokar, Rath-Shambaugh, Ludwiczak, Narayan, & Rottman, 1994). The complex is composed of catalytic enzyme, methyltransferase-like 3 (METTL3), and cofactors, including METTL14, Wilms tumor 1-associated protein (WTAP) and KIAA1429 (Bokar, Shambaugh, Polayes, Matera, & Rottman, 1997; J. Liu et al., 2014; Ping et al., 2014; Schwartz, Mumbach, et al., 2014; Y. Wang et al., 2014). The METTL3 complex recognizes and methylates mRNAs at conserved RRACH motifs (R = A or G; H = A, C, or U) across various species, often in mRNA 3′ UTRs and coding DNA sequence (CDS) (Dominissini et al., 2012; Ke et al., 2015; Meyer et al., 2012; Yue, Liu, & He, 2015). Recently, another m^6A methyltransferase, METTL16, has been identified and shown to deposit m^6A in U6 snRNA and pre-mRNAs, regulating the alternative splicing through intron retention (Gu, Patton, Shimba, & Reddy, 1996; Pendleton et al., 2017b; Sergiev, Serebryakova, Bogdanov, & Dontsova, 2008; Warda et al., 2017). Notably, METTL16 methylates the conserved sequence, UACAGAGAA, in U6 snRNA and methionine adenosyltransferase 2A (MAT2A) pre-mRNA, thereby regulating the expression of MAT2A in response to intracellular S-adenosylmethionine (SAM) level (Pendleton et al., 2017b).

RNA m^6A modification is dynamic and reversible, attributed to the discovery of two demethylases catalyzing the oxidative demethylation of m^6A: one is fat-mass and obesity-associated protein (FTO), the first demethylase identified to reverse m^6A modifications in nuclear RNA (Jia et al., 2011); a second m^6A demethylase of the same family, α-ketoglutarate-dependent dioxygenase alkB homolog 5 (ALKBH5), affects mouse fertility and spermatogenesis (Zheng et al., 2013). The identification of both these enzymes and characterization of their function on demethylation of m^6A in mRNA provided the first evidence of reversible post-transcriptional modification in RNA transcribed by RNA polymerase II, including mRNAs and a set of non-coding RNAs.

The biological function of RNA m^6A modification is exerted by the m^6A-binding proteins or called “readers”. Rechavi and colleagues initially identified YTH-domain-containing proteins, YTHDF2 and YTHDF3 as m^6A reader proteins in an m^6A RNA pull down experiment without characterizing their function (Dominissini et al., 2012). There are five members of YTH-domain proteins in mammalian cells: YTHDF1–3, which are primarily localized in the cytoplasm, and YTHDC1 and YTHDC2, which exhibit nucleus localization (Patil et al., 2016; X. Wang et al., 2014; X. Wang et al., 2015; Xu et al., 2014). The study of YTHDF2 in Hela cells showing the regulatory function of YTHDF2 on expediting m^6A-modified mRNA decay provides the first evidence of m^6A reader protein involving in significant biological functions (X. Wang et al., 2014). In contrast to YTHDF2, YTHDF1 does not show a considerable effect on mRNA decay, instead it is shown to promote translation by interacting with eIF3 and other translation initiation factors (X. Wang et al., 2015). The function of YTHDF1 on translation regulation can be enhanced by cooperating with another YTH-domain protein, YTHDF3, which interacts with ribosomal 40S/60S subunits (A. Li et al., 2017; Shi et al., 2017b). YTHDC1, a

nucleus-enriched splicing regulator before it was known to interact with m^{6}A, has been demonstrated its role in m^{6}A-regulated splicing and mRNA export from nucleus (Roundtree et al., 2017; Xiao et al., 2016). YTHDC1 is also shown to mediate the function of *XIST*, a noncoding RNA that contains at least 76 m^{6}A sites and is critical for silencing genes on one X chromosome in female cells (Lee, 2009; Patil et al., 2016). The function of another m^{6}A reader protein, YTHDC2, remains poorly understood. Recent studies show that YTHDC2 regulates the transition from proliferation to differentiation in the germline by enhancing the translation efficiency of its targets and also decreasing their mRNA abundance (Bailey et al., 2017; P. J. Hsu et al., 2017). In addition to YTH-domain containing proteins, other m^{6}A reader proteins, include HNRNPA2B1 and insulin-like growth factor 2 mRNA-binding proteins (IGF2BPs) (Alarcon, Goodarzi, et al., 2015; Huang et al., 2018).

1.3.2 mRNA m^{6}A modification in disease and development

Recent studies have elucidated the roles of m^{6}A modification in stem cell fate determination and endothelial-to-hematopoietic transition during embryogenesis (Batista et al., 2014; Geula et al., 2015; Lv et al., 2018; Yoon et al., 2017b; C. Zhang et al., 2017b; B. S. Zhao, Wang, et al., 2017b) as well as in leukemia development (Barbieri et al., 2017b; Z. Li et al., 2017b; Vu et al., 2017b; Weng et al., 2018). Interestingly, deficiency in m^{6}A writer complex, METTL3 and METTL14, leads to distinct outcomes in different types of stem cells. For example, *Mettl3* or *Mettl14* KO promoted differentiation in HSCs (Barbieri et al., 2017b; Vu et al., 2017b; Weng et al., 2018), while resulting in enhanced stem cell self-renewal and maintenance in mouse embryonic stem cells (mESCs) and embryonic neuronal stem cells (NSCs) (Batista et al., 2014; Yoon et al., 2017b). Besides, the physiological function of m^{6}A in stem cells and leukemia are mediated through different mechanisms. In stem cells, m^{6}A

modifications regulate stem cell fate determination by m6A-mediated decay of mRNAs encoding stem cell fate determinant (Batista et al., 2014; Yoon et al., 2017b), while in acute myeloid leukemia (AML), METTL3 and METTL14 promote leukemogenesis as m^6A modifications stabilize the mRNAs of oncogenes and/or increase their translation (Barbieri et al., 2017b; Vu et al., 2017b; Weng et al., 2018). Furthermore, previous studies have reported that the leukemogenic functions of FTO and METTL14 are independent of YTHDF reader proteins (Z. Li et al., 2017b; Weng et al., 2018). Noting that, we focus on Ythdf2, a well-recognized m^6A reader promoting targeted mRNA decay to investigate its role in the context of HSC maintenance. We hypothesize that manipulation of Ythdf2 might potentially influence the life span of a great number of m^6A-marked mRNAs, thus impacting adult HSC self-renewal versus differentiation and facilitating HSC expansion.

Chapter 2 : Materials and Methods

Sections of chapters 2-8 have previously been published and are adapted and reprinted here with permission, alongside new, never-before published material. Li, Z., Qian, P., Shao, W. Shi, H., He, X.C., Gogol, M.,. . . Li, L. (2018). Suppression of m(6)A reader Ythdf2 promotes hematopoietic stem cell expansion. *Cell Res*, 28(9), 904-917.

2.1 Mice.

Ythdf2 conditional KO mice were generated by Chuan He and Bin Shen group. Mice were housed in the animal facility at Stowers Institute for Medical Research (SIMR) and handled according to Institute and NIH guidelines. All procedures were approved by the IACUC of SIMR.

2.2 Flow cytometry and HSPC sorting.

Mouse HSPCs, progenitors, and lineage cells were harvested from BM (femur and tibia) and spleen. Red blood cells were lysed using a 0.16 M ammonium chloride solution, and the cells were filtered with 70μm strainers to generate single cell suspensions. For mouse HSC identification, cells were stained with antibodies against Sca-1 (D7), c-Kit (2B8), CD34 (RAM34), Flk2 (A2F10), CD48 (HM48-1), CD150 (TC15-12F12.2), together with lineage cocktail including CD3 (145-2C11), CD4 (RM4-5), CD8 (53-6.7), Mac-1 (M1/70), Gr1 (RB6-8C5), CD45R (B220, RA3-6B2), IgM (Il-41) and Ter119 (TER-119). For progenitors and lineage cells, cells were stained with antibodies as previously described (Qian et al., 2016). 7-aminoactinomycin D (7-AAD) (A1310, Life technologies) was used to exclude dead cells. hUCB samples were acquired from the St. Louis Cord Blood Bank. Mononuclear cells were isolated with Lymphoprep™ (StemCell technologies), followed by isolation of human $CD34^+$ cord blood cells by human CD34 MicroBead Kit UltraPure (Miltenyi Biotec). To quantify hUCB HSPCs, cells were stained with antibodies against CD34 (581), CD38 (HIT2), CD45RA (HI100), CD90

(5E10), CD49f (GoH3), EPCR/CD201 (RCR-401). Cell sorting and analyses were performed on MoFlo (Dako), InFlux Cell Sorter (BD Biosciences), and/or MACSQuant (Miltenyi Biotec). Data analysis was performed using FlowJo software.

2.3 Homing assay.

In vivo homing assays were performed as previously described (X. C. He et al., 2014). Basically, whole bone marrow (WBM) cells from CD45.2 mice were labelled with 5 μM 5-(and -6)-carboxyfluorescein diacetate succinimidyl ester (CFDA SE) (Molecular Probes) at 37˚C for 10 mins, washed three times, and 1×10^6 WBM were transplanted into lethally irradiated *ptprc* mice. After 18 hours, femurs and tibias were flushed, and CFDA SE^+ cells were determined.

2.4 Competitive reconstitution assay.

Competitive reconstitution assays were performed by intravenous transplantation of 2 $\times10^5$, 7.5 $\times10^4$ or 2.5 $\times10^4$ donor-derived WBM cells from *wt* or *Ythdf2* KO mice (CD45.2), together with 2×10^5 rescue cells (CD45.1) into groups of ten lethally irradiated (10 Gy) *ptprc* recipient mice. For secondary transplantation, primary transplant recipients were sacrificed. BM cells were dissected from femur and tibia, and then transplanted mouse-to-mouse at a dosage of 1×10^6 cells into irradiated secondary recipient mice. Baytril water was given to recipient mice three days before irradiation and continued for another two weeks after irradiation. Primary and secondary competitive repopulating unit (CRU) frequencies were measured using ELDA software (Hu & Smyth, 2009), in which successful engraftment was defined as the presence of a distinct $CD45.2^+$ $CD45.1^-$ population ≥5% and ≥1% of total hematopoietic cells in peripheral blood, respectively (Purton & Scadden, 2007). Also, the secondary transplantation recipient mice that died before 16 weeks post transplantation were counted for failed engraftment.

For rescue experiment, LSK cells were sorted out from *wt* and *Ythdf2* KO mouse BM and cultured overnight in StemSpan SFEM medium (Stem Cell Technologies) supplemented with 10μg/mL heparin (Sigma), 0.5× penicillin/streptomycin (Sigma), 10ng/mL recombinant mouse (rm) SCF (Biovision, Inc.), and 20ng/mL Tpo (Cell Sciences, Inc.) (Perry et al., 2011) at 37^0C 5% CO_2 5% O_2. Control shRNA and shRNA targeting mouse *Tal1* were delivered into LSK cells by lentivirus at 100 MOI. To enhance the efficiency of infection, ViroMag Transduction Reagent (OZ Biosciences) were used following manufacturer's directions. GFP^+ cells were sorted out at 5 days post infection and cultured for another 3 days to expand before transplantation. Upon transplantation, equal numbers of GFP^+ cells from each group were transplanted with 10^5 rescue BM cells into lethally irradiated recipients.

2.5 Cell cycle and apoptosis assays.

Cell cycle analysis was performed with FITC mouse anti-human Ki67 set (BD Pharmingen) according to the manufacturer's instructions. Briefly, 5×10^6 BM cells were isolated and stained with HSC antibodies as described above. Cells were fixed by 4% paraformaldehyde at 4˚C overnight or room temperature (RT) for 1 hour, and then permeabilized with 0.2% triton X-100 on ice for 15 mins. Cells were washed with PBS containing 2% FBS, and then were incubated with Ki-67 antibody at RT for 1 hour in the dark, and SYTOX Red (Invitrogen) at RT for another 5 mins, followed by flow cytometric analysis with InFlux Cell Sorter (BD Biosciences). For apoptosis analysis, Annexin V (Invitrogen) and SYTOX Red staining of 5×10^6 BM cells was performed according to the manufacturer's protocol.

2.6 m^6A RNA-IP-seq.

Two replicates of 10^5 LT-HSC (LSK $CD34^-$ $Flk2^-$), ST-HSC (LSK $CD34^+$ $FLK2^-$) and MPP (LSK $CD34^+$ $FLK2^+$) from C57BL/6J mouse were sorted into TRIzol (Invitrogen), and total

RNA was isolated according to the manufacturer's instructions. RNA was fragmented to ~100 nucleotide fragments with Ambion fragmentation reagent (2 mins incubation at 70^0C). The samples were then subjected to Turbo DNase treatment (Ambion), followed by a phenol-chloroform extraction, and resuspension in 85µl of nuclease-free water, and 5µl was saved as input. Then the remaining 80µl RNA fragments were diluted into IPP buffer (150mM NaCl, 0.1% NP-40, 10mM Tris-HCl, pH 7.5). RNA was incubated with 25µl of protein-G magnetic beads, previously bound to 3µg of anti-m^6A plyclonal antibody (Synaptic Systems), for 3 hours at 4^0C in IPP buffer. Beads were washed twice with 200µl IPP buffer, twice with 200µl low-salt buffer (50mM NaCl, 0.1% NP-40, 10mM Tris-HCl, pH 7.5) and twice with 200µl high-salt buffer (500mM NaCl, 0.1% NP-40, 10mM Tris-HCl, pH 7.5). Beads were then treated with 300µl Elution Buffer (5mM Tris-HCL pH 7.5, 1mM EDTA pH 8.0, 0.05% SDS, 4.2µl Proteinase K (20 mg/ml)) for 1.5 hours at 50^0C, and RNA was recovered with phenol:chloroform extraction followed by ethanol precipitation. Three human $CD34^+$ umbilical cord blood cells were isolated as described above and isolated total RNA with TRIzol. RNA was fragmented to ~100 nucleotide fragments with Ambion fragmentation reagent (2 mins 50 secs incubation at 70^0C). The samples were then subjected to Turbo DNase treatment (Ambion), followed by a phenol:chloroform extraction, and resuspension in 18µl of nuclease-free water, and 1µl was saved as input. m^6A RNA IP was performed with EpiMark® N6-Methyladenosine Enrichment Kit following manufacturer's instructions.

Following m^6A preparation of RNA, quality was assessed on Agilent 2100 Bioanalyzer, and 1ng (mouse) or 10ng (human) RNA was used to generate RNAseq libraries according to the manufacturer's directions for the SMARTer Stranded Total RNA-Seq Kit – Pico Input Mammalian (Takara Bio Inc) using 16 cycles (mouse) or 13 cycles (human) PCR2 amplification.

This method uses random priming and a template switching oligo to generate complimentary DNA, followed by the ligation of barcoded adapters; ribosomal-derived cDNA is then removed through probe-directed enzyme cleavage and subsequent enrichment of un-cleaved fragments. We modified the protocol to retain lower molecular weight sample fragments by using a 1.2x SPRI bead concentration for PCR1 cleanup. To remove dimerized adapters, libraries underwent 160-600 bp size selection with a Pippin Prep (Sage Science) 2% gel. The resulting libraries were checked for quality and quantity using the Bioanalyzer and Qubit Fluorometer (Life Technologies). Then equal molar libraries were pooled and requantified. For mouse m^6A-seq, libraries were sequenced as 50 bp single read on the Illumina HiSeq 2500 instrument using HiSeq Control Software 2.2.58. Following sequencing, Illumina Primary Analysis version RTA 1.18.64 and Secondary Analysis version bcl2fastq2 v2.18 were run to demultiplex reads for all libraries and generate FASTQ files. For human m^6A-seq, libraries were sequenced as 75 bp single read on the Illumina NextSeq instrument using NextSeq Control Software 2.1.2. Following sequencing, Illumina Primary Analysis version NextSeq RTA 2.4.11 and Secondary Analysis version bcl2fastq2 v2.18 were run to demultiplex reads for all libraries and generate FASTQ files.

2.7 Plasmid construction and stable cell line generation.

Mouse Ythdf2 (mYthdf2) was cloned from commercial cDNA clone (ORIGENE # MC200730) into vector pcDNA5/FRT/Flag plasmid using primers listed: mYthdf2 ORF Clone BamhI F: 5’-CGC GGA TCC TCG GCC AGC CTC TTG GA-3’ and mYthdf2 ORF Clone NotI R: 5’-ATA AGA ATG CGG CCG CCT ATT TCC CAC GAC CTT GAC GT-3’. Then Flag-mYthdf2 was subcloned under EF1a promoter in pSicoR-EF1a-IRES-EGFP lentiviral construct (Gibson Assembly®, forward primer: 5’-GTC GAC GGT ACC GCG GGC CCA TGG ATT

ACA AGG ATG ACG ACG-3' and reverse primer: 5'-GAG GGA GAG GGG CGG ATC CCC TAT TTC CCA CGA CCT TGA CGT-3'). Human Ythdf2 (hYthdf2) was cloned from plasmid provided by Chuan He lab using primers indicated: Forward 5'-CGT TCG AAA TGT CGG CCA GCA GCC TCT-3'; Reverse 5'-TCC CCC GGG TTA TTT CCC ACG ACC TT-3'. Then hYthdf2 was cloned into pSicoR-EF1a-IRES-EGFP constructs under EF1a promoter by BstBI and XmaI restriction digestions and ligation. To generate Flag-mYthdf2 HPC7 stable cell line, lentiviruses were generated by transfection of pSicoR-EF1a-Flag-mYthdf2-IRES-EGFP constructs together with the psPAX2 and pMD2.G plasmids at a ratio of 10:7.5:2.5 into 293T cells using calcium phosphate transfection. The virus particles were harvested 48, 72, and 96 hours post transfection, filtered by 0.45 micrometers filter unit (Millipore), and then centrifuged at 18,000 RPM, 4˚C for 2 hours. HPC7 cells were infected with recombinant lentivirus-transducing units in the presence of 4μg/mL polybrene (Sigma). 48 hours after infection, GFP^+ cells were sorted and cultured for experiments.

2.8 irCLIP-seq and data analysis.

For irCLIP-seq, we modified the procedure from the previously reported methods (Simsek et al., 2017; Zarnegar et al., 2016). In brief, irCLIP was performed on ~3×10^8 Flag-Ythdf2 HPC7 cells by UV crosslinking cells at 0.4J/cm^2 for 3 times. Whole-cell lysates were generated in lysis buffer (150mM KCl, 10mM HEPES pH 7.6, 2mM EDTA, 0.5% NP-40, 0.5mM DTT, 1:100 protease inhibitor cocktail, 400U/ml RNase inhibitor; 1ml cell pellet and 2ml lysis buffer). Pipetted up and down several times, and then the mRNP lysate was incubated on ice for 5 mins and shock-frozen at -80^0C with liquid nitrogen. The mRNP lysate was thawed on ice and centrifuged at 15,000g for 15 mins to clear the lysate. Flag-Ythdf2 was isolated with 30μl of protein-G magnetic beads per 1ml lysate, previously bound to 2μg of anti-Flag monoclonal

antibody (Sigma) for 2 hours at 4^0C on rotation. The beads were collected, washed eight times with 1ml ice-cold NT2 buffer (200mM NaCl, 50mM HEPES pH 7.6, 2mM EDTA, 0.05% NP-40, 0.5mM DTT, 200U/ml RNase inhibitor) and one time with 200µl irCLIP NT2 buffer (50mM Tris, pH 7.5; 150mM NaCl; 1mM MgCl2; 0.0005% NP-40). mRNP complex was digested with RNase 1 (Thermo Fisher #AM2294) at 0.4U/µl in irCLIP NT2 buffer (aqueous volume of 30µl and supplemented with 6 µl of PEG400 (16.7% final)). The nuclease reaction was incubated at 30^0C for 15 mins in an Eppendorf Thermomixer, 15 s 1,400 r.p.m., 90 s rest. Nuclease digestions were stopped by addition of 0.5mL of ice-cold high-stringency buffer (20mM Tris, pH 7.5; 120mM NaCl; 25mM KCl; 5mM EDTA; 1% Trition-X100; 1% Na-deoxycholate). Immunoprecipitates were then quickly rinsed with 0.25mL then with 0.05mL of ice-cold irCLIP NT2 buffer. The irCLIP adaptor ligation and library construction followed previously reported protocol (Zarnegar et al., 2016).

Data were demultiplexed using FAST-iCLIP version 0.9.3 and aligned to mouse genome mm10 from UCSC using STAR (2.4.2a) with parameters "--outFilterScoreMinOverLread 0 --outFilterMatchNminOverLread 0 --outFilterMatchNmin 0". RPM-normalized genome browser tracks were created in R (3.4.1) and plotted using the Gviz package (1.20.0). Enriched motifs were identified by taking midpoints of each binding site found in all three replicates, adding 20 bases up and downstream, and running MEME (4.11.1) with parameters "-dna -mod zoops -revcomp -minw 5 -maxw 10 -nmotifs 10 -maxsize 1000000". After motifs were identified, we ran tomtom (4.11.1) against transfac (1-2017) to identify known binding sites. Gene Ontology enrichment analysis was performed using a hypergeometric test in R. GO terms were considered enriched if they had a BH-adjusted p-value less than 0.05. Selected terms of interest are shown in the bar plot. Bars in the bar plot indicate percentage of genes in the list being tested having the

term divided by the percentage of genes in the genome having the term. Peaks found by FAST-iCLIP in all three replicates were assigned to various features in the genome. Promoters were defined as upstream 150 bases from the TSS. "trans_stop" was defined as upstream and downstream 200 bases from the transcript start site.

2.9 Cord blood transduction.

Cord blood transduction was conducted as described previously (Rentas et al., 2016). Briefly, fresh $CD34^+$ cord blood cells or flow-sorted $CD34^+$ $CD38^-$ cells were prestimulated for 12-18 hours in StemSpan medium (StemCell Technologies) supplemented with growth factors interleukin 6(IL-6; 20ng/ml, Peprotech), stem cell factor (SCF; 100ng/ml, Peprotech), Flt3 ligand (FLT3-L; 100ng/ml, Peprotech) and thrombopoietin (TPO; 20ng/ml, Peprotech). Lentiviruses were then added in the same medium at a multiplicity of infection (MOI) of 50-200 for 24 hours. Cells were then given 2 days after transduction before *in vitro* or *in vivo* assays. Human *YTHDF2* was knockdown by shRNA targeting 5'-AAGGACGTTCCCAATAGCCAA-3' near the N terminus of CDS as used in a previous report (Shlush et al., 2014). Scramble shRNA (seed sequence 5'- GCGCGATAGCGCTAATAAT-3') was used as control.

2.10 Clonogenic progenitor assays.

Flow-sorted GFP^+ cord blood cells from 10-day cultured transduced cells (12,000 per ml) were resuspended in semi-solid methylcellulose medium (Methocult H4034; StemCell Technologies). Colony counts were carried out after 14 days of incubation.

2.11 Human umbilical cord blood HSPC culture.

Two days after transduction, human cord blood $CD34^+$ or $CD34^+$ $CD38^-$ cells were collected and determined GFP^+ percentage by flow cytometry. To ensure that equal numbers of GFP^+ cells were cultured before expansion, we added identically cultured GFP^- cells to the one

with higher GFP^+ percentage to match the % GFP^+ between control and hYthdf2 KD. Then cells were seeded at a density of 10^5 per ml in StemSpan medium (StemCell Technologies) supplemented with growth factors IL-6 (20ng/ml), SCF (100ng/ml), FLT3-L (100ng/ml), TPO (20ng/ml) and CHIR99021 (250 nM) (Stemgent)(Perry et al., 2011).

2.12 Human HSC xenotransplantation.

For human cord blood HSC *ex vivo* expansion analysis, 10^5 sorted $CD34^+$ $CD38^-$ cells were transduced with human *YTHDF2* shRNA or control shRNA for 3 days and then analyzed for transduction efficiency (%$GFP^{-/+}$) and stem cell markers. On day 10, cultured cells were collected for stem cell marker analysis. For hUCB HSC primary limiting dilution assay (LDA), $CD34^+$ cells were enriched as described above and transduced with human *YTHDF2* shRNA or control shRNA at 50 MOI. Media were changed at 24 hours post infection. Equal number of GFP^+ cells were sorted out from control or *YTHDF2* KD cells on 3 days post infection and cultured overnight. Three doses, 50K, 20K and 10K, of sorted GFP^+ cells were transplanted into sublethally irradiated (3.25Gy) NSG mice, respectively. The cut-off for HSC engraftment was an exhibition of more than 1% human $CD45^+$ GFP^+ cells out of total $CD45^+$ cells in BM of primary transplantation recipients. For hUCB HSC secondary LDA assay, BM cells from highest two doses primary recipients were collected and mixed together at 10 weeks post transplantation. Three doses, 1.2×10^7, 8×10^6, 4×10^6, of BM cells were transplanted into sublethally irradiated (3.25Gy) NSG mice, respectively. The cut-off for HSC engraftment was an exhibition of more than 0.2% human $CD45^+$ GFP^+ cells out of total $CD45^+$ cells in BM of secondary transplantation recipients. HSC frequency was assessed using ELDA software (Hu & Smyth, 2009). For all human cord blood xenotransplantation experiments, female NSG mice aged 6-8 weeks were used.

2.13 m^{6}A-seq data analysis.

Human and mouse m^{6}A-seq data were aligned to the transcriptome of hg19 and mm10. In order to identify m^{6}A peaks, hg19 and mm10, transcriptome was divided into 25 nucleotide-wide tiles. The number of reads in the m^{6}A IP and non-IP (control) sample was counted in each tile, and p value was calculated with Fisher exact test and adjusted for multiple testing. Tiles with significant m^{6}A signal enrichment (adjust-Pval <= 0.05) were merged into bigger regions. Regions smaller than 100 bp were discarded, and regions over 200 bp were divided into 100 to 200 bp sub-regions; m^{6}A signal over control was calculated at each region; and regions with at least 2-fold enrichment in all replicates were identified as m^{6}A peaks. m^{6}A peaks distribution and m^{6}A marked genes were determined by overlapping all m^{6}A peaks with hg19 and mm10 RefGene annotation. m^{6}A marked genes were identified by overlapping m^{6}A peaks with hg19 RefGene. To filter for transcription factors, genes marked by m^{6}A in all three samples were compared against human transcription factor database (http://fantom.gsc.riken.jp/5/sstar/Browse_Transcription_Factors_hg19). GO term analysis was then performed using R package enrich GO. m^{6}A marked human transcription factors were used as searching list, and all the expressed genes were used as background. Hemopoiesis related BP terms with significant enrichment were used to generate Figure 3c.

2.14 RNA-seq.

Human cord blood CD34$^+$ cells were transduced with control or human *YTHDF2* KD lentivirus and sorted out for GFP$^+$ CD34$^+$ 10 days later. Three replicates of 12,000 GFP$^+$ CD34$^+$ cells were sorted for each group and were used to extract total RNA. Four nanograms of high quality total RNA was used for cDNA synthesis and library preparation according to the manufacturer's directions with the SMART-Seq v4 Ultra Low Input RNA Kit for Sequencing

(Takara, 634891) and Nextera XT (Illumina, FC-131-1096). Resulting short fragment libraries were checked for quality and quantity using an Agilent 2100 Bioanalyzer and Invitrogen Qubit Fluorometer. Equal molar libraries were pooled, requantified, and sequenced as 75 base pair single reads on a High Output flow cell on the Illumina NextSeq 500 instrument. Following sequencing, Illumina Primary Analysis version NextSeq RTA 2.4.11 and Secondary Analysis version bcl2fastq2 2.18 were run to demultiplex reads for all libraries and generate FASTQ files.

For RNA-seq analysis, reads were aligned to UCSC genome hg38 with Tophat version 2.0.13 with default parameters, using Ensembl 87 gene models. Read counts were generated using HTSeq-count with -m intersection-nonempty. Reads were also aligned to ERCC control sequences and counts tabulated. A scaling factor was calculated based on the median of the ERCC counts for each sample and used for normalization. Differentially expressed genes were found using the edgeR package (3.18.1) in R (3.4.1). Differentially expressed genes were required to have a BH-adjusted p-value < .05 and a 2-fold change in expression.

2.15 RNA stability assay.

15,000 sorted LT-, ST-HSCs and MPPs were cultured in StemSpan SFEM medium (Stem Cell Technologies) supplemented with 10μg/mL heparin (Sigma), 0.5× penicillin/streptomycin (Sigma), 10ng/mL recombinant mouse (rm) SCF (Biovision, Inc.), and 20ng/mL Tpo (Cell Sciences, Inc.) (Perry et al., 2011) at 37^0C 5% CO_2 5% O_2. Sorted cells were treated with 5μM actinomycin D (Sigma) for inhibition of mRNA transcription. Cells were harvested at 0 hour or 4 hours post treatment, and total RNA was extracted and used for RNA-seq.

2.16 m^6A RNA methylation quantification.

Mouse BM Lineage negative cells from *wt* and *Ythdf2* KO mice were enriched with mouse Lineage Cell Depletion Kit (Miltenyi Biotec), followed by total RNA extraction with

TRIzol (Invitrogen). The quantification of m^6A RNA methylation in Lin^- cells were performed with m^6A RNA Methylation Quantification Kit (Abcam ab185912) following manufacturer's protocol. 200ng total RNA were used per replicates for either group.

2.17 qPCR analysis.

10^5 LSK cells were sorted from *wt* and *Ythdf2* KO mice. Total RNA was extracted with TRIzol (Invitrogen). cDNA synthesis was conducted with High-Capacity RNA-to-cDNA™ Kit (Thermo) following manufacturer's protocol. qPCR primers used are listed Table 2.1.

mouse Tal1 qPCR primer F	CGCTGCTCTATAGCCTTAGCC
mouse Tal1 qPCR primer R	CTCTTCACCCGGTTGTTGTT
mouse Gata2 qPCR primer F	CAACCCTTACTACGCCAACC
mouse Gata2 qPCR primer R	GCTGTGCAACAAGTGTGGTC
mouse Runx1 qPCR primer F	CCAGCCTCTCTGCAGAACTT
mouse Runx1 qPCR primer R	GGAGATGGACGGCAGAGTAG
mouse Stat5a qPCR primer F	AGAAGCAAGTGTCCCTGGAG
mouse Stat5a qPCR primer R	GTCGTCCAGGATGATGGTCT
mouse Actb qPCR primer F	TGTCACCAACTGGGACGATA
mouse Actb qPCR primer R	ACCCTCATAGATGGGCACAG

Table 2.1 qPCR primers used to verify the expressional levels of transcription factors in *wt* and *Ythdf2* KO HSPCs.

2.18 Western blot and intracellular staining.

To validate the KO or KD efficiency in *Ythdf2* KO mouse model or hUCB, 33,000 $cKit^+$ cells or 120,000 GFP^+ cells were sorted from BM or transfected hUCB samples, respectively. Hela cells transduced to overexpress human YTHDF2 were used validate overexpression efficiency as shown in supplementary information Figure S8b. Immunoblotting was performed with anti-YTHDF2 rabbit polyclonal antibody (MBL, RN123PW) and β-actin mouse monoclonal antibody (NOVUS, NB600-501). Secondary antibodies used were IRDye 800CW

Goat anti-Mouse IgG and IRDye 800CW Goat anti-Rabbit IgG antibodies (LI-COR). For intracellular staining, BM cells from *wt* and *Ythdf2* KO mice were stained with HSC markers as above, then fixed with the Cytofix/Cytoperm kit (BD Biosciences) according to the manufacturer's instructions. Fixed and permeabilized cells were immunostained with anti YTHDF2 antibody (MBL RN123PW), anti TAL1 antibody (Santacruz sc-393287), anti GATA2 antibody (Santacruz sc-267), anti RUNX1 antibody (Santacruz sc-365644), anti STAT5 antibody (Santacruz sc-74442) and detected by Alexa-488 donkey anti-rabbit IgG antibody (Invitrogen).

2.19 Single cell immunostaining.

10,000 LSKs from *wt* and *Ythdf2* KO mice were sorted onto Poly-L-lysine coating slides, which were placed in a moisture chamber and incubated at 4^0C for 30 mins to allow cells settling onto the slides. Cells were fixed with chilled methanol at RT for 10 mins, blocked with universal blocking reagent (BioGenex) at RT for 30 mins, and stained with mouse TAL1 antibody (Santa Cruz, SC393287) or mouse IgG control (Abcam) at 4˚C overnight. Cells were then stained with Alexa Fluor 488 donkey anti-mouse IgG (Thermo Fisher Scientific) at 4˚C for 30 mins. Images were taken on a PerkinElmer Ultraview spinning disk system with Yokagawa CS-X1 disk. All emission was collected onto a C9100-23 Hamamatsu EM-CCD using Velocity software (PerkinElmer). For Z-stacks, the step size was set at 400nm. Staining intensity per image was quantified by ImageJ program.

2.20 FISH in conjugation with fluorescent immunostaining.

Sorted LSKs were spun onto microscope glass slide (Fisher Scientific Cat. No. 12-544-4) using a Cytospin™ 4 Cytocentrifuge at 800 rpm for 1 min with medium acceleration (Thermo Scientific, cat. no. A78300003), followed by an immediate immersion into 4% PFA (diluted from 16% (wt/vol) aqueous solution, Electron Microscopy Sciences, cat. no. 15710). Cells were

fixed at RT (25 ± 2 °C) for 30 mins. RNA in situ hybridization was performed using RNAscope multiplex fluorescent detection kit according to the manufacturer's instructions (Advanced Cell Diagnostics) with a couple of modifications: Antigen retrieval was unnecessary, and digestion was performed with 1:15 diluted proteinase III solution for 10 mins at RT. RNAscope probes targeting mouse *Tal1* and *Gata2* were designed and produced by ACDbio. After the *in situ* hybridization was completed, slides were rinsed twice with PBST and directly processed with background blocking (Background buster solution, Innovex, cat. no. NB306) and primary antibody incubation. Anti-YTHDF2 (MBL, 1: 500) and anti-Dcp1α (Santa Cruz, SC100706, 1:200) antibodies were diluted with antibody diluent reagent buffer (Life technologies, cat. no. 003118) and incubated at 4°C overnight. Donkey anti- rabbit Alexa Fluor 488 (Invitrogen, 1:500) and donkey anti-mouse Alexa Fluor 633 (Invitrogen, 1:500) were used for protein target multiplexing.

2.21 Statistical analysis.

Statistical analyses were done using Student's *t* test. The results are shown as the mean ± s.e.m.

2.22 Data availability.

All sequencing data, including the m^6A-seq, irCLIP-seq and RNA-seq datasets, are available through the Gene Expression Omnibus (GEO) under accession GSE107957. Original Data Repository at http://www.stowers.org/research/publications/LIBPB-1248.

Chapter 3 : Ythdf2 KO leads to increase in phenotypic HSCs in primary mice

Sections of chapters 2-8 have previously been published and are adapted and reprinted here with permission, alongside new, never-before published material. Li, Z., Qian, P., Shao, W. Shi, H., He, X.C., Gogol, M.,. . . Li, L. (2018). Suppression of m(6)A reader Ythdf2 promotes hematopoietic stem cell expansion. *Cell Res*, 28(9), 904-917.

3.1 Examine the phenotype of Ythdf2 KO in mouse bone marrow

In this chapter, I will examine the effect of Ythdf2 on hematopoiesis in the primary mice with the advent of cell surface markers and flow cytometry. To test this, we first crossed the Ythdf2 conditional knockout (KO) mice with a PolyI:C (pI:pC)-inducible *Mx1-Cre* mouse line (Kuhn, Schwenk, Aguet, & Rajewsky, 1995) to specifically reduce *Ythdf2* expression in hematopoietic cells (hereafter *Ythdf2* KO mice) (Figure 3.1A and B). Four weeks after pI:pC injections, we observed a significant increase in both frequency and absolute number of long-term HSCs (Lin^- $Sca1^+$ $cKit^+$ (LSK) $CD34^-$ $Flk2^-$; LT-HSCs) and short-term HSCs (LSK $CD34^+$ $Flk2^-$; ST-HSCs), but not in multipotent progenitors (LSK $CD34^+$ $Flk2^+$; MPPs) in *Ythdf2* KO mice compared to littermate *wild type (wt)* mice (Figure 3.1C to E). Although *Ythdf2* KO led to increased BM cellularity, the absolute number of committed progenitors, including common myeloid progenitors (CMPs), granulocyte-macrophage progenitors (GMPs), megakaryocyte-erythrocyte progenitors (MEPs) and common lymphoid progenitors (CLPs), as well as mature lineage cells, erythrocytes, myeloid cells, B cells and T cells, showed no significant difference between *Ythdf2* KO and *wt* mice (Figure 3.1Fto H).

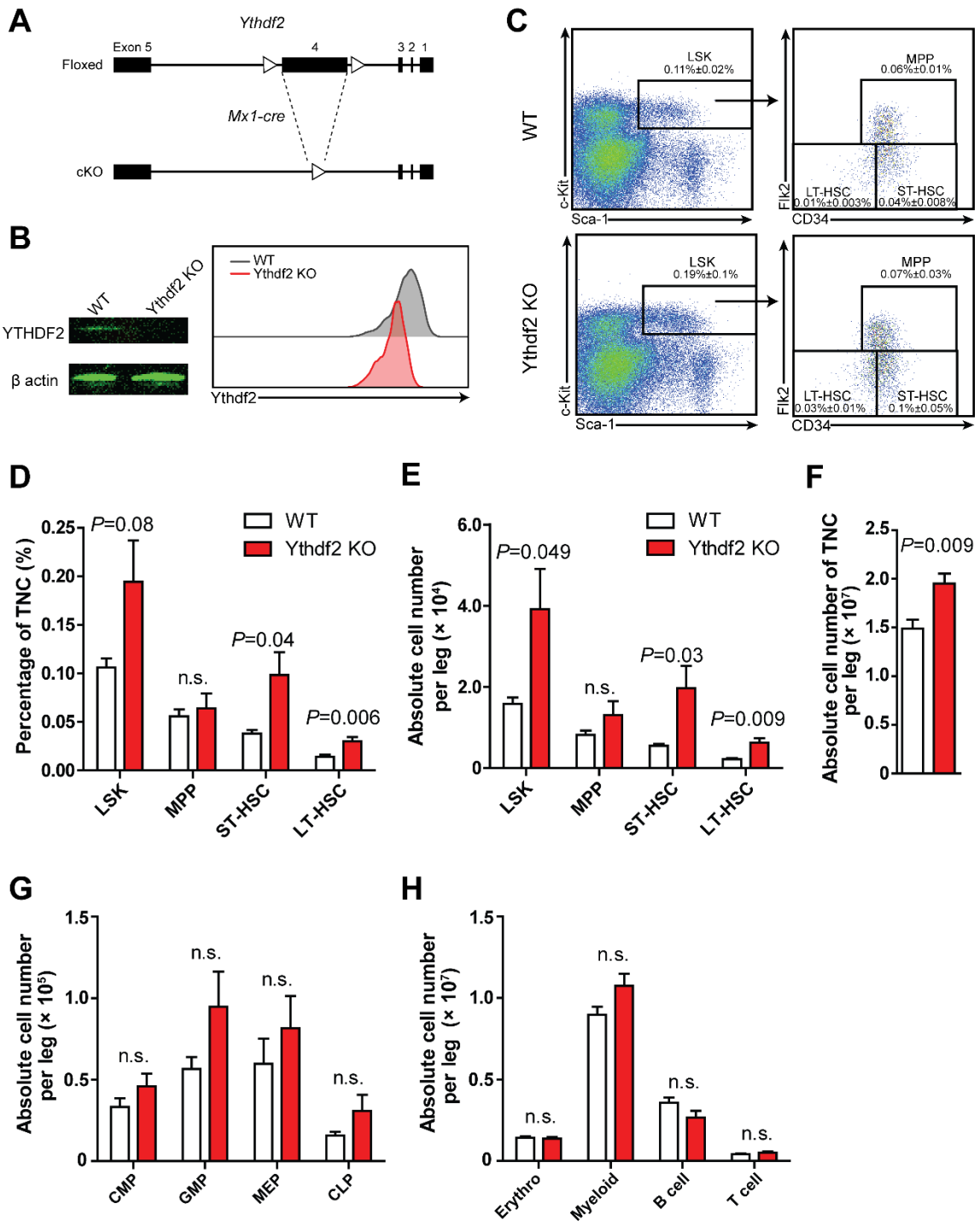

Figure 3.1 *Ythdf2* KO leads to increase in phenotypic HSCs in mice.
(**A**) Deletion of Ythdf2 in the HSPCs of *Mx1-cre;Ythdf2*$^{f/f}$ conditional KO (cKO) mice. (**B**) Western blot (left) and histogram (right) showing intracellular flow validation of KO Ythdf2 in mouse HSPCs. (**C**) Representative flow plots of HSPCs in BM from *wt* and *Ythdf2* KO mice (n = 5 for each group). (**D** and **E**) Frequency in total nucleated cells (TNC) (**D**) and absolute cell number (**E**) of HSPCs in BM from *wt* and *Ythdf2* KO mice (n = 5 for each group). (**F**) Absolute number of BM TNC from *wt* and *Ythdf2* KO mice (n= 5 for each group). (**G** and **H**) Absolute

number of committed progenitors (**G**) and lineage cells (**H**) in BM of *wt* and *Ythdf2* KO mice (n = 5 for each group). Data shown as mean ± s.e.m. Unpaired t-test. n.s., nonsignificant.

3.2 *Ythdf2* KO results in lower apoptotic rate in HSPCs without affecting cell cycle

HSC quiescence has been well documented to play an essential role in maintaining LT-HSC function and self-renewal capacity, disruption of which results in HSC exhaustion and places HSC under higher risk of tumorigenic mutagenesis (Jude, Gaudet, Speck, & Ernst, 2008; Kohli & Passegue, 2014; Nakamura-Ishizu, Takizawa, & Suda, 2014; Sanchez-Aguilera & Mendez-Ferrer, 2017). Given that we observed an increase in the number of phenotypic HSCs, we asked whether this is due to faster cell cycle, which may impair HSC quiescence and functionality. Cell cycle analysis revealed no discernible change of quiescence in HSCs or MPPs after *Ythdf2* KO (Figure 3.2A). Notably, the percentage of apoptotic cells in *Ythdf2* KO LT-, ST-HSCs and MPPs significantly reduced compared to *wt* controls (Figure 3.2B).

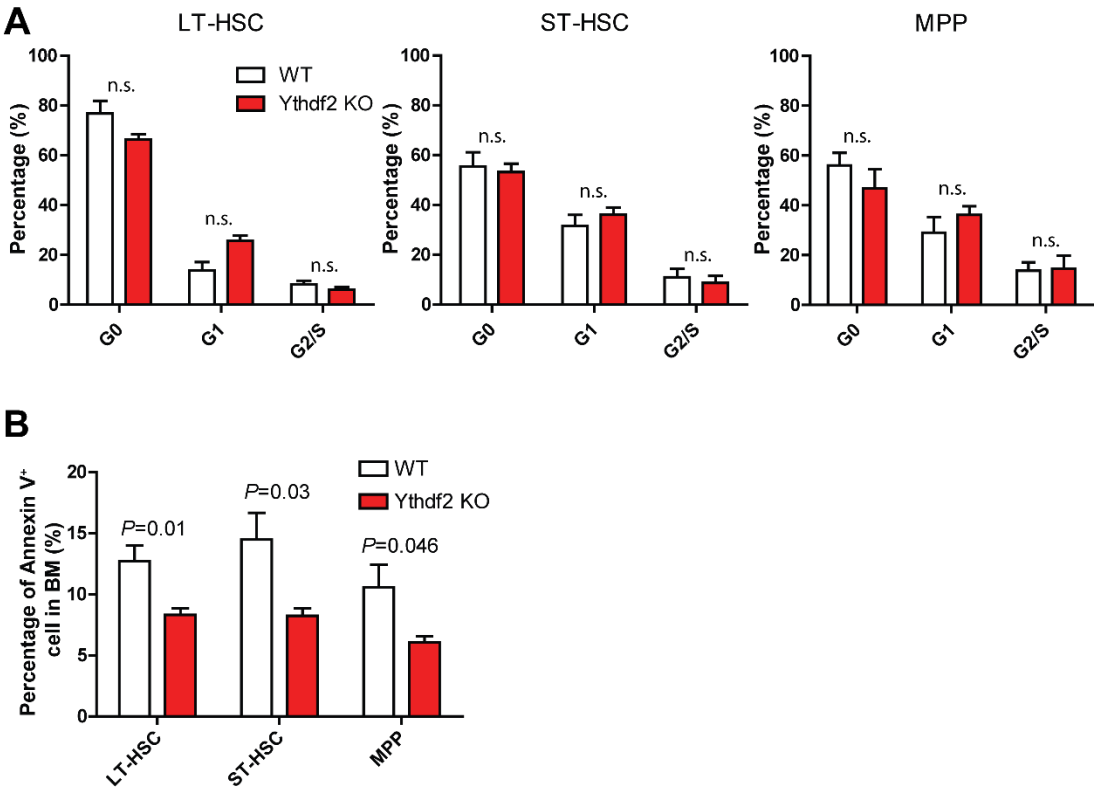

Figure 3.2 *Ythdf2* KO results in lower apoptotic rate in HSPCs without affecting cell cycle. (**A**) Cell cycle analysis of HSPCs in *wt* (n = 3) and *Ythdf2* KO (n = 4) mice. (**B**) Apoptosis analysis of BM HSPCs in *wt* and *Ythdf2* KO mice (n = 5 for each group). Data shown as mean ± s.e.m. Unpaired t-test. n.s., nonsignificant.

3.3 Determine the splenic hematopoiesis in Ythdf2 KO mouse

Adult splenic hematopoiesis, a type of extramedullary hematopoiesis, usually reflects pathological circumstances, such as immune response, within the organism (Kim, 2010). To further identify any potential HSC defects in *Ythdf2* KO mice, we examined the number of HSCs, committed progenitors, and mature lineages in the spleen and found no significant differences between *wt* and *Ythdf2* KO mice (Figure 3.3A-E). In summary, *Ythdf2* KO in primary mice specifically increases HSC numbers with no bias or defects in either progenitor or lineage cells.

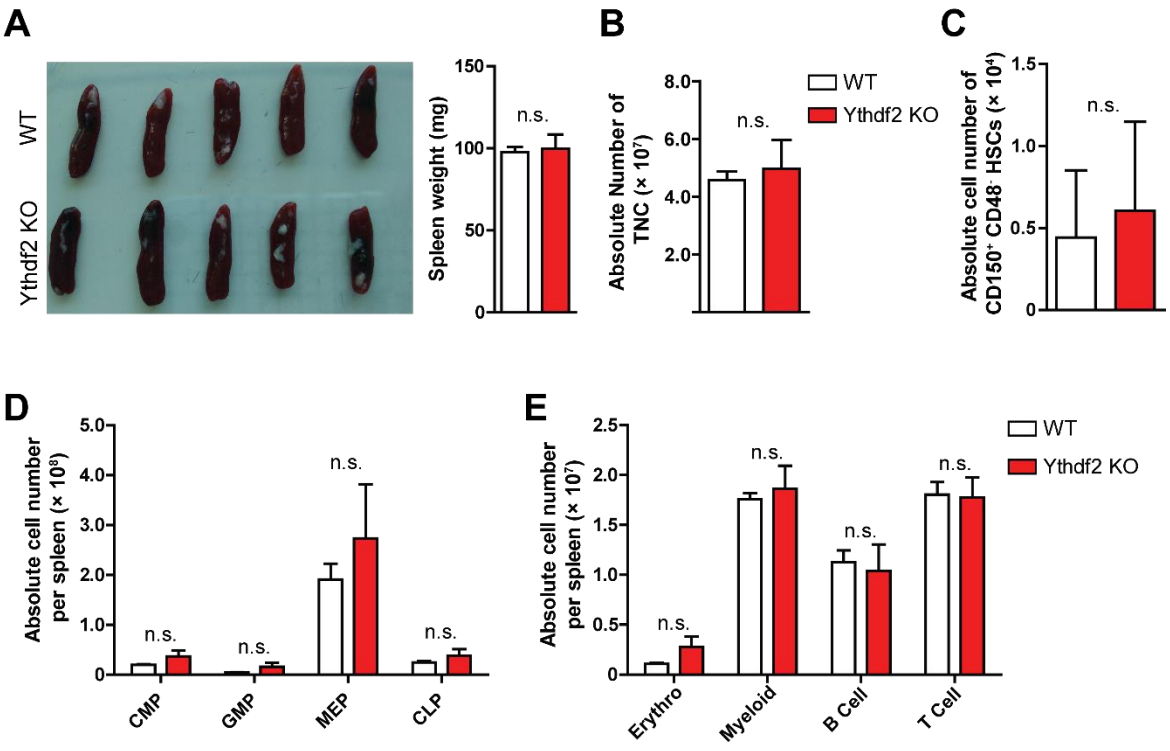

Figure 3.3 Splenic hematopoiesis is normal in *Ythdf2* KO mice.
(**A**) Images and weight of spleens from *wt* and *Ythdf2* KO mice. (**B** to **E**) Absolute number of TNC (**B**), LSK CD48$^-$ CD150$^+$ HSCs (**C**), committed progenitors (**D**) and lineage cells (**E**) in the spleen of *wt* (n = 3) and *Ythdf2* KO (n = 4) mice. Data shown as mean ± s.e.m. Unpaired t-test. n.s., nonsignificant.

Chapter 4 : *Ythdf2* KO expands functional HSCs in mice

Sections of chapters 2-8 have previously been published and are adapted and reprinted here with permission, alongside new, never-before published material. Li, Z., Qian, P., Shao, W. Shi, H., He, X.C., Gogol, M.,. . . Li, L. (2018). Suppression of m(6)A reader Ythdf2 promotes hematopoietic stem cell expansion. *Cell Res*, 28(9), 904-917.

4.1 Determine the frequency of reconstitution units from *Ythdf2* KO mouse BM in primary transplantation recipients

To determine whether *Ythdf2* KO expands functional HSCs, we initially executed limited dilution, competitive repopulation unit assay (LDA) by transplanting 2×10^5, 7.5×10^4 or 2.5×10^4 donor BM cells (CD45.2), together with 2×10^5 recipient BM cells derived from the *ptprc* mutant strain (CD45.1), into lethally irradiated recipient mice (Figure 4.1A). Consistent with an increased number of phenotypic HSCs in *Ythdf2* KO mice, we found that competitive repopulating units (CRUs) increased 2.2-fold in *Ythdf2* KO HSCs compared to controls (Figure 4.1B). In the 2×10^5 group, compared to controls, we observed a significant increase in the overall repopulation rate from *Ythdf2* KO donor cells at 16 weeks post transplantation (Figure 4.1C). Moreover, recipients of *Ythdf2* KO BM cells, compared to that of controls, exhibited markedly higher frequency and absolute number of donor derived LT-HSCs and ST-HSCs, but not MPPs in BM (Figure 4.1D and E). Furthermore, we found that donor derived committed progenitors and mature lineages in BM from transplantation recipients of mutant and *wt* cells showed no significant changes (Figure 4.1F and G). To exclude the possibility that homing ability may contribute to higher engraftment of *Ythdf2* KO cells, we performed a short-term homing assay by transplanting 1×10^6 carboxyfluorescein diacetate succinimidyl ester (CFDA SE)-labelled BM cells from KO mice or their control littermates into lethally irradiated recipient

mice, and found no significant difference in their homing capacity between mutant and *wt* controls (Figure 4.1H).

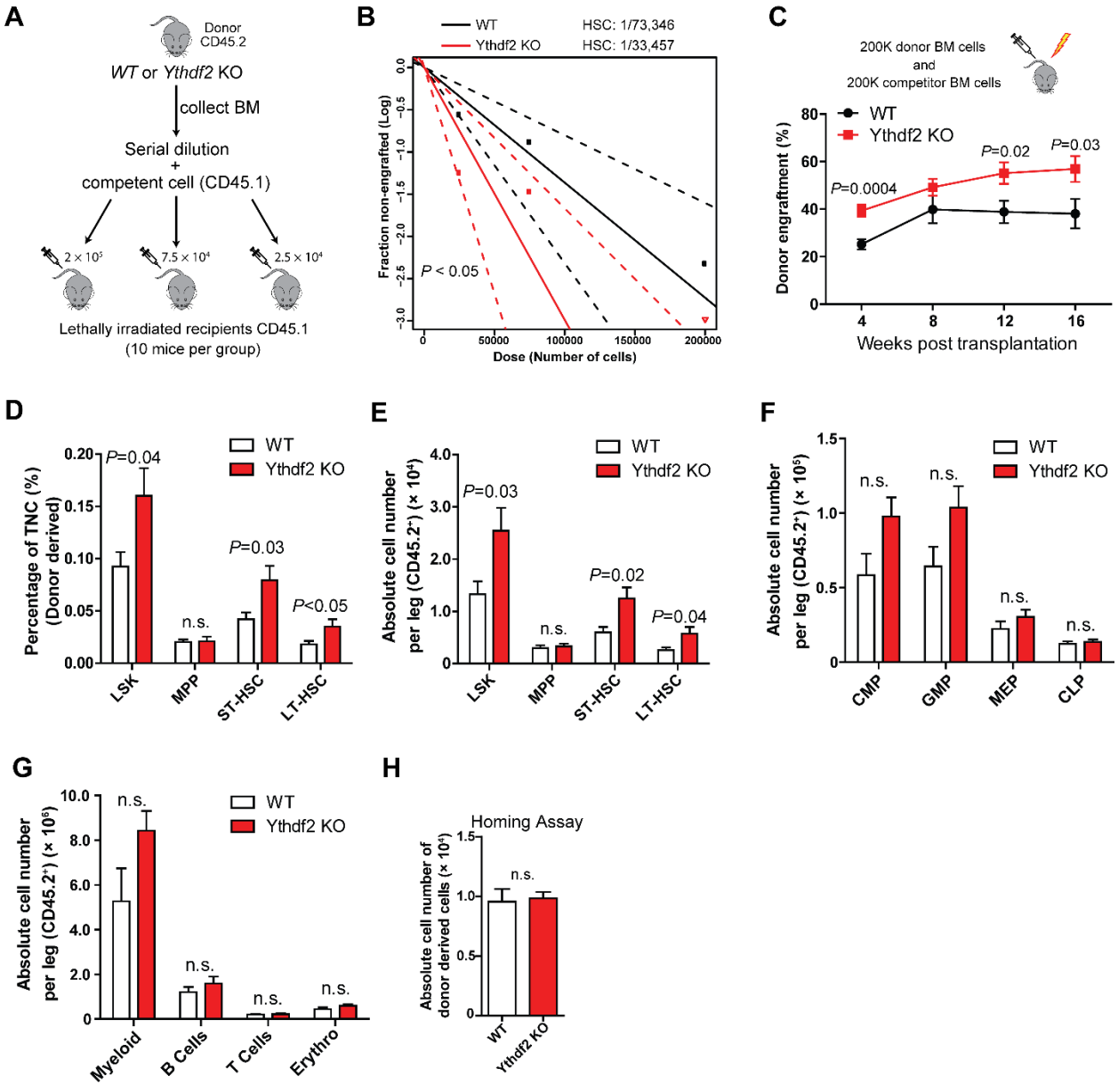

Figure 4.1 *Ythdf2* KO HSCs expand in primary transplanted recipient mice.
(**A**) Experimental scheme for limiting dilution transplantation assay (LDA) to determine the frequency of functional HSCs. (**B**) Primary LDA to determine the CRU frequency by ELDA (Extreme Limiting Dilution Analysis) at 16 weeks post transplantation (n = 10 per group). (**C**) Competitive reconstitution assay by transplanting 200K whole bone marrow (WBM) cells with 200K rescue cells into irradiated recipients (n = 10 for each group). (**D** and **E**) Frequency in TNC

(**D**) and absolute cell number (**E**) of donor derived HSPCs in BM from transplantation recipient mice as (**C**) (n = 10 for each group). (**F**and **G**) Absolute cell number of donor derived ($CD45.2^+$) committed progenitors (**F**) and lineage cells (**G**) in BM from primary 200K BM transplantation recipient mice (n= 9-10 for each group). (**H**) Homing ability of *wt* and *Ythdf2* KO cells was determined by transplanting 1×10^6 CFDA SE-labelled BM cells into lethally irradiated mice. 18 hours later, BM was analyzed for homed events (n = 6 mice per group). Data shown as mean ± s.e.m. Unpaired t-test. n.s., nonsignificant.

4.2 Examine the frequency of LT-HSCs from *Ythdf2* KO mouse BM in secondary transplantation recipients

The gold standard test of HSC potential is the serial transplant assay. The most immature HSC should be able to sustain hematopoiesis throughout serial transplantation (Lemischka, Raulet, & Mulligan, 1986; Purton & Scadden, 2007; Rosendaal, Hodgson, & Bradley, 1979). Thus, to determine the long-term repopulation ability of HSCs from *Ythdf2* KO mice, we conducted the secondary transplantation with BM cells derived from primary recipients. Notably, we found that compared to controls, CRUs from *Ythdf2* KO cells revealed a 3.5-fold increase (Figure 4.2A) and exhibited no signs of leukemia in both BM and spleen at 16 weeks after secondary transplantation (Figure 4.2 B-G).

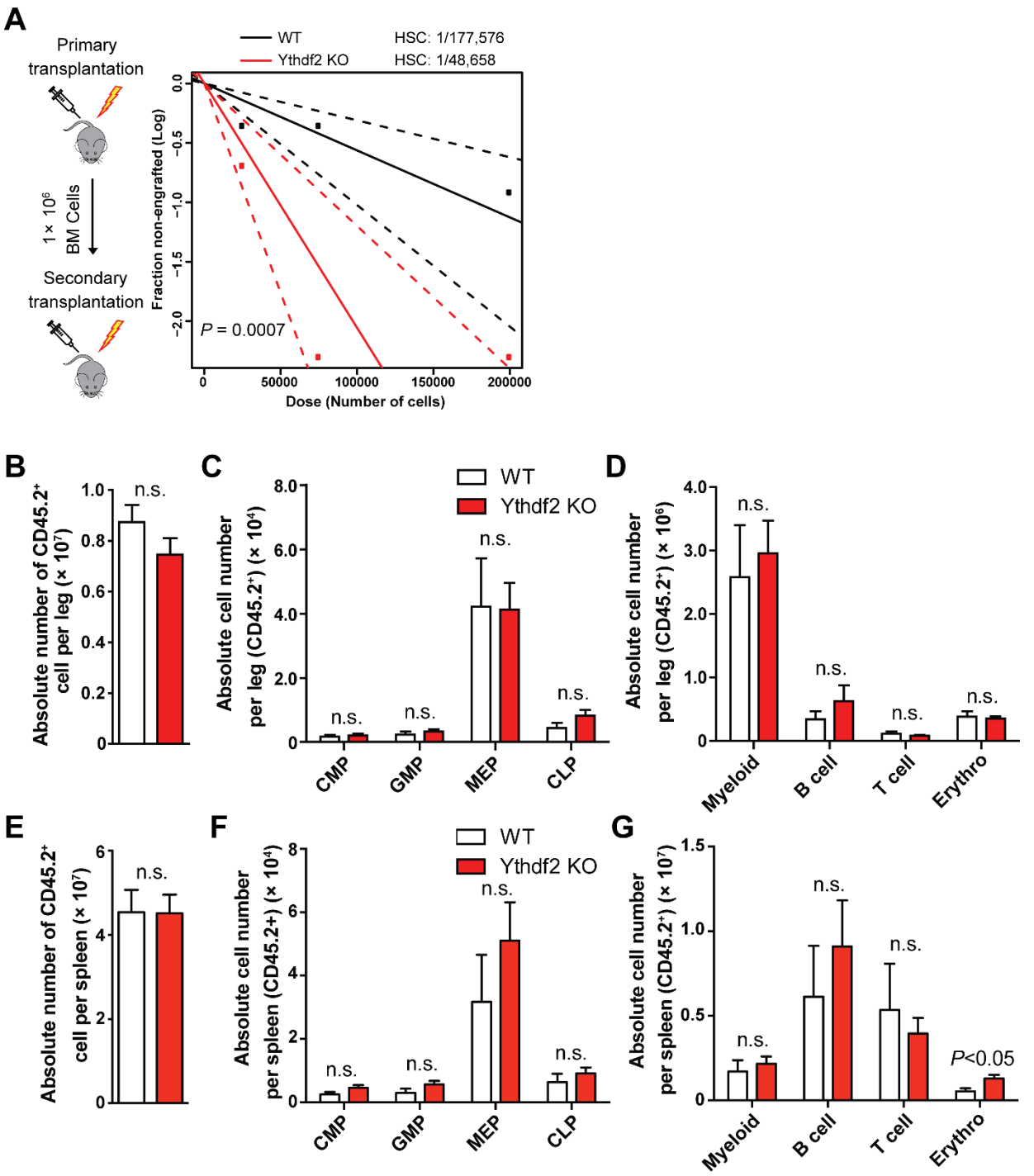

Figure 4.2 *Ythdf2* KO HSCs further expand in secondary transplant recipient mice without inducing leukemia.

(**A**) Secondary LDA to determine the long-term CRU frequency by ELDA at 16 weeks after secondary transplantation (n = 10). (**B** to **D**) Absolute cell number of donor derived ($CD45.2^+$) TNC (**B**), committed progenitors (**C**) and lineage cells (**D**) in the BM from secondary 200K transplantation recipient mice at 16 weeks after secondary transplantation (n= 7-10 for each group). (**E** to **G**) Absolute cell number of donor derived ($CD45.2^+$) TNC (**E**), committed progenitors (**F**) and lineage cells (**G**) in the spleen from secondary 200K transplantation recipient

mice at 16 weeks after secondary transplantation (n= 7-10 for each group). Data shown as mean ± s.e.m. Unpaired t-test. n.s., nonsignificant.

4.3 Test the long-term effect of *Ythdf2* KO in primary mice under homeostasis condition

Expansion of a clonal population of blood cells derived from a single HSC, known as clonal hematopoiesis, may endow higher risk of accumulating mutations that enhance HSC self-renewal, leading to hematological malignancies with the passage of time (Bowman, Busque, & Levine, 2018). Thus, we questioned whether depletion of Ythdf2 would result in abnormal hematopoiesis in primary mice along with aging. To test this, we examined the stem cells, progenitor cells, and lineages in both BM and spleen at over 5 months post pI:pC injections (Figure 4.3A). Although we observed a modest increase in the number of LT-HSCs in BM from *Ythdf2* KO mice compared to that of controls (Figure 4.3C), there were no discernible differences between *Ythdf2* KO and control mice in total nucleated cell (TNC), progenitors and lineage cells from either BM or spleen (Figure 4.3B and D to J). These observations indicate that the long-term effect of *Ythdf2* KO *in vivo* neither skews lineage differentiation nor facilitates aberrant proliferation, which is in line with previous reports that *Ythdf2* is not required for leukemogenesis (Z. Li et al., 2017a; Weng et al., 2018). To verify the frequency of functional HSCs in the BM at 5 months post pI:pC induction, we transplanted 7.5×10^4 BM cells from *wt* and *Ythdf2* KO mice with competent cells into lethally irradiated recipients. We found that *Ythdf2* KO led to significantly higher engraftment in recipients compared to *wt* controls, indicating that the number of functional, though not phenotypical, HSCs in 5-months post *Ythdf2* KO mice remained higher than that of control (Figure 4.3K). Taken together, these data reveal that *Ythdf2* KO results in specific and significant mouse HSC expansion *in vivo* without affecting lineage commitment.

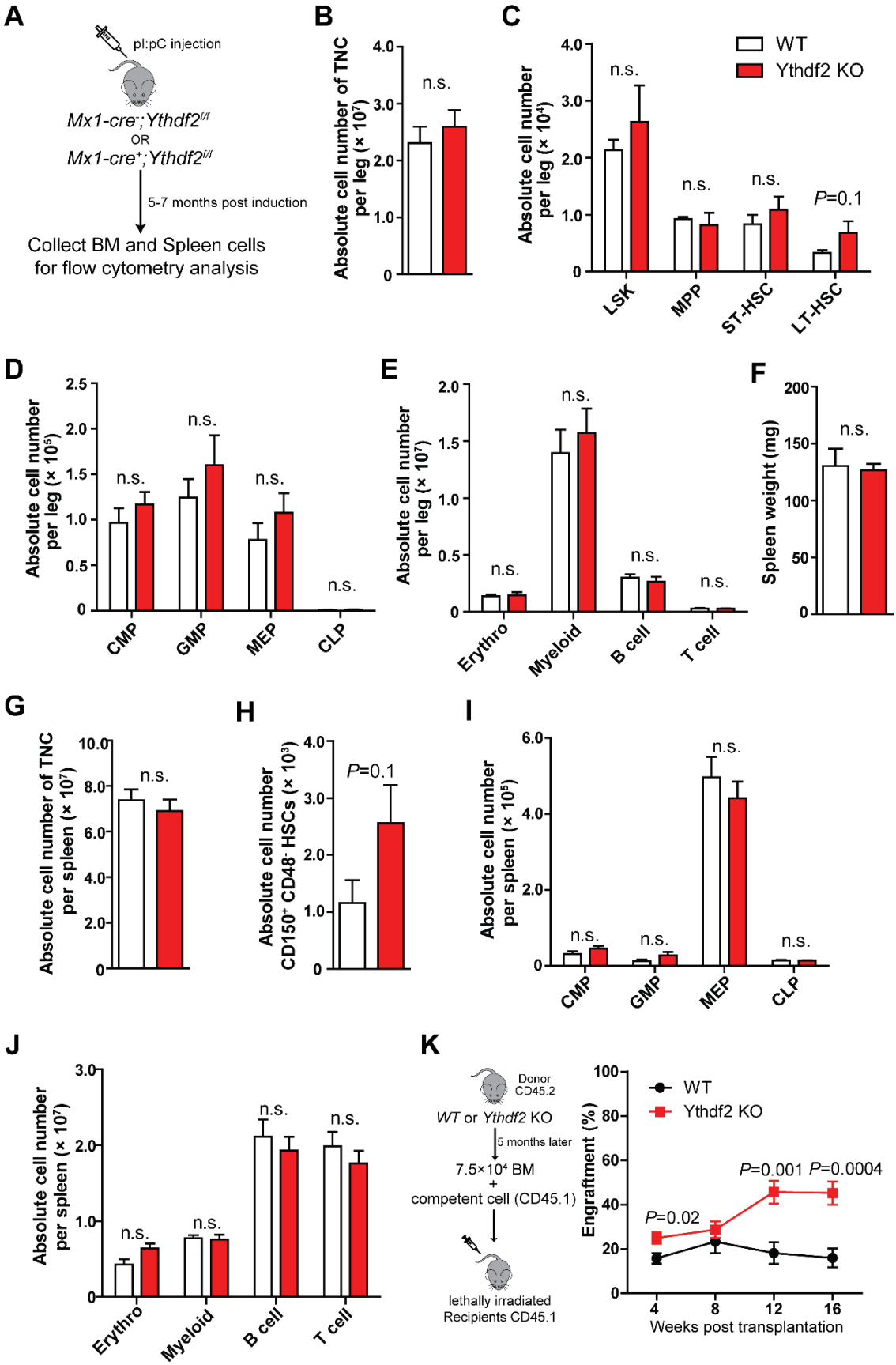
A
pI:pC injection
Mx1-cre⁻;Ythdf2f/f
OR
Mx1-cre⁺;Ythdf2f/f
5-7 months post induction
Collect BM and Spleen cells
for flow cytometry analysis
B
Absolute cell number of TNC per leg (× 10⁷)
n.s.
C
WT
Ythdf2 KO
Absolute cell number per leg (× 10⁴)
n.s.
n.s.
n.s.
P=0.1
LSK
MPP
ST-HSC
LT-HSC
D
Absolute cell number per leg (× 10⁵)
n.s.
n.s.
n.s.
n.s.
CMP
GMP
MEP
CLP
E
Absolute cell number per leg (× 10⁷)
n.s.
n.s.
n.s.
n.s.
Erythro
Myeloid
B cell
T cell
F
Spleen weight (mg)
n.s.
G
Absolute cell number of TNC per spleen (× 10⁷)
n.s.
H
Absolute cell number CD150⁺ CD48⁻ HSCs (× 10³)
P=0.1
I
Absolute cell number per spleen (× 10⁵)
n.s.
n.s.
n.s.
n.s.
CMP
GMP
MEP
CLP
J
Absolute cell number per spleen (× 10⁷)
n.s.
n.s.
n.s.
n.s.
Erythro
Myeloid
B cell
T cell
K
Donor CD45.2
WT or Ythdf2 KO
5 months later
7.5×10⁴ BM
+
competent cell (CD45.1)
lethally irradiated
Recipients CD45.1
WT
Ythdf2 KO
Engraftment (%)
P=0.02
P=0.001
P=0.0004
Weeks post transplantation

Figure 4.3 *Ythdf2* KO has long-term effect on mouse HSC expansion *in vivo* without inducing lineage bias.
(**A**) BM and spleen collected from *wt* and *Ythdf2* KO mice were analyzed by flow cytometry at 5-7 months post pI:pC inductions. (**B** to **E**) Absolute cell number of TNC (**B**), HSPCs (**C**), committed progenitors (**D**) and lineage cells (**E**) in the BM of *wt* and *Ythdf2* KO mice at 5-7 months post induction. (n = 4-7 mice per group). (**F**) The weight of spleens from *wt* and *Ythdf2* KO mice at 5-7 months post induction. (n = 4-7 mice per group). (**G** to **J**) Absolute cell number of TNC (**G**), LSK $CD48^{-}$ $CD150^{+}$ HSCs (**H**), committed progenitors (**I**) and lineage cells (**J**) in the spleen of *wt* and *Ythdf2* KO mice at 5-7 months post induction. (n = 4-7 mice per group). (**K**) 5 months post pI:pC injection, 75k WBM from *wt* and *Ythdf2* KO mice were transplanted with 200K rescue cells into lethally irradiated recipients. Peripheral blood from transplantation recipients were analyzed every 4 weeks post transplantation to determine the donor derived engraftment (n = 10 for each group). Data shown as mean ± s.e.m. Unpaired t-test. n.s., nonsignificant.

Chapter 5 : Ythdf2 regulates HSC self-renewal gene expression by m^{6}A-mediated mRNA decay

Sections of chapters 2-8 have previously been published and are adapted and reprinted here with permission, alongside new, never-before published material. Li, Z., Qian, P., Shao, W. Shi, H., He, X.C., Gogol, M.,. . . Li, L. (2018). Suppression of m(6)A reader Ythdf2 promotes hematopoietic stem cell expansion. *Cell Res*, 28(9), 904-917.

5.1 Molecular characterization of m^{6}A modification in mouse HSPCs

In this chapter, I will explore the underlying mechanism of how *Ythdf2* KO expands HSCs. According to the previous study on the function of YTHDF2, it is an m^{6}A reader protein that recognizes m^{6}A-marked mRNAs and promotes mRNA decay by recruiting to mRNA decay site (X. Wang et al., 2014). However, the transcriptome-wide map of m^{6}A in mouse HSCs remains unknown. Thus, we first mapped the m^{6}A methylome by methylated RNA immunoprecipitation combined with high-throughput sequencing (MeRIP-seq or m^{6}A-seq) in LT-HSCs, ST-HSCs, and MPPs sorted from adult C57BL/6J mice (Dominissini et al., 2012; Meyer et al., 2012; Schwartz et al., 2013). m^{6}A peaks were selected by identifying significantly enriched overlapping peaks from two independent replicates. Consistent with previous studies (Dominissini et al., 2012; Meyer et al., 2012), we found that m^{6}A peaks were abundant in mRNA open reading frame (ORF), in 3' untranslated regions (UTRs), and around the stop codon in all three HSPC populations (Figure 5.1A and B). Transcripts of moderately expressed genes were more likely to be methylated (Figure 5.1C). Intriguingly, we found that m^{6}A modifications were enriched in the mRNAs of transcription factors, such as *Gata2*, *Etv6, Stat5* and *Tal1*, which have been documented to be critical for HSC self-renewal and stem cell state maintenance (de Pater et al., 2013; Ebina & Rossi, 2015; Hock et al., 2004; Kato et al., 2005; Lim et al., 2012; Orkin & Zon, 2008; Reynaud et al., 2005; Z. Wang, Li, Tse, & Bunting, 2009), suggesting the m^{6}A

modification could play critical roles in HSC regulation (Table 5.1). Given the accumulating evidence that m^6A mRNA methylation regulates stem cell fate determination by facilitating the decay of mRNAs coding for transcription factors and genes in key signaling pathways involved in self-renewal and differentiation (Batista et al., 2014; Geula et al., 2015; H. B. Li et al., 2017; Z. Li et al., 2017a; Yoon et al., 2017a; C. Zhang et al., 2017a; B. S. Zhao, Wang, et al., 2017a), we next measured the mRNA degradation rates in LT-, ST-HSCs, and MPPs by monitoring mRNA levels after transcription inhibition with actinomycin D. We found that degradation rates of methylated mRNAs were significantly faster than unmethylated mRNAs in ST-HSCs, and MPPs but not LT-HSCs (Figure 5.1D).

Gata2	**Gfi1**	**Pbx1**
Lmo2	**Etv6**	**Erg**
Runx1	**Tal1**	**Hoxa9**
Meis1	**Kmt2a**	**Kmt2b**
Kmt2c	**Kmt2d**	**Bmi1**
Sox4	**Evi1**	**Stat3**
Stat5a	**Hoxb4**	**Zfx**
Foxo3	**Foxp1**	

Table 5.1 Key transcription factors critical for HSC self-renewal and maintenance are labeled by m^6A in HSPCs.

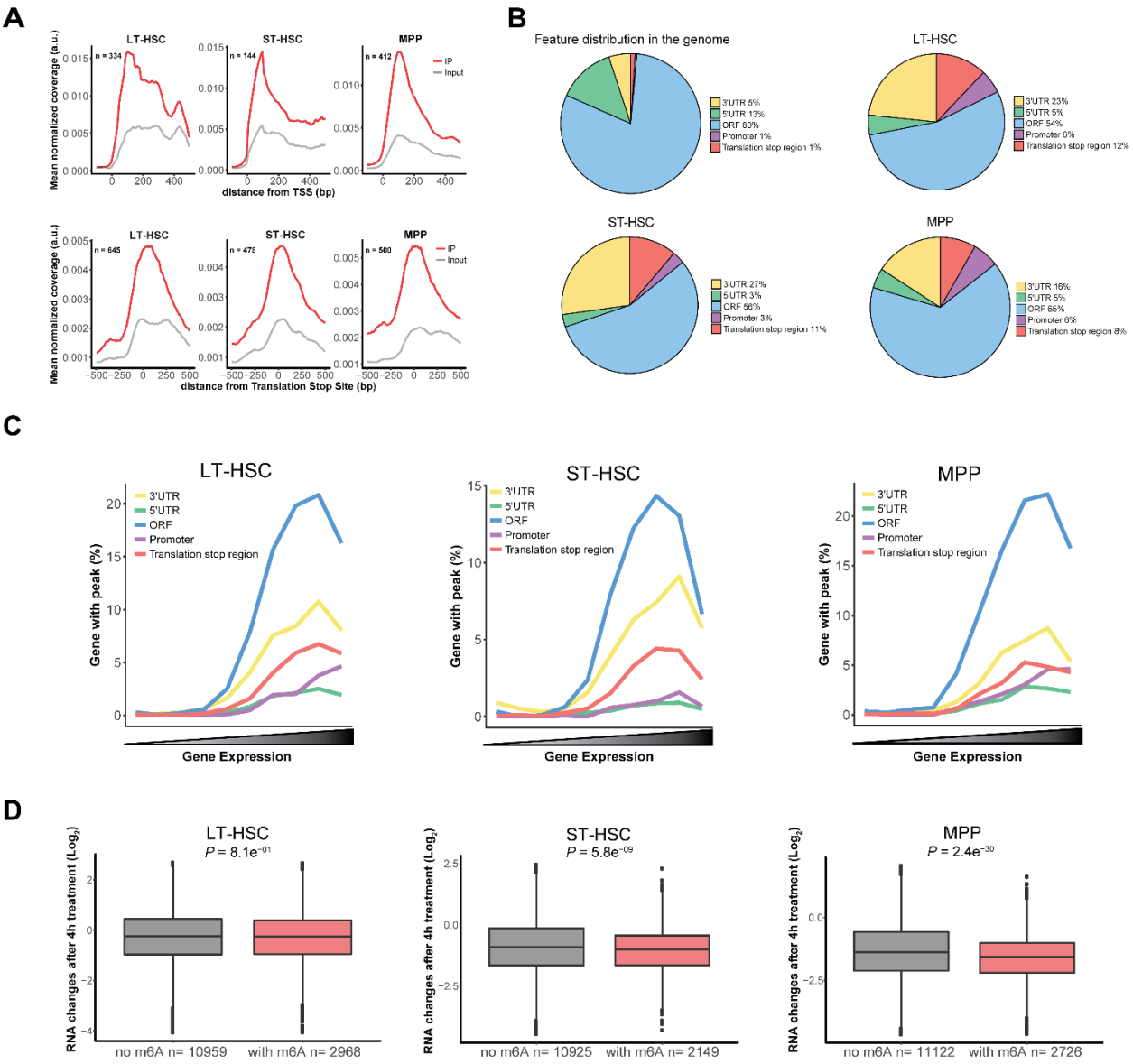

Figure 5.1 Molecular characterization of m^{6}A modification in mouse HSPCs.
(**A**) Metagene profiles depicting sequence coverage in windows surrounding the TSS (up) and stop codon (down). Coverage of m^{6}A IP and control (input) fragments indicated in red and grey, respectively. (**B**) Pie chart presenting the fraction of m^{6}A peaks in each of five transcript segments. (**C**) Fraction of genes in mouse HPSCs with m^{6}A peaks in each of the segments as a function of expression level. (**D**) m^{6}A-tagged and non-m^{6}A-tagged mRNA degradation rates as determined by analysis of the expression level at 0 hour and 4 hours post actinomycin D treatment in HSPCs.

5.2 Define Ythdf2 functionality by irCLIP-seq

In this section, I will examine the mRNA targets of YTHDF2 in mouse multipotent hematopoietic precursor cell line HPC-7. In the previous section, I identified the transcriptome-wide map of m^6A in HSPCs and showed that mRNAs encoding transcription factors essential for stem cell self-renewal are enriched. Next, I asked whether YTHDF2 recognizes and mediates the degradation of these mRNAs. Thus, I performed infrared UV-crosslinking immunoprecipitation sequencing (irCLIP-seq) in HPC-7 cells (Figure 5.2A). irCLIP-seq, a derivation of CLIP assay, is a powerful technique for interrogating direct protein–RNA interactions with high efficiency and sensitivity (Zarnegar et al., 2016). I first repeated the published experiment (Zarnegar, 2016) as a pilot test and showed successful pulled down hnRNP-RNA complex as published data (Figure 5.2B). Though it would be best to profile the mRNA targets of YTHDF2 in mouse HSPCs, several commercial antibodies of YTHDF2 failed to pull down clear YTHDF2-RNA complex as visualized on nitrocellulose membrane (data not shown). Thus, to improve the efficiency of pulling down YTHDF2-RNA complex, I generated stable HPC-7 cell line expressing Flag-YTHDF2 driven by mammalian EF1α promoter. The efficiency of immunoprecipitation of YTHDF2 with anti-FLAG antibody from control or Flag-YTHDF2 overexpression HPC-7 cell lysates was confirmed by western blot with anti-YTHDF2 antibody (Figure 5.2C). I then performed irCLIP-seq to determine the mRNA targets of YTHDF2 in HPC-7 cells overexpressing Flag-YTHDF2 as indicated (Figure 5.2D and E). The results showed that YTHDF2 binding sites were enriched with the conserved m^6A motif and exhibited the characteristic of m^6A distribution features (Figure 5.2F and G). Consistent with the previous report that YTHDF2 function as a m^6A reader protein (X. Wang et al., 2014), we found that 57.8% of Ythdf2 target mRNAs contained m^6A peaks (Figure 5.2H).

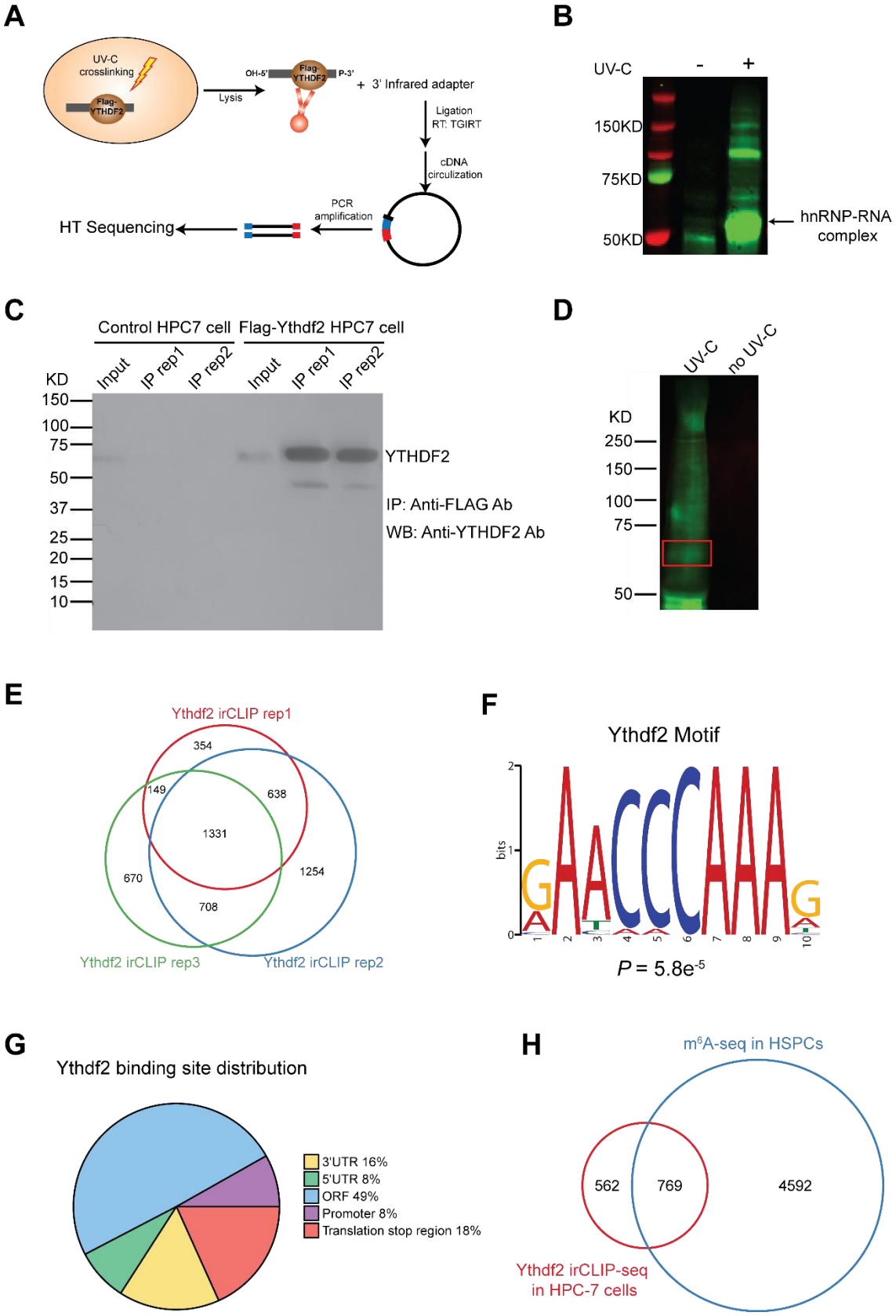
A
UV-C crosslinking
Flag-YTHDF2
Lysis
OH-5'
Flag-YTHDF2
P-3'
+ 3' Infrared adapter
Ligation RT: TGIRT
cDNA circulization
PCR amplification
HT Sequencing
B
UV-C
-
+
150KD
75KD
50KD
hnRNP-RNA complex
C
Control HPC7 cell
Flag-Ythdf2 HPC7 cell
Input
IP rep1
IP rep2
Input
IP rep1
IP rep2
KD
150
100
75
50
37
25
20
15
10
YTHDF2
IP: Anti-FLAG Ab
WB: Anti-YTHDF2 Ab
D
UV-C
no UV-C
KD
250
150
100
75
50
E
Ythdf2 irCLIP rep1
354
149
638
1331
670
1254
708
Ythdf2 irCLIP rep3
Ythdf2 irCLIP rep2
F
Ythdf2 Motif
bits
P = 5.8e-5
G
Ythdf2 binding site distribution
3'UTR 16%
5'UTR 8%
ORF 49%
Promoter 8%
Translation stop region 18%
H
m6A-seq in HSPCs
562
769
4592
Ythdf2 irCLIP-seq in HPC-7 cells

Figure 5.2 Define Ythdf2 functionality by irCLIP-seq.
(**A**) Schematic of irCLIP-seq workflow. (**B**) irCLIP membrane image showing IR800 labeled RNA-hnRNP complex isolated from Hela cells. (**C**) Immunoprecipitation of YTHDF2 in control or Flag-YTHDF2 overexpressed HPC-7 cells. (**D**) irCLIP membrane image showing IR800 labeled RNA-Ythdf2 complex. Red box indicates the RNA-YTHDF2 complex collected for library construction. Samples without UV crosslinking serve as controls. (**E**) Venn diagram showing intersection genes identified in three independent Ythdf2 irCLIP-seq experiments. (**F**) YTHDF2-binding motif identified by MEME with all irCLIP peaks found in all three replicates. (**G**) Pie chart depicting the fraction of YTHDF2-binding peaks in each of five transcript segments. (**H**) Venn diagram showing overlap of Ythdf2 binding targets and m^6A labeled mRNAs.

5.3 YTHDF2 binds to m^6A-labeled mRNAs encoding transcription factors essential for HSC self-renewal and results in their degradation

To investigate the molecular mechanism underlying YTHDF2 regulation of HSC self-renewal, I first performed Gene Ontology (GO) analysis of Ythdf2 target transcripts. This analysis revealed enrichment of genes related to hematopoietic or lymphoid organ development, suggesting the involvement of Ythdf2 in the regulation of hematopoiesis (Figure 5.3A). Notably, we found that Ythdf2 bound to transcription factor mRNAs, such as that of *Tal1* and *Gata2*, on sites largely overlapping with m^6A peaks (Figure 5.3B and C, Table 5.1). Then I tested the effect of Ythdf2 KO on RNA metabolism. I did not observe a significant difference in the total RNA mass in LSK $Flk2^-$ cells isolated from *wt* and *Ythdf2* KO mice (Figure 5.3D). Though m^6A modification constituted only 0.1-0.4% of adenosine nucleotide in mammal cells (B. S. Zhao, Roundtree, & He, 2017), we found that *Ythdf2* KO led to increased level of m^6A content in total RNA from BM Lin^- cells, suggesting that Ythdf2 specifically regulates the stability of m^6A-marked mRNAs (Figure 5.3E). Consistently, qPCR analysis of total mRNA revealed increased levels of *Tal1*, *Gata2*, *Runx1* and *Stat5a* (representative mRNAs with m^6A modifications in HSPCs) in *Ythdf2* KO LSK cells compared to *wt* controls (Figure 5.3F).

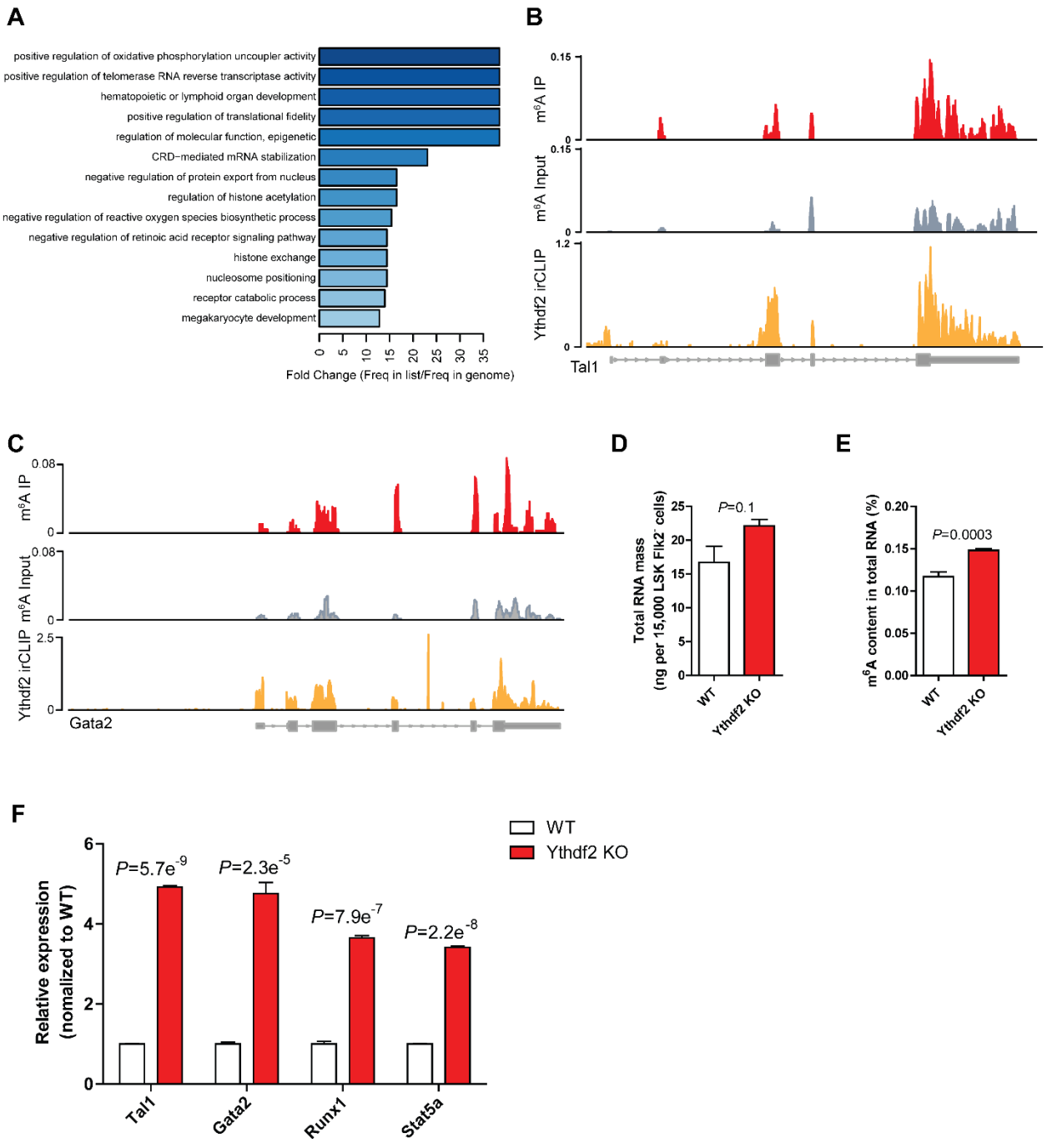

Figure 5.3 YTHDF2 specifically binds to m^{6}A-labeled mRNAs and results in degradation. (**A**) GO enrichment analysis of YTHDF2 targets from intersect genes of three YTHDF2 irCLIPseq replicates. (**B** and **C**) Representative tracks of Tal1(**B**) and Gata2 (**C**) harboring m^{6}A peaks and YTHDF2 irCLIP peaks. Coverage of m^{6}A immunoprecipitation and input fragments indicated in red and grey, respectively. YTHDF2 irCLIP reads highlighted in yellow. (**D**) Total RNA was extracted from 15,000 sorted BM LSK Flk2- cells. (**E**) Quantification of m^{6}A RNA methylation in wt and Ythdf2 KO Lin- cells (n = 6). (**F**) qPCR analysis of total mRNA of sorted LSK cells from wt and Ythdf2 KO mice. All Ct values were first normalized to *Actb* control (not

m6A-tagged) and the ratio (Ythdf2 KO over wt) was then calculated. (n = 3). Data shown as mean ± s.e.m. Unpaired t-test. n.s., nonsignificant.

Then I asked whether increased expression level of mRNAs encoding key transcription factors would result in higher protein levels in *Yhtdf2* KO HSCs. To test this, I performed intracellular flow cytometry and found that *Ythdf2* KO HSPCs exhibited significant increases in the intensities of m^6A-labeled transcription factors involved in stem cell self-renewal, such as TAL1, GATA2, RUNX1 and STAT5, indicative of a suppressive role of Ythdf2 in HSC self-renewal (Figure 5.4A). A previous study has shown that Ythdf2 regulates RNA metabolism through localizing the bound mRNAs to mRNA decay sites (X. Wang et al., 2014). To further explore the mechanism of Ythdf2 in regulating HSC self-renewal, we performed fluorescence in situ hybridization (FISH) of *Tal1* mRNA and fluorescence immunostaining of YTHDF2 and DCP1a, a marker of mRNA decay sites (Kedersha & Anderson, 2007; Sheth & Parker, 2003), and analyzed their relative spatial distribution in sorted *wt* and *Ythdf2* KO HSPCs. Co-localization of *Tal1* mRNA, Dcp1a and Ythdf2 was observed in *wt* cells, while substantially reduced in *Ythdf2* KO controls (Figure 5.4B and C). Furthermore, a similar observation was confirmed by co-staining *Gata2* mRNA FISH with Ythdf2 and Dcp1a in *wt* or *Ythdf2* KO HSPCs (Figure 5.4D and E). To determine whether the increased transcription factors, such as *Tal1*, expression accounted for the HSC expansion in *Ythdf2* KO mice, we performed rescue experiments using short hairpin (sh) RNA-mediated *Tal1* KD in *wt* and *Ythdf2* KO LSK cells, followed by transplantation into lethally irradiated recipients. Depletion of *Tal1* in HSPCs significantly impaired the reconstitution capacity of *wt* cells as reported previously (Lacombe et al., 2010) and also rescued in partial the increased engraftment of *Ythdf2* KO cells (Figure 5.4F).

Overall, these data indicate that Ythdf2 regulates HSC self-renewal by enabling the degradation of mRNAs encoding transcription factors essential for stem cell self-renewal.

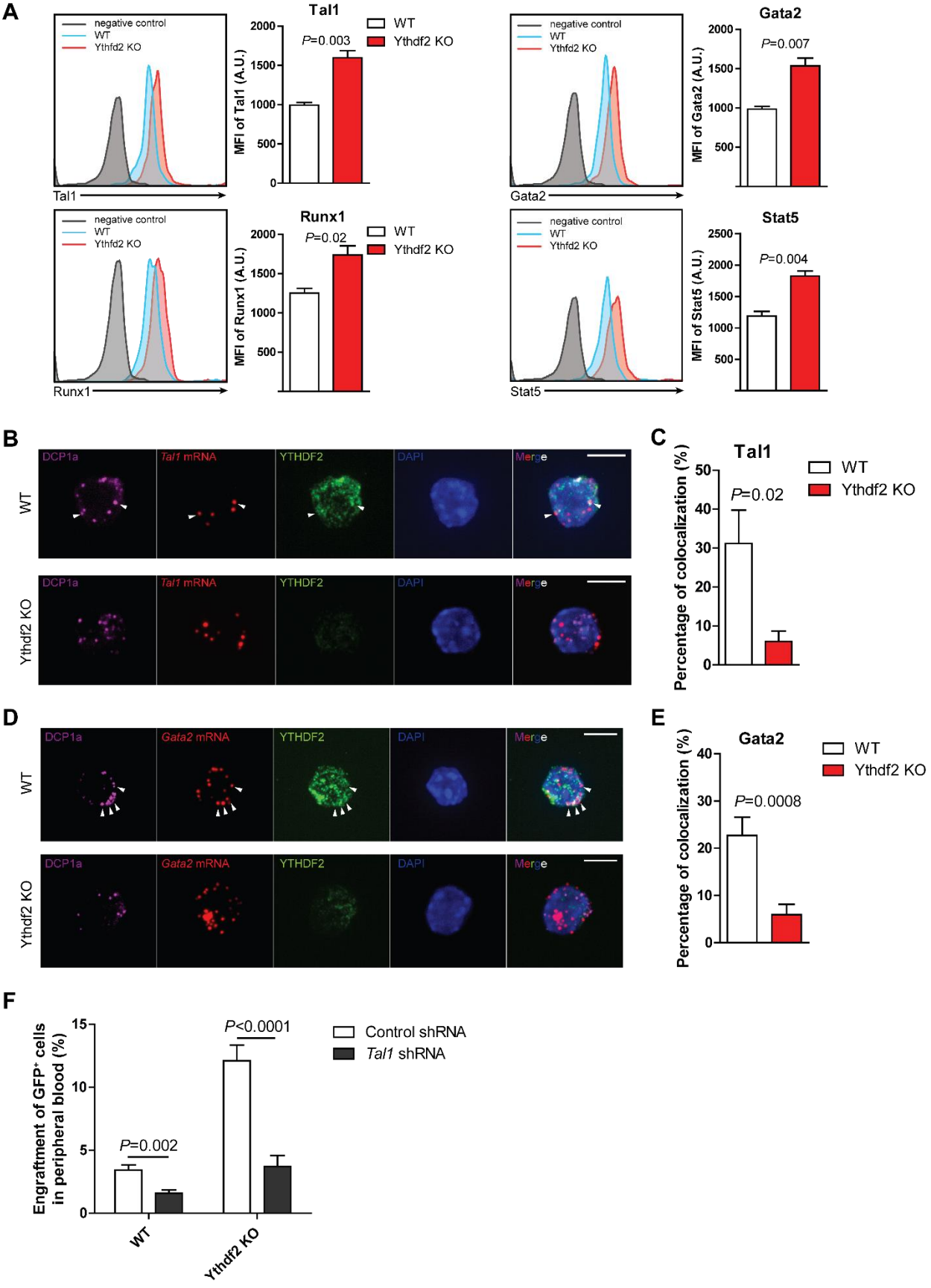
A
negative control
WT
Ythfd2 KO
Tal1
MFI of Tal1 (A.U.)
P=0.003
WT
Ythdf2 KO
Gata2
MFI of Gata2 (A.U.)
P=0.007
Runx1
MFI of Runx1 (A.U.)
P=0.02
Stat5
MFI of Stat5 (A.U.)
P=0.004
B
DCP1a
Tal1 mRNA
YTHDF2
DAPI
Merge
WT
Ythdf2 KO
C
Tal1
Percentage of colocalization (%)
P=0.02
WT
Ythdf2 KO
D
Gata2 mRNA
E
Gata2
P=0.0008
F
Engraftment of GFP+ cells in peripheral blood (%)
P=0.002
P<0.0001
Control shRNA
Tal1 shRNA

Figure 5.4 YTHDF2 regulates HSC self-renewal by promoting m^{6}A-marked mRNA decay. (**A**) Quantification (right) and histogram (left) showing intracellular flow validation of increased expression of TAL1, GATA2, RUNX1 and STAT5 in *Ythdf2* KO LT-HSCs comparing to *wt* LT-HSCs (n = 3 mice per group). (**B**) Fluorescence in situ hybridization of *Tal1* mRNA (red) and fluorescence immunostaining of DCP1a (P-body marker) (magenta), YTHDF2 (green) in wt and Ythdf2 KO HSPCs. Arrows indicate colocalized staining. Scale bars, 5 μm. (**C**) Quantification of *Tal1* mRNA and DCP1a co-localization in sorted LSK cells from wt and Ythdf2 KO mice. Percentage indicates the average frequency of the Tal1 mRNA that colocalized with DCP1a over total Tal1 mRNA level in each LSK cells (n = 9–17). (**D**) Fluorescence in situ hybridization of *Gata2* mRNA (red) and fluorescence immunostaining of Dcp1a (P-body marker) (magenta), Ythdf2 (green) in *wt* and *Ythdf2* KO HSPCs. Arrows indicate co-localized staining. Scale bars, 5 μm. (**E**) Quantification of *Gata2* mRNA and DCP1a colocalization in sorted LSK cells from *wt* and *Ythdf2* KO mice. Percentage indicates the average frequency of the *Gata2* mRNA that co-localized with DCP1a over total *Gata2* mRNA level in each LSK cells (n = 12-20). (**F**) Percentage of GFP$^+$ cells in the CD45$^+$ population at 4 weeks post transplantation (n = 10). Data shown as mean ± s.e.m. Unpaired t-test. n.s., nonsignificant.

Chapter 6 : Dissecting the role of Ythdf2 in human UCB HSPCs by m^{6}A-seq and RNA-seq

Sections of chapters 2-8 have previously been published and are adapted and reprinted here with permission, alongside new, never-before published material. Li, Z., Qian, P., Shao, W. Shi, H., He, X.C., Gogol, M.,. . . Li, L. (2018). Suppression of m(6)A reader Ythdf2 promotes hematopoietic stem cell expansion. *Cell Res*, 28(9), 904-917.

The limited number of HSCs in a single human umbilical cord blood unit has been an obstacle for clinical applications, such as HSC transplantation (Walasek et al., 2012). Our observation that *Ythdf2* KO resulted in an increase of phenotypic and functional mouse HSCs prompted us to test whether *YTHDF2* KD could facilitate human UCB HSC expansion. We first performed m^{6}A-seq with CD34$^+$ cells isolated from 3 individual hUCB samples (Figure 6.1A). m^{6}A modifications predominantly occurred in mRNAs (~95%), preferential in mRNA ORF regions, 3'UTRs, and near the stop codon, as expected (~90%) (Figure 6.1B-D). We further compared m^{6}A landscapes in mouse and hUCB HSPCs and found that 2,239 genes were commonly m^{6}A tagged (Figure 6.1E). These commonly m^{6}A-tagged transcripts were enriched for genes related to hematopoiesis and stem cell maintenance (Figure 6.1F). Due to the enrichment of m^{6}A labeling in the mRNAs of transcription factors responsible for mouse HSC self-renewal, we next characterized the m^{6}A-marked transcription factor transcripts in hUCB CD34$^+$ cells by performing GO term analysis. Among the 722 identified m^{6}A-labeled transcription factor mRNAs, major GO terms were related to cell fate commitment and stem cell maintenance (Figure 6.1G). For example, *HOXB4*, overexpression of which has been reported to expand human and mouse HSCs *ex vivo* (Amsellem et al., 2003; Antonchuk et al., 2002), was marked by m^{6}A in hUCB CD34$^+$ cells (Figure 6.1H). Other transcription factors required for HSC self-renewal and critical to induce HSCs from other cell types (Ebina & Rossi, 2015;

Galan-Caridad et al., 2007), such as *Zfx, RUNX1* and *FOSB,* were also m^6A-tagged in hUCB $CD34^+$ cells (Table 6.1).

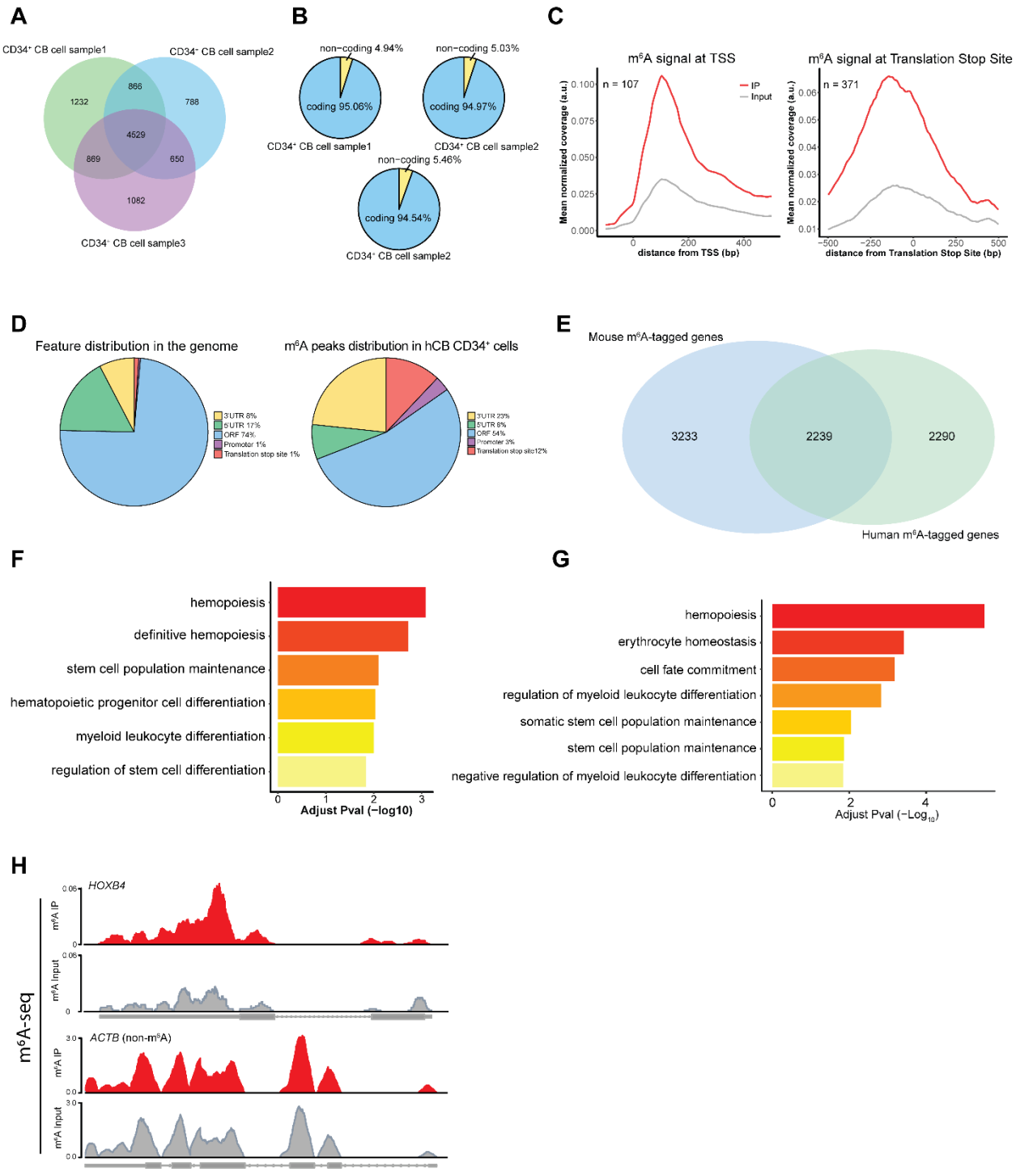

Figure 6.1 Determine the RNA methylome in human UCB HSPCs by m^{6}A-seq.
(**A**) Venn diagram showing intersection genes identified in three independent m^{6}A-seq experiments, using three independent cord blood samples. (**B**) Percentage of mRNAs and noncoding RNAs containing m^{6}A peaks. (**C**) Metagene profiles depicting sequence coverage in windows surrounding the TSS (left) and stop codon (right). Coverage of m^{6}A IP and control (input) fragments indicated in red and grey, respectively. (**D**) Pie chart presenting the fraction of

m^{6}A peaks in each of five non-overlapping transcript segments. (**E**) Venn diagram showing shared and unique m^{6}A-tagged genes in mouse and hUCB HSPCs. (**F**) GO enrichment analysis of m^{6}A-tagged transcripts shared in both mouse and hUCB HSPCs. (**G**) GO enrichment analysis of the transcription factors harboring m^{6}A modifications in hUCB CD34+ cells. (**H**) Representative tracks of HOXB4 harboring m^{6}A peaks. Color codes are the same as in (**C**).

To further dissect the role of YTHDF2 in hUCB HSPCs, we performed RNA-seq with control or *YTHDF2* KD hUCB CD34$^+$ cells (Figure 6.2A). The efficiency of knockdown YTHDF2 was verified at both protein and RNA level by western blot and RNA-seq, respectively (Figure 6.2B and C). Remarkably, transcripts marked by m^{6}A, including *HOXB4* and other HSC self-renewal related transcription factors, showed significant increases of input mRNA reads in the *YTHDF2* KD cells compared to the control, without noticeable changes for non-m^{6}A labelled genes (Figure 6.2D-F and Figure 6.3). These results support the role of YTHDF2 in regulating hUCB HSC self-renewal through RNA degradation.

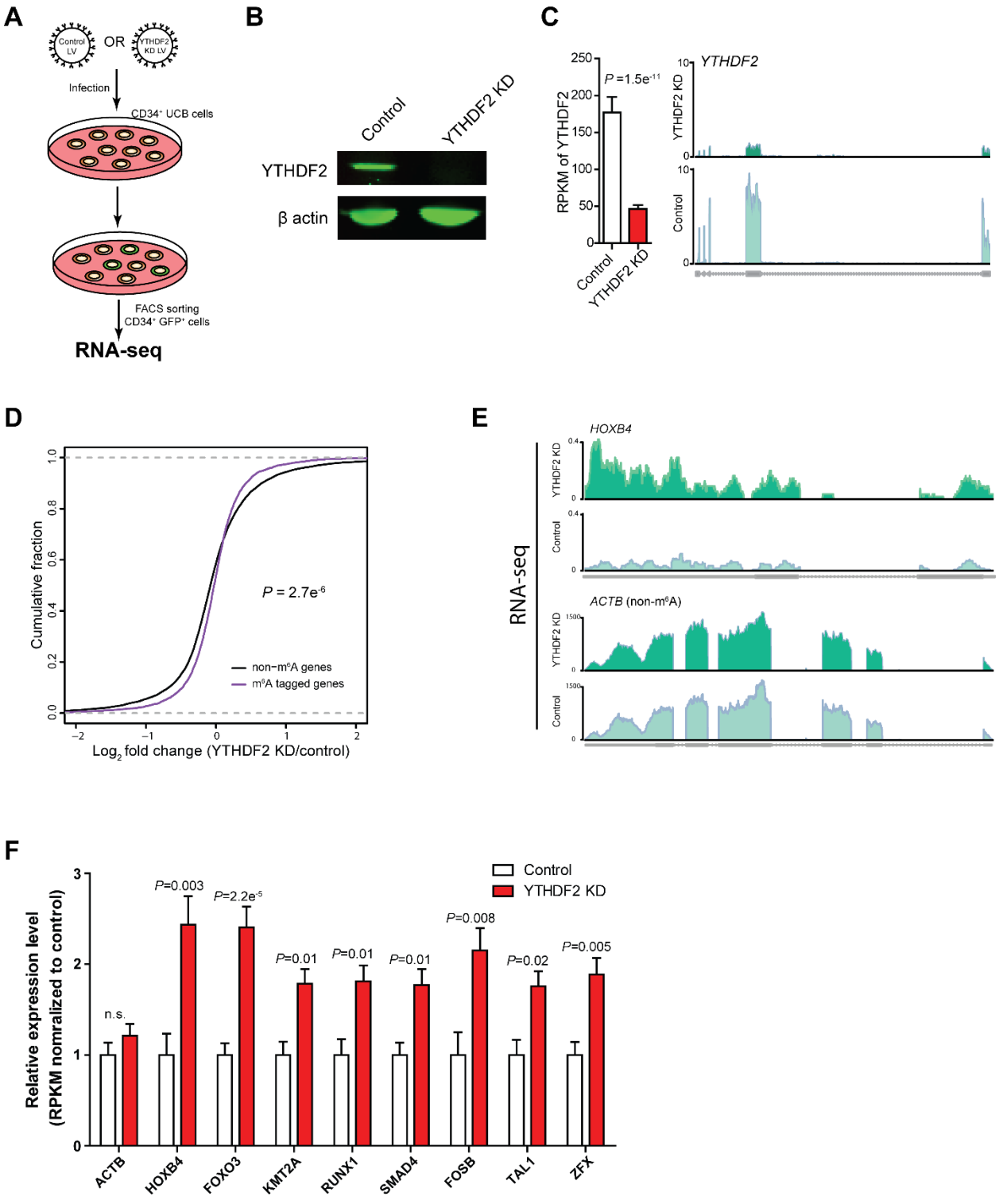

Figure 6.2 Dissect the mechanism of YTHDF2 regulating m^{6}A-labeled mRNAs by RNA-seq.

(**A**) Lentivirus mediated YTHDF2 KD in hUCB CD34$^+$ HSPCs for RNA-seq. (**B**) Western blotting of YTHDF2 (up) and β-Actin (down) in sorted GFP$^+$ control and *YTHDF2* KD hUCB cells, showing knockdown efficiency of YTHDF2. (**C**) Expression level (left) and representative

track plot (right) of YTHDF2 from RNA-seq analysis of control and *YTHDF2* KD hUCB CD34$^+$ cells, showing knockdown efficiency of YTHDF2. (**D**) Cumulative distribution of $\log_2$ (fold change) for m^{6}A-marked genes (purple line) and non-m^{6}A-marked genes (black line) with control and YTHDF2 KD hUCB CD34$^+$ cells. (**E**) Representative coverage plots from the RNA-seq analysis, showing increased reads of m^{6}A-tagged gene *HOXB4* but not a non-m^{6}A-tagged gene *ACTB* in YTHDF2 KD compared with control hUCB CD34$^+$ cells. RPKM from RNA-seq analysis were normalized to controls. Adjusted P-value indicated. n.s. nonsignificant

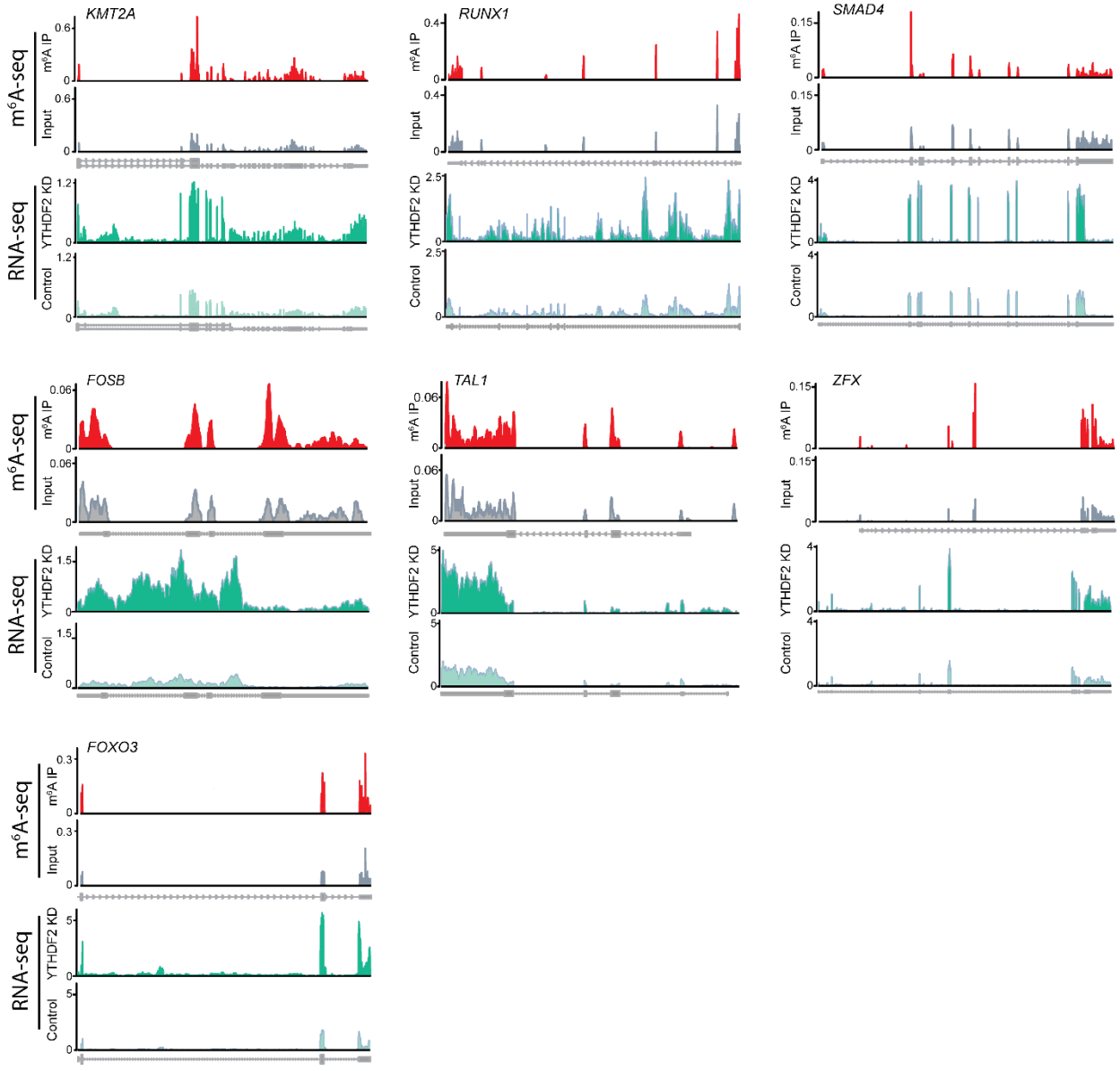

Figure 6.3 Track files of m^{6}A-seq and RNA-seq for genes presented in Figure 6.2. Representative track plots of indicated transcription factors harboring m^{6}A peaks (up) and their representative coverage plots from the RNA-seq analysis (bottom).

Chapter 7 : Expansion of human UCB HSCs by *YTHDF2* Knockdown

Sections of chapters 2-8 have previously been published and are adapted and reprinted here with permission, alongside new, never-before published material. Li, Z., Qian, P., Shao, W. Shi, H., He, X.C., Gogol, M.,. . . Li, L. (2018). Suppression of m(6)A reader Ythdf2 promotes hematopoietic stem cell expansion. *Cell Res*, 28(9), 904-917.

7.1 *YTHDF2* KD facilitates expansion of human cord blood HSCs ex vivo.

In this chapter, I will explore whether suppression of YTHDF2 can expand human HSCs. I next performed shRNA-induced *YTHDF2* KD in hUCB HSPCs followed by expansion *ex vivo* for 7 days. After 7 days *ex vivo* culture, lentiviral mediated KD of YTHDF2 resulted in an average 14.3-fold and 13.6-fold increase, respectively, in the frequency and absolute number of $CD34^+$ $CD38^-$ $CD45RA^-$ $EPCR^+$ phenotypic HSCs (Figure 7.1 A-C). Next I sorted out the lentivirus infected GFP^+ cells from control or *YTHDF2* KD groups by FACS and performed the colony-forming cell (CFC) assay which measures progenitor cells in a given population using semisolid agar- or well-defined methylcellulose-based culture media, which are commercially available (Purton & Scadden, 2007). Two weeks post culture, the number of colonies derived from *YTHDF2* KD cells exhibited a 5.1-fold increase in CFUs relative to control cells. Among different CFU categories, more dramatic increase was seen in the most primitive CFU-granulocyte erythrocyte monocyte megakaryocyte (GEMM) colony type and burst forming unit-erythroid (BFU-E), reflecting higher expression level of key transcription factors for hematopoiesis, such as *TAL1*, in *YTHDF2* KD hUCB cells (Figure 7.1D and E). Interestingly, the apoptotic rate was significantly reduced in *YTHDF2* KD hUCB HSPCs compared to control cells, similar to the trend of HSCs in *Ythdf2* KO mouse (Figure 7.1F). We next compared the effect of overexpression of *YTHDF2* on HSPC function. The efficiency of YTHDF2 overexpression was verified by western blot (Figure 7.1G). Overexpression of *YTHDF2* reduced

clonogenic potential of hUCB HSPCs by 2.2-fold, confirming that YTHDF2 negatively regulates HSC maintenance *ex vivo* (Figure 7.1H).

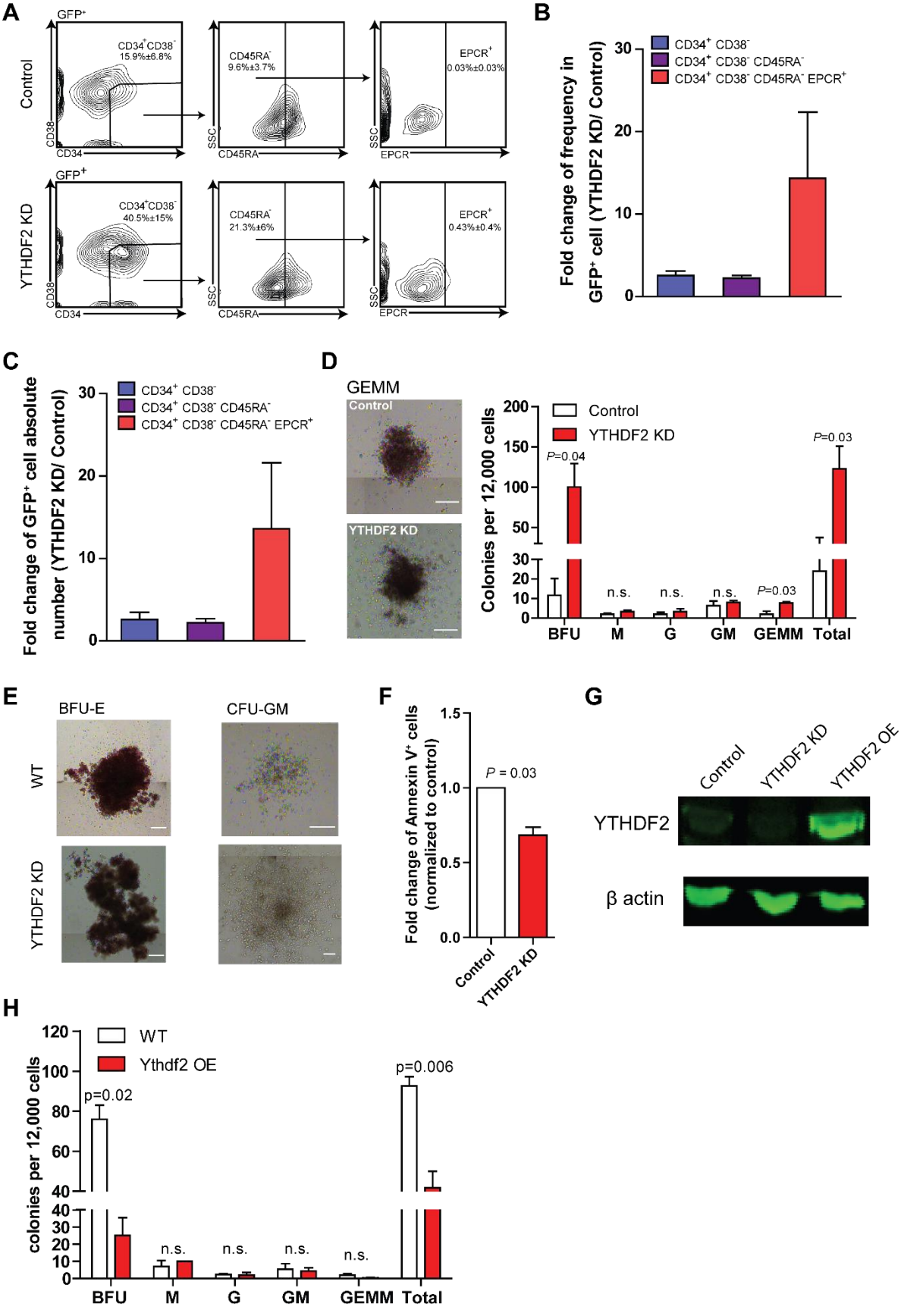
A
GFP+
Control
CD34+CD38-
15.9%±6.8%
CD45RA-
9.6%±3.7%
EPCR+
0.03%±0.03%
YTHDF2 KD
CD34+CD38-
40.5%±15%
CD45RA-
21.3%±6%
EPCR+
0.43%±0.4%
CD38
CD34
SSC
CD45RA
EPCR
B
Fold change of frequency in GFP+ cell (YTHDF2 KD/ Control)
CD34+ CD38-
CD34+ CD38- CD45RA-
CD34+ CD38- CD45RA- EPCR+
C
Fold change of GFP+ cell absolute number (YTHDF2 KD/ Control)
D
GEMM
Control
YTHDF2 KD
Colonies per 12,000 cells
P=0.04
P=0.03
n.s.
BFU
M
G
GM
GEMM
Total
E
BFU-E
CFU-GM
WT
YTHDF2 KD
F
Fold change of Annexin V+ cells (normalized to control)
P = 0.03
G
Control
YTHDF2 KD
YTHDF2 OE
YTHDF2
β actin
H
WT
Ythdf2 OE
colonies per 12,000 cells
p=0.02
p=0.006

Figure 7.1 *YTHDF2* KD facilitates expansion of human cord blood HSCs ex vivo.
(**A**) Representative flow plots of GFP+ CD34+ CD38- CD45RA- EPCR+ HSCs in control and *YTHDF2* KD hUCB cells post 7 days culture. (**B** and **C**) Fold change of frequency (**B**) and absolute number (**C**) of indicated cells in YTHDF2 KD over control cells after 7 days culture. (**D**) CFU output from transduced $CD34^+$ $CD38^-$ hUCB cells and images of CFU the granulocyte-erythrocyte-monocyte-megakaryocytes (GEMMs) (scale bar, 200 μm). (**E**) Images of burst forming unit-erythroid (BFU-E) (left) and colony-forming unit-granulocyte/macrophage (CFU-GM) (right) from 7 days cultured control or YTHDF2 KD hUCB cells (scale bar, 200 μm). Three independent cord blood samples were used, and this was repeated twice for (**A**) to (**E**). (**F**) Apoptosis analysis of $CD34^+$ $CD38^-$ cells in 7-day cultures of transduced $CD34^+$ hUCB cells by Annexin V staining (n = 3 independent CB samples). (**G**) Confirmation of YTHDF2 protein knockdown and overexpression in transduced Hela cells. (**H**) CFU production by YTHDF2 overexpression (OE) and control transduced CD34+ CD38- CB from day 10 cultures (n = 3 independent human samples). Data shown as mean ± SEM. Unpaired t-test. n.s. nonsignificant

7.2 *YTHDF2* KD facilitates expansion of human cord blood functional LT-HSCs

To determine whether *YTHDF2* KD can expand human HSCs *in vivo,* we performed LDA by transplanting GFP^+ cells sorted from hUCB $CD34^+$ cells infected with control and *YTHDF2* shRNA at day 4 post infection (Figure 7.2A). For hUCB HSC primary LDA assay, in brief, $CD34^+$ cells were enriched as described above and transduced with human *YTHDF2* shRNA or control shRNA at 50 MOI. Media were changed at 24 hours post infection. Equal number of GFP^+ cells were sorted out from control or *YTHDF2* KD cells on 3 days post infection and cultured overnight. Three doses, 50K, 20K and 10K, of sorted GFP^+ cells were transplanted into sublethally irradiated (3.25Gy) NSG mice, respectively. At 10 weeks post transplantation, we analyzed BM cells from recipient NOD/SCID *Il2rg*^{null} (NSG) mice and measured the functional HSC frequency after *in vivo* expansion. Notably, compared to control group, recipients of *YTHDF2* KD cells displayed a 9-fold increase in human hematopoietic cell ($hCD45^+$ GFP^+) engraftment in BM (Figure 7.2B and C, Table 7.1). *YTHDF2* KD significantly increased the percentage of myeloid, megakaryocyte and erythrocyte in the BM of primary recipients without changes in the proportions of each lineage (Figure 7.2E-G). Accordingly, I

found that the HSC frequency in *YTHDF2* KD cells was increased 4.4-fold relative to that in control cells (Figure 7.2D).

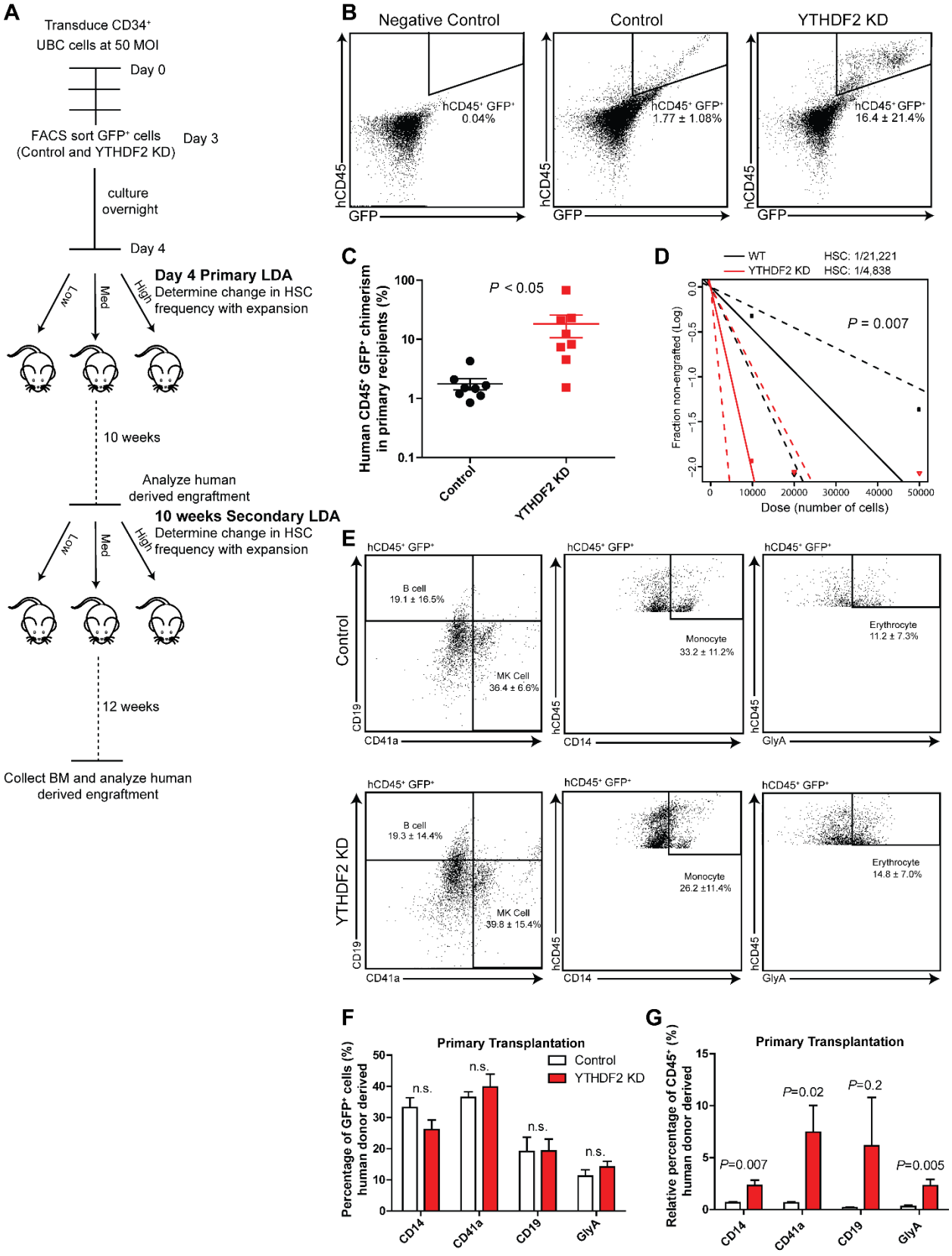
A
Transduce CD34+
UBC cells at 50 MOI
Day 0
FACS sort GFP+ cells
(Control and YTHDF2 KD)
Day 3
culture
overnight
Day 4
Day 4 Primary LDA
Determine change in HSC
frequency with expansion
Low
Med
High
10 weeks
Analyze human
derived engraftment
10 weeks Secondary LDA
Determine change in HSC
frequency with expansion
12 weeks
Collect BM and analyze human
derived engraftment
B
Negative Control
Control
YTHDF2 KD
hCD45+ GFP+
0.04%
1.77 ± 1.08%
16.4 ± 21.4%
hCD45
GFP
C
Human CD45+ GFP+ chimerism
in primary recipients (%)
P < 0.05
Control
YTHDF2 KD
D
WT HSC: 1/21,221
YTHDF2 KD HSC: 1/4,838
P = 0.007
Fraction non-engrafted (Log)
Dose (number of cells)
E
Control
YTHDF2 KD
B cell
19.1 ± 16.5%
19.3 ± 14.4%
MK Cell
36.4 ± 6.6%
39.8 ± 15.4%
Monocyte
33.2 ± 11.2%
26.2 ±11.4%
Erythrocyte
11.2 ± 7.3%
14.8 ± 7.0%
CD19
CD41a
CD14
GlyA
F
Primary Transplantation
Control
YTHDF2 KD
Percentage of GFP+ cells (%)
human donor derived
n.s.
G
Primary Transplantation
Relative percentage of CD45+ (%)
human donor derived
P=0.007
P=0.02
P=0.2
P=0.005

Figure 7.2 *YTHDF2* KD hUCB HSCs expand in primary transplanted recipient mice. (**A**) Experimental scheme for measuring frequency of HSCs after in vivo expansion. (**B**) Representative flow plots of $hCD45^+$ GFP^+ reconstitution from primary recipient mice receiving the highest two cell doses. hCD45, human CD45 (**C**) $hCD45^+$ GFP^+ engraftment in BM from the primary recipient mice that received the highest two doses (n = 8). (**D**) HSC frequency determined by primary LDA. Dashed lines indicate 95% confidence intervals. (**E**) Representative flow plots of $hCD45^+$ GFP^+ monocyte, megakaryocyte (MK cell), B cell and erythrocyte in primary NSG recipient BM. (**F** and **G**) Percentage of lineage cells in $hCD45^+$ GFP^+ (**F**) and in total $CD45^+$ (**G**) BM cells from primary NSG recipients at 10 weeks post transplantation (n = 13-15). Data shown as mean ± s.e.m. Unpaired t-test. n.s., nonsignificant.

Next, I confirmed the long-term capability of *YTHDF2* KD hUCB HSCs to be reconstituted and to undergo self-renewal; 12 weeks after transplantation of BM from primary recipients into sublethally irradiated secondary NSG recipient mice, human hematopoietic cell chimerism in BM were higher in the *YTHDF2* KD group, as compared to that in the control group (Figure 7.3A, B and D). CRUs from *YTHDF2* KD cells revealed an 8-fold increase relative to that in control cells (Figure 7.3C and Table 7.1). These data demonstrate that *YTHDF2* KD remarkably facilitates the expansion of both phenotypic and long-term functional hUCB HSCs *in vivo*.

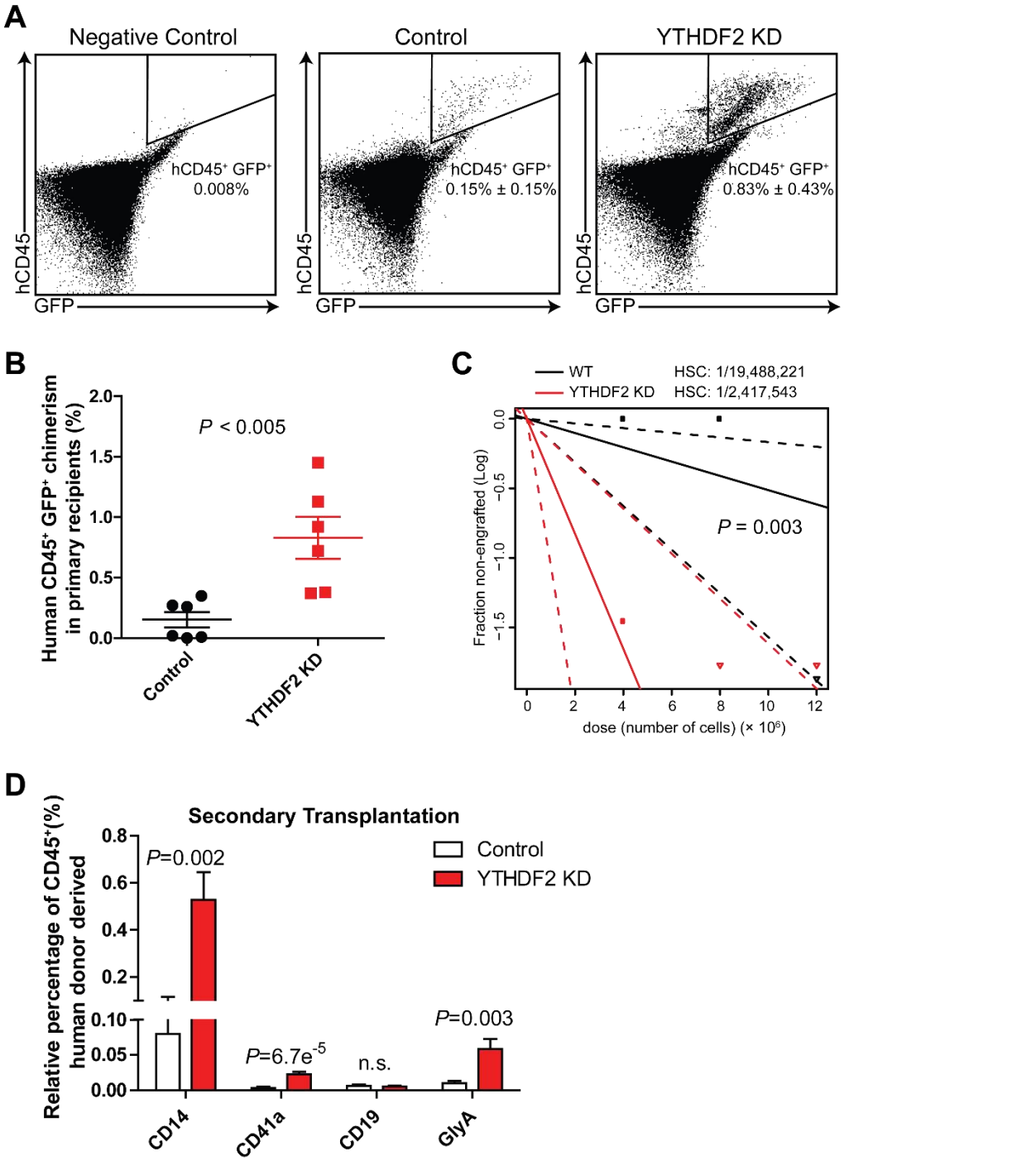

Figure 7.3 *YTHDF2* KD HSCs further expand in secondary transplanted recipient mice. (**A**) Representative flow plots of hCD45$^+$ GFP$^+$ reconstitution from secondary recipient mice receiving the highest two cell doses. (**B**) hCD45$^+$ GFP$^+$ engraftment in BM from secondary recipient mice that received the highest two doses (n = 6). (**C**) HSC frequency determined by secondary LDA. Dashed lines indicate 95% confidence intervals. (**D**) Summary of human donor derived lineage chimerisms in total CD45$^+$ BM cells from secondary NSG recipients at 12 weeks post transplantation (n = 6). Data shown as mean ± s.e.m. Unpaired t-test. n.s., nonsignificant.

Chapter 8 : Discussion

Sections of chapters 2-8 have previously been published and are adapted and reprinted here with permission, alongside new, never-before published material. Li, Z., Qian, P., Shao, W. Shi, H., He, X.C., Gogol, M.,. . . Li, L. (2018). Suppression of m(6)A reader Ythdf2 promotes hematopoietic stem cell expansion. *Cell Res*, 28(9), 904-917.

Although recent studies shed light on the biological functions of mRNA m^6A modifications (Alarcon, Goodarzi, et al., 2015; Alarcon, Lee, Goodarzi, Halberg, & Tavazoie, 2015; Bertero et al., 2018; T. Chen et al., 2015; Fustin et al., 2013; Haussmann et al., 2016; Huang et al., 2018; Ivanova et al., 2017; Lence et al., 2016; N. Liu et al., 2015; Pendleton et al., 2017a; Schwartz, Bernstein, et al., 2014; Shi et al., 2017a; Slobodin et al., 2017; Wojtas et al., 2017; Xiao et al., 2016; S. Zhang et al., 2017; Zheng et al., 2013; J. Zhou et al., 2015), our work identifies Ythdf2 as an important regulator of human and mouse HSC self-renewal by coupling the post-transcriptional m^6A modification to the degradation of mRNAs encoding key transcription factors for self-renewal. Repression of Ythdf2 in mouse HSPCs and hUCB HSCs leads to increased expression of multiple key TFs critical for self-renewal, thereby facilitating *ex vivo* expansion of both phenotypic and functional HSCs without noticeable lineage bias and leukemia potential. In addition, stem cell niches, to some extent, may contribute to Ythdf2 suppression-mediated mouse HSC expansion as *Mx1-cre* can be activated in mesenchyme stromal cells (Joseph et al., 2013). It would be intriguing to study the function of *Ythdf2* on MSCs and how repression of Ythdf2 in both HSCs and MSCs may synergistically expand HSCs *in vivo*. Our *ex vivo* expansion of human HSCs showed that suppression of Ythdf2 in HSCs is able to expand HSCs, as seen in this study.

Given the broad and complicated impact of m^6A writer complex *Mettl3* and *Mettl14* on mRNA splicing, translation, and pri-miRNA processing (Alarcon, Lee, et al., 2015; Barbieri et

al., 2017a; N. Liu et al., 2015), *Mettl3* or *Mettl14* depletion results in distinct outcomes in normal stem cells and leukemia. Recent studies have demonstrated that *Mettl3* and *Mettl14* play essential roles in leukemia development and leukemia stem cell maintenance (Barbieri et al., 2017a; Vu et al., 2017a; Weng et al., 2018). In contrast, Ythdf2 is mainly involved in m^6A-mediated mRNA decay by which stem cells are shown to be influenced (Batista et al., 2014; Shlush et al., 2014; Yoon et al., 2017a; C. Zhang et al., 2017a). Therefore, manipulating *Ythdf2* would extend the half-life of specific m^6A-marked mRNAs encoding TFs critical for stem cell self-renewal without affecting other aspects of mRNA processing. In line with this, our data clearly show that *Ythdf2* depletion in HSCs neither skews the lineage commitment nor induces hematological malignancies, reducing the risk of leukemogenesis with expanded HSCs. Furthermore, stem cell self-renewal is a complex process involving promoting cell division, inhibiting apoptosis, preventing differentiation, and stemness retention (S. He, Nakada, & Morrison, 2009). Our observation that *Ythdf2*-deficient HSCs exhibited lower apoptotic rates accounts for at least one aspect of stem cell self-renewal mechanism. We believe that stemness retention is another mechanism underlying the Ythdf2-mediated HSC expansion.

A major limitation in using hUCB HSC transplantation is the insufficient number of HSCs in one hUCB unit. Albeit previous studies have revealed that Dlk1, SR1, Musashi2 and UM171 can expand hUCB HSCs by targeting Notch, AHR signaling or other unknown pathway (Boitano et al., 2010; Chou, Flygare, & Lodish, 2013; Fares et al., 2014; Rentas et al., 2016), our work provides a novel and potent way to target multiple key TFs critical for HSC self-renewal and to enhance the expansion of HSCs. Reducing Ythdf2 level and function during *in vitro* culture via small chemicals or AAV-mediated KD allows the Ythdf2 level and function to restore after transplantation *in vivo*, and thus not affect normal HSC maintenance and function in human

patients. Furthermore, we envision that combining our method with previous ones may facilitate the expansion of not only human HSCs, but also other stem cells, rendering a potential approach for future stem cell-based therapies.

References

Adams, J. M., & Cory, S. (1975). Modified nucleosides and bizarre 5'-termini in mouse myeloma mRNA. *Nature, 255*(5503), 28-33.

Alarcon, C. R., Goodarzi, H., Lee, H., Liu, X., Tavazoie, S., & Tavazoie, S. F. (2015). HNRNPA2B1 Is a Mediator of m(6)A-Dependent Nuclear RNA Processing Events. *Cell, 162*(6), 1299-1308. doi: 10.1016/j.cell.2015.08.011

Alarcon, C. R., Lee, H., Goodarzi, H., Halberg, N., & Tavazoie, S. F. (2015). N6-methyladenosine marks primary microRNAs for processing. *Nature, 519*(7544), 482-485. doi: 10.1038/nature14281

Amsellem, S., Pflumio, F., Bardinet, D., Izac, B., Charneau, P., Romeo, P. H., . . . Fichelson, S. (2003). Ex vivo expansion of human hematopoietic stem cells by direct delivery of the HOXB4 homeoprotein. *Nat Med, 9*(11), 1423-1427. doi: 10.1038/nm953

Antonchuk, J., Sauvageau, G., & Humphries, R. K. (2002). HOXB4-induced expansion of adult hematopoietic stem cells ex vivo. *Cell, 109*(1), 39-45.

Armitage, J. O. (1994). Bone marrow transplantation. *N Engl J Med, 330*(12), 827-838. doi: 10.1056/NEJM199403243301206

Bailey, A. S., Batista, P. J., Gold, R. S., Chen, Y. G., de Rooij, D. G., Chang, H. Y., & Fuller, M. T. (2017). The conserved RNA helicase YTHDC2 regulates the transition from proliferation to differentiation in the germline. *Elife, 6*. doi: 10.7554/eLife.26116

Barbieri, I., Tzelepis, K., Pandolfini, L., Shi, J., Millan-Zambrano, G., Robson, S. C., . . . Kouzarides, T. (2017a). Promoter-bound METTL3 maintains myeloid leukaemia by m(6)A-dependent translation control. *Nature*. doi: 10.1038/nature24678

Barbieri, I., Tzelepis, K., Pandolfini, L., Shi, J., Millan-Zambrano, G., Robson, S. C., . . . Kouzarides, T. (2017b). Promoter-bound METTL3 maintains myeloid leukaemia by m(6)A-dependent translation control. *Nature, 552*(7683), 126-131. doi: 10.1038/nature24678

Batista, P. J., Molinie, B., Wang, J., Qu, K., Zhang, J., Li, L., . . . Chang, H. Y. (2014). m(6)A RNA modification controls cell fate transition in mammalian embryonic stem cells. *Cell Stem Cell, 15*(6), 707-719. doi: 10.1016/j.stem.2014.09.019

Bertero, A., Brown, S., Madrigal, P., Osnato, A., Ortmann, D., Yiangou, L., . . . Vallier, L. (2018). The SMAD2/3 interactome reveals that TGFbeta controls m(6)A mRNA methylation in pluripotency. *Nature*. doi: 10.1038/nature25784

Bhardwaj, G., Murdoch, B., Wu, D., Baker, D. P., Williams, K. P., Chadwick, K., . . . Bhatia, M. (2001). Sonic hedgehog induces the proliferation of primitive human hematopoietic cells via BMP regulation. *Nat Immunol, 2*(2), 172-180. doi: 10.1038/84282

Boitano, A. E., Wang, J., Romeo, R., Bouchez, L. C., Parker, A. E., Sutton, S. E., . . . Cooke, M. P. (2010). Aryl hydrocarbon receptor antagonists promote the expansion of human hematopoietic stem cells. *Science, 329*(5997), 1345-1348. doi: 10.1126/science.1191536

Bokar, J. A., Rath-Shambaugh, M. E., Ludwiczak, R., Narayan, P., & Rottman, F. (1994). Characterization and partial purification of mRNA N6-adenosine methyltransferase from HeLa cell nuclei. Internal mRNA methylation requires a multisubunit complex. *J Biol Chem, 269*(26), 17697-17704.

Bokar, J. A., Shambaugh, M. E., Polayes, D., Matera, A. G., & Rottman, F. M. (1997). Purification and cDNA cloning of the AdoMet-binding subunit of the human mRNA (N6-adenosine)-methyltransferase. *RNA, 3*(11), 1233-1247.

Bowman, R. L., Busque, L., & Levine, R. L. (2018). Clonal Hematopoiesis and Evolution to Hematopoietic Malignancies. *Cell Stem Cell, 22*(2), 157-170. doi: 10.1016/j.stem.2018.01.011

Bruns, I., Lucas, D., Pinho, S., Ahmed, J., Lambert, M. P., Kunisaki, Y., . . . Frenette, P. S. (2014). Megakaryocytes regulate hematopoietic stem cell quiescence through CXCL4 secretion. *Nat Med, 20*(11), 1315-1320. doi: 10.1038/nm.3707

Butko, E., Pouget, C., & Traver, D. (2016). Complex regulation of HSC emergence by the Notch signaling pathway. *Dev Biol, 409*(1), 129-138. doi: 10.1016/j.ydbio.2015.11.008

Cabezas-Wallscheid, N., Buettner, F., Sommerkamp, P., Klimmeck, D., Ladel, L., Thalheimer, F. B., . . . Trumpp, A. (2017). Vitamin A-Retinoic Acid Signaling Regulates Hematopoietic Stem Cell Dormancy. *Cell, 169*(5), 807-823 e819. doi: 10.1016/j.cell.2017.04.018

Cai, X., Gaudet, J. J., Mangan, J. K., Chen, M. J., De Obaldia, M. E., Oo, Z., . . . Speck, N. A. (2011). Runx1 loss minimally impacts long-term hematopoietic stem cells. *PLoS One, 6*(12), e28430. doi: 10.1371/journal.pone.0028430

Calvi, L. M., Adams, G. B., Weibrecht, K. W., Weber, J. M., Olson, D. P., Knight, M. C., . . . Scadden, D. T. (2003). Osteoblastic cells regulate the haematopoietic stem cell niche. *Nature, 425*(6960), 841-846. doi: 10.1038/nature02040

Cantara, W. A., Crain, P. F., Rozenski, J., McCloskey, J. A., Harris, K. A., Zhang, X., . . . Agris, P. F. (2011). The RNA Modification Database, RNAMDB: 2011 update. *Nucleic Acids Res, 39*(Database issue), D195-201. doi: 10.1093/nar/gkq1028

Challen, G. A., Sun, D., Jeong, M., Luo, M., Jelinek, J., Berg, J. S., . . . Goodell, M. A. (2011). Dnmt3a is essential for hematopoietic stem cell differentiation. *Nat Genet, 44*(1), 23-31. doi: 10.1038/ng.1009

Chen, M. J., Yokomizo, T., Zeigler, B. M., Dzierzak, E., & Speck, N. A. (2009). Runx1 is required for the endothelial to haematopoietic cell transition but not thereafter. *Nature, 457*(7231), 887-891. doi: 10.1038/nature07619

Chen, T., Hao, Y. J., Zhang, Y., Li, M. M., Wang, M., Han, W., . . . Zhou, Q. (2015). m(6)A RNA methylation is regulated by microRNAs and promotes reprogramming to pluripotency. *Cell Stem Cell, 16*(3), 289-301. doi: 10.1016/j.stem.2015.01.016

Chou, S., Flygare, J., & Lodish, H. F. (2013). Fetal hepatic progenitors support long-term expansion of hematopoietic stem cells. *Exp Hematol, 41*(5), 479-490 e474. doi: 10.1016/j.exphem.2013.02.003

Chow, A., Lucas, D., Hidalgo, A., Mendez-Ferrer, S., Hashimoto, D., Scheiermann, C., . . . Frenette, P. S. (2011). Bone marrow CD169+ macrophages promote the retention of hematopoietic stem and progenitor cells in the mesenchymal stem cell niche. *J Exp Med, 208*(2), 261-271. doi: 10.1084/jem.20101688

Christopher, M. J., Rao, M., Liu, F., Woloszynek, J. R., & Link, D. C. (2011). Expression of the G-CSF receptor in monocytic cells is sufficient to mediate hematopoietic progenitor mobilization by G-CSF in mice. *J Exp Med, 208*(2), 251-260. doi: 10.1084/jem.20101700

Cobas, M., Wilson, A., Ernst, B., Mancini, S. J., MacDonald, H. R., Kemler, R., & Radtke, F. (2004). Beta-catenin is dispensable for hematopoiesis and lymphopoiesis. *J Exp Med, 199*(2), 221-229. doi: 10.1084/jem.20031615

Cohn, W. E. (1960). Pseudouridine, a carbon-carbon linked ribonucleoside in ribonucleic acids: isolation, structure, and chemical characteristics. *J Biol Chem, 235*, 1488-1498.

Copley, M. R., Beer, P. A., & Eaves, C. J. (2012). Hematopoietic stem cell heterogeneity takes center stage. *Cell Stem Cell, 10*(6), 690-697. doi: 10.1016/j.stem.2012.05.006

de Haan, G., Weersing, E., Dontje, B., van Os, R., Bystrykh, L. V., Vellenga, E., & Miller, G. (2003). In vitro generation of long-term repopulating hematopoietic stem cells by fibroblast growth factor-1. *Dev Cell, 4*(2), 241-251.

de Pater, E., Kaimakis, P., Vink, C. S., Yokomizo, T., Yamada-Inagawa, T., van der Linden, R., . . . Dzierzak, E. (2013). Gata2 is required for HSC generation and survival. *J Exp Med, 210*(13), 2843-2850. doi: 10.1084/jem.20130751

Degos, L., & Wang, Z. Y. (2001). All trans retinoic acid in acute promyelocytic leukemia. *Oncogene, 20*(49), 7140-7145. doi: 10.1038/sj.onc.1204763

Delaney, C., Varnum-Finney, B., Aoyama, K., Brashem-Stein, C., & Bernstein, I. D. (2005). Dose-dependent effects of the Notch ligand Delta1 on ex vivo differentiation and in vivo marrow repopulating ability of cord blood cells. *Blood, 106*(8), 2693-2699. doi: 10.1182/blood-2005-03-1131

Dendrou, C. A., Petersen, J., Rossjohn, J., & Fugger, L. (2018). HLA variation and disease. *Nat Rev Immunol, 18*(5), 325-339. doi: 10.1038/nri.2017.143

Desrosiers, R., Friderici, K., & Rottman, F. (1974). Identification of methylated nucleosides in messenger RNA from Novikoff hepatoma cells. *Proc Natl Acad Sci U S A, 71*(10), 3971-3975.

Ding, L., & Morrison, S. J. (2013). Haematopoietic stem cells and early lymphoid progenitors occupy distinct bone marrow niches. *Nature, 495*(7440), 231-235. doi: 10.1038/nature11885

Dominissini, D., Moshitch-Moshkovitz, S., Schwartz, S., Salmon-Divon, M., Ungar, L., Osenberg, S., . . . Rechavi, G. (2012). Topology of the human and mouse m6A RNA methylomes revealed by m6A-seq. *Nature, 485*(7397), 201-206. doi: 10.1038/nature11112

Ebina, W., & Rossi, D. J. (2015). Transcription factor-mediated reprogramming toward hematopoietic stem cells. *EMBO J, 34*(6), 694-709. doi: 10.15252/embj.201490804

Erlich, H. A., Opelz, G., & Hansen, J. (2001). HLA DNA typing and transplantation. *Immunity, 14*(4), 347-356.

Fares, I., Chagraoui, J., Gareau, Y., Gingras, S., Ruel, R., Mayotte, N., . . . Sauvageau, G. (2014). Cord blood expansion. Pyrimidoindole derivatives are agonists of human hematopoietic stem cell self-renewal. *Science, 345*(6203), 1509-1512. doi: 10.1126/science.1256337

Furuichi, Y., Morgan, M., Shatkin, A. J., Jelinek, W., Salditt-Georgieff, M., & Darnell, J. E. (1975). Methylated, blocked 5 termini in HeLa cell mRNA. *Proc Natl Acad Sci U S A, 72*(5), 1904-1908.

Fustin, J. M., Doi, M., Yamaguchi, Y., Hida, H., Nishimura, S., Yoshida, M., . . . Okamura, H. (2013). RNA-methylation-dependent RNA processing controls the speed of the circadian clock. *Cell, 155*(4), 793-806. doi: 10.1016/j.cell.2013.10.026

Galan-Caridad, J. M., Harel, S., Arenzana, T. L., Hou, Z. E., Doetsch, F. K., Mirny, L. A., & Reizis, B. (2007). Zfx controls the self-renewal of embryonic and hematopoietic stem cells. *Cell, 129*(2), 345-357. doi: 10.1016/j.cell.2007.03.014

Geula, S., Moshitch-Moshkovitz, S., Dominissini, D., Mansour, A. A., Kol, N., Salmon-Divon, M., . . . Hanna, J. H. (2015). Stem cells. m6A mRNA methylation facilitates resolution of naive pluripotency toward differentiation. *Science, 347*(6225), 1002-1006. doi: 10.1126/science.1261417

Ghiaur, G., Yegnasubramanian, S., Perkins, B., Gucwa, J. L., Gerber, J. M., & Jones, R. J. (2013). Regulation of human hematopoietic stem cell self-renewal by the microenvironment's control of retinoic acid signaling. *Proc Natl Acad Sci U S A, 110*(40), 16121-16126. doi: 10.1073/pnas.1305937110

Gratwohl, A., Pasquini, M. C., Aljurf, M., Atsuta, Y., Baldomero, H., Foeken, L., . . . Marrow, T. (2015). One million haemopoietic stem-cell transplants: a retrospective observational study. *Lancet Haematol, 2*(3), e91-100. doi: 10.1016/S2352-3026(15)00028-9

Gu, J., Patton, J. R., Shimba, S., & Reddy, R. (1996). Localization of modified nucleotides in Schizosaccharomyces pombe spliceosomal small nuclear RNAs: modified nucleotides are clustered in functionally important regions. *RNA, 2*(9), 909-918.

Guiu, J., Shimizu, R., D'Altri, T., Fraser, S. T., Hatakeyama, J., Bresnick, E. H., . . . Bigas, A. (2013). Hes repressors are essential regulators of hematopoietic stem cell development downstream of Notch signaling. *J Exp Med, 210*(1), 71-84. doi: 10.1084/jem.20120993

Gutierrez-Vazquez, C., & Quintana, F. J. (2018). Regulation of the Immune Response by the Aryl Hydrocarbon Receptor. *Immunity, 48*(1), 19-33. doi: 10.1016/j.immuni.2017.12.012

Haas, S., Trumpp, A., & Milsom, M. D. (2018). Causes and Consequences of Hematopoietic Stem Cell Heterogeneity. *Cell Stem Cell, 22*(5), 627-638. doi: 10.1016/j.stem.2018.04.003

Hanahan, D., & Weinberg, R. A. (2011). Hallmarks of cancer: the next generation. *Cell, 144*(5), 646-674. doi: 10.1016/j.cell.2011.02.013

Haussmann, I. U., Bodi, Z., Sanchez-Moran, E., Mongan, N. P., Archer, N., Fray, R. G., & Soller, M. (2016). m6A potentiates Sxl alternative pre-mRNA splicing for robust Drosophila sex determination. *Nature, 540*(7632), 301-304. doi: 10.1038/nature20577

He, S., Nakada, D., & Morrison, S. J. (2009). Mechanisms of stem cell self-renewal. *Annu Rev Cell Dev Biol, 25*, 377-406. doi: 10.1146/annurev.cellbio.042308.113248

He, X. C., Li, Z., Sugimura, R., Ross, J., Zhao, M., & Li, L. (2014). Homing and migration assays of hematopoietic stem/progenitor cells. *Methods Mol Biol, 1185*, 279-284. doi: 10.1007/978-1-4939-1133-2_19

Hidalgo, I., Herrera-Merchan, A., Ligos, J. M., Carramolino, L., Nunez, J., Martinez, F., . . . Gonzalez, S. (2012). Ezh1 is required for hematopoietic stem cell maintenance and prevents senescence-like cell cycle arrest. *Cell Stem Cell, 11*(5), 649-662. doi: 10.1016/j.stem.2012.08.001

Hoang, T., Lambert, J. A., & Martin, R. (2016). SCL/TAL1 in Hematopoiesis and Cellular Reprogramming. *Curr Top Dev Biol, 118*, 163-204. doi: 10.1016/bs.ctdb.2016.01.004

Hock, H., Meade, E., Medeiros, S., Schindler, J. W., Valk, P. J., Fujiwara, Y., & Orkin, S. H. (2004). Tel/Etv6 is an essential and selective regulator of adult hematopoietic stem cell survival. *Genes Dev, 18*(19), 2336-2341. doi: 10.1101/gad.1239604

Horowitz, S., Horowitz, A., Nilsen, T. W., Munns, T. W., & Rottman, F. M. (1984). Mapping of N6-methyladenosine residues in bovine prolactin mRNA. *Proc Natl Acad Sci U S A, 81*(18), 5667-5671.

Hsu, P. J., Zhu, Y., Ma, H., Guo, Y., Shi, X., Liu, Y., . . . He, C. (2017). Ythdc2 is an N(6)-methyladenosine binding protein that regulates mammalian spermatogenesis. *Cell Res, 27*(9), 1115-1127. doi: 10.1038/cr.2017.99

Hsu, Y. C., & Fuchs, E. (2012). A family business: stem cell progeny join the niche to regulate homeostasis. *Nat Rev Mol Cell Biol, 13*(2), 103-114. doi: 10.1038/nrm3272

Hu, Y., & Smyth, G. K. (2009). ELDA: extreme limiting dilution analysis for comparing depleted and enriched populations in stem cell and other assays. *J Immunol Methods, 347*(1-2), 70-78. doi: 10.1016/j.jim.2009.06.008

Huang, H., Weng, H., Sun, W., Qin, X., Shi, H., Wu, H., . . . Chen, J. (2018). Recognition of RNA N(6)-methyladenosine by IGF2BP proteins enhances mRNA stability and translation. *Nat Cell Biol, 20*(3), 285-295. doi: 10.1038/s41556-018-0045-z

Itkin, T., Ludin, A., Gradus, B., Gur-Cohen, S., Kalinkovich, A., Schajnovitz, A., . . . Lapidot, T. (2012). FGF-2 expands murine hematopoietic stem and progenitor cells via proliferation of stromal cells, c-Kit activation, and CXCL12 down-regulation. *Blood, 120*(9), 1843-1855. doi: 10.1182/blood-2011-11-394692

Ivanova, I., Much, C., Di Giacomo, M., Azzi, C., Morgan, M., Moreira, P. N., . . . O'Carroll, D. (2017). The RNA m6A Reader YTHDF2 Is Essential for the Post-transcriptional Regulation of the Maternal Transcriptome and Oocyte Competence. *Mol Cell, 67*(6), 1059-1067 e1054. doi: 10.1016/j.molcel.2017.08.003

Iwama, A., Oguro, H., Negishi, M., Kato, Y., Morita, Y., Tsukui, H., . . . Nakauchi, H. (2004). Enhanced self-renewal of hematopoietic stem cells mediated by the polycomb gene product Bmi-1. *Immunity, 21*(6), 843-851. doi: 10.1016/j.immuni.2004.11.004

Jaroscak, J., Goltry, K., Smith, A., Waters-Pick, B., Martin, P. L., Driscoll, T. A., . . . Kurtzberg, J. (2003). Augmentation of umbilical cord blood (UCB) transplantation with ex vivo-expanded UCB cells: results of a phase 1 trial using the AastromReplicell System. *Blood, 101*(12), 5061-5067. doi: 10.1182/blood-2001-12-0290

Jeannet, G., Scheller, M., Scarpellino, L., Duboux, S., Gardiol, N., Back, J., . . . Held, W. (2008). Long-term, multilineage hematopoiesis occurs in the combined absence of beta-catenin and gamma-catenin. *Blood, 111*(1), 142-149. doi: 10.1182/blood-2007-07-102558

Jeong, M., Park, H. J., Celik, H., Ostrander, E. L., Reyes, J. M., Guzman, A., . . . Challen, G. A. (2018). Loss of Dnmt3a Immortalizes Hematopoietic Stem Cells In Vivo. *Cell Rep, 23*(1), 1-10. doi: 10.1016/j.celrep.2018.03.025

Jia, G., Fu, Y., Zhao, X., Dai, Q., Zheng, G., Yang, Y., . . . He, C. (2011). N6-methyladenosine in nuclear RNA is a major substrate of the obesity-associated FTO. *Nat Chem Biol, 7*(12), 885-887. doi: 10.1038/nchembio.687

Joseph, C., Quach, J. M., Walkley, C. R., Lane, S. W., Lo Celso, C., & Purton, L. E. (2013). Deciphering hematopoietic stem cells in their niches: a critical appraisal of genetic models, lineage tracing, and imaging strategies. *Cell Stem Cell, 13*(5), 520-533. doi: 10.1016/j.stem.2013.10.010

Jude, C. D., Gaudet, J. J., Speck, N. A., & Ernst, P. (2008). Leukemia and hematopoietic stem cells: balancing proliferation and quiescence. *Cell Cycle, 7*(5), 586-591. doi: 10.4161/cc.7.5.5549

Kamminga, L. M., Bystrykh, L. V., de Boer, A., Houwer, S., Douma, J., Weersing, E., . . . de Haan, G. (2006). The Polycomb group gene Ezh2 prevents hematopoietic stem cell exhaustion. *Blood, 107*(5), 2170-2179. doi: 10.1182/blood-2005-09-3585

Kanakry, C. G., Fuchs, E. J., & Luznik, L. (2016). Modern approaches to HLA-haploidentical blood or marrow transplantation. *Nat Rev Clin Oncol, 13*(1), 10-24. doi: 10.1038/nrclinonc.2015.128

Kato, Y., Iwama, A., Tadokoro, Y., Shimoda, K., Minoguchi, M., Akira, S., . . . Nakauchi, H. (2005). Selective activation of STAT5 unveils its role in stem cell self-renewal in normal and leukemic hematopoiesis. *J Exp Med, 202*(1), 169-179. doi: 10.1084/jem.20042541

Ke, S., Alemu, E. A., Mertens, C., Gantman, E. C., Fak, J. J., Mele, A., . . . Darnell, R. B. (2015). A majority of m6A residues are in the last exons, allowing the potential for 3' UTR regulation. *Genes Dev, 29*(19), 2037-2053. doi: 10.1101/gad.269415.115

Kedersha, N., & Anderson, P. (2007). Mammalian stress granules and processing bodies. *Methods Enzymol, 431*, 61-81. doi: 10.1016/S0076-6879(07)31005-7

Kim, C. H. (2010). Homeostatic and pathogenic extramedullary hematopoiesis. *J Blood Med, 1*, 13-19. doi: 10.2147/JBM.S7224

Koch, U., Wilson, A., Cobas, M., Kemler, R., Macdonald, H. R., & Radtke, F. (2008). Simultaneous loss of beta- and gamma-catenin does not perturb hematopoiesis or lymphopoiesis. *Blood, 111*(1), 160-164. doi: 10.1182/blood-2007-07-099754

Kode, A., Manavalan, J. S., Mosialou, I., Bhagat, G., Rathinam, C. V., Luo, N., . . . Kousteni, S. (2014). Leukaemogenesis induced by an activating beta-catenin mutation in osteoblasts. *Nature, 506*(7487), 240-244. doi: 10.1038/nature12883

Kohli, L., & Passegue, E. (2014). Surviving change: the metabolic journey of hematopoietic stem cells. *Trends Cell Biol, 24*(8), 479-487. doi: 10.1016/j.tcb.2014.04.001

Kuhn, R., Schwenk, F., Aguet, M., & Rajewsky, K. (1995). Inducible gene targeting in mice. *Science, 269*(5229), 1427-1429.

Lacombe, J., Herblot, S., Rojas-Sutterlin, S., Haman, A., Barakat, S., Iscove, N. N., . . . Hoang, T. (2010). Scl regulates the quiescence and the long-term competence of hematopoietic stem cells. *Blood, 115*(4), 792-803. doi: 10.1182/blood-2009-01-201384

Lavi, S., & Shatkin, A. J. (1975). Methylated simian virus 40-specific RNA from nuclei and cytoplasm of infected BSC-1 cells. *Proc Natl Acad Sci U S A, 72*(6), 2012-2016.

Lee, J. T. (2009). Lessons from X-chromosome inactivation: long ncRNA as guides and tethers to the epigenome. *Genes Dev, 23*(16), 1831-1842. doi: 10.1101/gad.1811209

Lemischka, I. R., Raulet, D. H., & Mulligan, R. C. (1986). Developmental potential and dynamic behavior of hematopoietic stem cells. *Cell, 45*(6), 917-927.

Lence, T., Akhtar, J., Bayer, M., Schmid, K., Spindler, L., Ho, C. H., . . . Roignant, J. Y. (2016). m6A modulates neuronal functions and sex determination in Drosophila. *Nature, 540*(7632), 242-247. doi: 10.1038/nature20568

Li, A., Chen, Y. S., Ping, X. L., Yang, X., Xiao, W., Yang, Y., . . . Yang, Y. G. (2017). Cytoplasmic m(6)A reader YTHDF3 promotes mRNA translation. *Cell Res, 27*(3), 444-447. doi: 10.1038/cr.2017.10

Li, H. B., Tong, J., Zhu, S., Batista, P. J., Duffy, E. E., Zhao, J., . . . Flavell, R. A. (2017). m6A mRNA methylation controls T cell homeostasis by targeting the IL-7/STAT5/SOCS pathways. *Nature, 548*(7667), 338-342. doi: 10.1038/nature23450

Li, L., & Clevers, H. (2010). Coexistence of quiescent and active adult stem cells in mammals. *Science, 327*(5965), 542-545. doi: 10.1126/science.1180794

Li, Z., Qian, P., Shao, W. Shi, H., He, X.C., Gogol, M.,. . . Li, L. (2018). Suppression of m(6)A reader Ythdf2 promotes hematopoietic stem cell expansion. *Cell Res*, 28(9), 904-917.

Li, Z., Weng, H., Su, R., Weng, X., Zuo, Z., Li, C., . . . Chen, J. (2017). FTO Plays an Oncogenic Role in Acute Myeloid Leukemia as a N(6)-Methyladenosine RNA Demethylase. *Cancer Cell, 31*(1), 127-141. doi: 10.1016/j.ccell.2016.11.017

Lim, K. C., Hosoya, T., Brandt, W., Ku, C. J., Hosoya-Ohmura, S., Camper, S. A., . . . Engel, J. D. (2012). Conditional Gata2 inactivation results in HSC loss and lymphatic mispatterning. *J Clin Invest, 122*(10), 3705-3717. doi: 10.1172/JCI61619

Ling, K. W., Ottersbach, K., van Hamburg, J. P., Oziemlak, A., Tsai, F. Y., Orkin, S. H., . . . Dzierzak, E. (2004). GATA-2 plays two functionally distinct roles during the ontogeny of hematopoietic stem cells. *J Exp Med, 200*(7), 871-882. doi: 10.1084/jem.20031556

Liu, J., Yue, Y., Han, D., Wang, X., Fu, Y., Zhang, L., . . . He, C. (2014). A METTL3-METTL14 complex mediates mammalian nuclear RNA N6-adenosine methylation. *Nat Chem Biol, 10*(2), 93-95. doi: 10.1038/nchembio.1432

Liu, N., Dai, Q., Zheng, G., He, C., Parisien, M., & Pan, T. (2015). N(6)-methyladenosine-dependent RNA structural switches regulate RNA-protein interactions. *Nature, 518*(7540), 560-564. doi: 10.1038/nature14234

Lopez-Otin, C., Blasco, M. A., Partridge, L., Serrano, M., & Kroemer, G. (2013). The hallmarks of aging. *Cell, 153*(6), 1194-1217. doi: 10.1016/j.cell.2013.05.039

Luis, T. C., Ichii, M., Brugman, M. H., Kincade, P., & Staal, F. J. (2012). Wnt signaling strength regulates normal hematopoiesis and its deregulation is involved in leukemia development. *Leukemia, 26*(3), 414-421. doi: 10.1038/leu.2011.387

Luis, T. C., Naber, B. A., Roozen, P. P., Brugman, M. H., de Haas, E. F., Ghazvini, M., . . . Staal, F. J. (2011). Canonical wnt signaling regulates hematopoiesis in a dosage-dependent fashion. *Cell Stem Cell, 9*(4), 345-356. doi: 10.1016/j.stem.2011.07.017

Lv, J., Zhang, Y., Gao, S., Zhang, C., Chen, Y., Li, W., . . . Liu, F. (2018). Endothelial-specific m(6)A modulates mouse hematopoietic stem and progenitor cell development via Notch signaling. *Cell Res, 28*(2), 249-252. doi: 10.1038/cr.2017.143

Makova, K. D., & Hardison, R. C. (2015). The effects of chromatin organization on variation in mutation rates in the genome. *Nat Rev Genet, 16*(4), 213-223. doi: 10.1038/nrg3890

Mendelson, A., & Frenette, P. S. (2014). Hematopoietic stem cell niche maintenance during homeostasis and regeneration. *Nat Med, 20*(8), 833-846. doi: 10.1038/nm.3647

Mendez-Ferrer, S., Michurina, T. V., Ferraro, F., Mazloom, A. R., Macarthur, B. D., Lira, S. A., . . . Frenette, P. S. (2010). Mesenchymal and haematopoietic stem cells form a unique bone marrow niche. *Nature, 466*(7308), 829-834. doi: 10.1038/nature09262

Meuwissen, H. J., Gatti, R. A., Terasaki, P. I., Hong, R., & Good, R. A. (1969). Treatment of lymphopenic hypogammaglobulinemia and bone-marrow aplasia by transplantation of allogeneic marrow. Crucial role of histocompatiility matching. *N Engl J Med, 281*(13), 691-697. doi: 10.1056/NEJM196909252811302

Meyer, K. D., Saletore, Y., Zumbo, P., Elemento, O., Mason, C. E., & Jaffrey, S. R. (2012). Comprehensive analysis of mRNA methylation reveals enrichment in 3' UTRs and near stop codons. *Cell, 149*(7), 1635-1646. doi: 10.1016/j.cell.2012.05.003

Mikkola, H. K., & Orkin, S. H. (2006). The journey of developing hematopoietic stem cells. *Development, 133*(19), 3733-3744. doi: 10.1242/dev.02568

Miller, C. L., Audet, J., & Eaves, C. J. (2002). Ex vivo expansion of human and murine hematopoietic stem cells. *Methods Mol Med, 63*, 189-208. doi: 10.1385/1-59259-140-X:189

Muller, A. M., Medvinsky, A., Strouboulis, J., Grosveld, F., & Dzierzak, E. (1994). Development of hematopoietic stem cell activity in the mouse embryo. *Immunity, 1*(4), 291-301.

Nakamura-Ishizu, A., Takizawa, H., & Suda, T. (2014). The analysis, roles and regulation of quiescence in hematopoietic stem cells. *Development, 141*(24), 4656-4666. doi: 10.1242/dev.106575

Nikiforow, S., & Ritz, J. (2016). Dramatic Expansion of HSCs: New Possibilities for HSC Transplants? *Cell Stem Cell, 18*(1), 10-12. doi: 10.1016/j.stem.2015.12.011

Ntziachristos, P., Abdel-Wahab, O., & Aifantis, I. (2016). Emerging concepts of epigenetic dysregulation in hematological malignancies. *Nat Immunol, 17*(9), 1016-1024. doi: 10.1038/ni.3517

Orkin, S. H., & Zon, L. I. (2008). Hematopoiesis: an evolving paradigm for stem cell biology. *Cell, 132*(4), 631-644. doi: 10.1016/j.cell.2008.01.025

Patil, D. P., Chen, C. K., Pickering, B. F., Chow, A., Jackson, C., Guttman, M., & Jaffrey, S. R. (2016). m(6)A RNA methylation promotes XIST-mediated transcriptional repression. *Nature, 537*(7620), 369-373. doi: 10.1038/nature19342

Pendleton, K. E., Chen, B., Liu, K., Hunter, O. V., Xie, Y., Tu, B. P., & Conrad, N. K. (2017a). The U6 snRNA m6A Methyltransferase METTL16 Regulates SAM Synthetase Intron Retention. *Cell, 169*(5), 824-835 e814. doi: 10.1016/j.cell.2017.05.003

Pendleton, K. E., Chen, B., Liu, K., Hunter, O. V., Xie, Y., Tu, B. P., & Conrad, N. K. (2017b). The U6 snRNA m(6)A Methyltransferase METTL16 Regulates SAM Synthetase Intron Retention. *Cell, 169*(5), 824-835 e814. doi: 10.1016/j.cell.2017.05.003

Perry, J. M., He, X. C., Sugimura, R., Grindley, J. C., Haug, J. S., Ding, S., & Li, L. (2011). Cooperation between both Wnt/{beta}-catenin and PTEN/PI3K/Akt signaling promotes primitive hematopoietic stem cell self-renewal and expansion. *Genes Dev, 25*(18), 1928-1942. doi: 10.1101/gad.17421911

Ping, X. L., Sun, B. F., Wang, L., Xiao, W., Yang, X., Wang, W. J., . . . Yang, Y. G. (2014). Mammalian WTAP is a regulatory subunit of the RNA N6-methyladenosine methyltransferase. *Cell Res, 24*(2), 177-189. doi: 10.1038/cr.2014.3

Purton, L. E., & Scadden, D. T. (2007). Limiting factors in murine hematopoietic stem cell assays. *Cell Stem Cell, 1*(3), 263-270. doi: 10.1016/j.stem.2007.08.016

Qian, P., De Kumar, B., He, X. C., Nolte, C., Gogol, M., Ahn, Y., . . . Li, L. (2018). Retinoid-Sensitive Epigenetic Regulation of the Hoxb Cluster Maintains Normal Hematopoiesis and Inhibits Leukemogenesis. *Cell Stem Cell, 22*(5), 740-754 e747. doi: 10.1016/j.stem.2018.04.012

Qian, P., He, X. C., Paulson, A., Li, Z., Tao, F., Perry, J. M., . . . Li, L. (2016). The Dlk1-Gtl2 Locus Preserves LT-HSC Function by Inhibiting the PI3K-mTOR Pathway to Restrict Mitochondrial Metabolism. *Cell Stem Cell, 18*(2), 214-228. doi: 10.1016/j.stem.2015.11.001

Raaijmakers, M. H., Mukherjee, S., Guo, S., Zhang, S., Kobayashi, T., Schoonmaker, J. A., . . . Scadden, D. T. (2010). Bone progenitor dysfunction induces myelodysplasia and secondary leukaemia. *Nature, 464*(7290), 852-857. doi: 10.1038/nature08851

Ramalho-Santos, M., & Willenbring, H. (2007). On the origin of the term "stem cell". *Cell Stem Cell, 1*(1), 35-38. doi: 10.1016/j.stem.2007.05.013

Rentas, S., Holzapfel, N., Belew, M. S., Pratt, G., Voisin, V., Wilhelm, B. T., . . . Hope, K. J. (2016). Musashi-2 attenuates AHR signalling to expand human haematopoietic stem cells. *Nature, 532*(7600), 508-511. doi: 10.1038/nature17665

Reynaud, D., Ravet, E., Titeux, M., Mazurier, F., Renia, L., Dubart-Kupperschmitt, A., . . . Pflumio, F. (2005). SCL/TAL1 expression level regulates human hematopoietic stem cell self-renewal and engraftment. *Blood, 106*(7), 2318-2328. doi: 10.1182/blood-2005-02-0557

Rizo, A., Dontje, B., Vellenga, E., de Haan, G., & Schuringa, J. J. (2008). Long-term maintenance of human hematopoietic stem/progenitor cells by expression of BMI1. *Blood, 111*(5), 2621-2630. doi: 10.1182/blood-2007-08-106666

Rosendaal, M., Hodgson, G. S., & Bradley, T. R. (1979). Organization of haemopoietic stem cells: the generation-age hypothesis. *Cell Tissue Kinet, 12*(1), 17-29.

Roundtree, I. A., Luo, G. Z., Zhang, Z., Wang, X., Zhou, T., Cui, Y., . . . He, C. (2017). YTHDC1 mediates nuclear export of N(6)-methyladenosine methylated mRNAs. *Elife, 6*. doi: 10.7554/eLife.31311

Rowe, R. G., Mandelbaum, J., Zon, L. I., & Daley, G. Q. (2016). Engineering Hematopoietic Stem Cells: Lessons from Development. *Cell Stem Cell, 18*(6), 707-720. doi: 10.1016/j.stem.2016.05.016

Sanchez-Aguilera, A., & Mendez-Ferrer, S. (2017). The hematopoietic stem-cell niche in health and leukemia. *Cell Mol Life Sci, 74*(4), 579-590. doi: 10.1007/s00018-016-2306-y

Schiedlmeier, B., Klump, H., Will, E., Arman-Kalcek, G., Li, Z., Wang, Z., . . . Ostertag, W. (2003). High-level ectopic HOXB4 expression confers a profound in vivo competitive growth advantage on human cord blood CD34+ cells, but impairs lymphomyeloid differentiation. *Blood, 101*(5), 1759-1768. doi: 10.1182/blood-2002-03-0767

Schroeder, T. (2010). Hematopoietic stem cell heterogeneity: subtypes, not unpredictable behavior. *Cell Stem Cell, 6*(3), 203-207. doi: 10.1016/j.stem.2010.02.006

Schwartz, S., Agarwala, S. D., Mumbach, M. R., Jovanovic, M., Mertins, P., Shishkin, A., . . . Regev, A. (2013). High-resolution mapping reveals a conserved, widespread, dynamic mRNA methylation program in yeast meiosis. *Cell, 155*(6), 1409-1421. doi: 10.1016/j.cell.2013.10.047

Schwartz, S., Bernstein, D. A., Mumbach, M. R., Jovanovic, M., Herbst, R. H., Leon-Ricardo, B. X., . . . Regev, A. (2014). Transcriptome-wide mapping reveals widespread dynamic-regulated pseudouridylation of ncRNA and mRNA. *Cell, 159*(1), 148-162. doi: 10.1016/j.cell.2014.08.028

Schwartz, S., Mumbach, M. R., Jovanovic, M., Wang, T., Maciag, K., Bushkin, G. G., . . . Regev, A. (2014). Perturbation of m6A writers reveals two distinct classes of mRNA methylation at internal and 5' sites. *Cell Rep, 8*(1), 284-296. doi: 10.1016/j.celrep.2014.05.048

Sergiev, P. V., Serebryakova, M. V., Bogdanov, A. A., & Dontsova, O. A. (2008). The ybiN gene of Escherichia coli encodes adenine-N6 methyltransferase specific for modification of A1618 of 23 S ribosomal RNA, a methylated residue located close to the ribosomal exit tunnel. *J Mol Biol, 375*(1), 291-300. doi: 10.1016/j.jmb.2007.10.051

Sheth, U., & Parker, R. (2003). Decapping and decay of messenger RNA occur in cytoplasmic processing bodies. *Science, 300*(5620), 805-808. doi: 10.1126/science.1082320

Shi, H., Wang, X., Lu, Z., Zhao, B. S., Ma, H., Hsu, P. J., . . . He, C. (2017a). YTHDF3 facilitates translation and decay of N6-methyladenosine-modified RNA. *Cell Res, 27*(3), 315-328. doi: 10.1038/cr.2017.15

Shi, H., Wang, X., Lu, Z., Zhao, B. S., Ma, H., Hsu, P. J., . . . He, C. (2017b). YTHDF3 facilitates translation and decay of N(6)-methyladenosine-modified RNA. *Cell Res, 27*(3), 315-328. doi: 10.1038/cr.2017.15

Shlomchik, W. D. (2007). Graft-versus-host disease. *Nat Rev Immunol, 7*(5), 340-352. doi: 10.1038/nri2000

Shlush, L. I., Zandi, S., Mitchell, A., Chen, W. C., Brandwein, J. M., Gupta, V., . . . Dick, J. E. (2014). Identification of pre-leukaemic haematopoietic stem cells in acute leukaemia. *Nature, 506*(7488), 328-333. doi: 10.1038/nature13038

Simsek, D., Tiu, G. C., Flynn, R. A., Byeon, G. W., Leppek, K., Xu, A. F., . . . Barna, M. (2017). The Mammalian Ribo-interactome Reveals Ribosome Functional Diversity and Heterogeneity. *Cell, 169*(6), 1051-1065 e1018. doi: 10.1016/j.cell.2017.05.022

Slobodin, B., Han, R., Calderone, V., Vrielink, J. A., Loayza-Puch, F., Elkon, R., & Agami, R. (2017). Transcription Impacts the Efficiency of mRNA Translation via Co-transcriptional N6-adenosine Methylation. *Cell, 169*(2), 326-337 e312. doi: 10.1016/j.cell.2017.03.031

Stanulovic, V. S., Cauchy, P., Assi, S. A., & Hoogenkamp, M. (2017). LMO2 is required for TAL1 DNA binding activity and initiation of definitive haematopoiesis at the haemangioblast stage. *Nucleic Acids Res, 45*(17), 9874-9888. doi: 10.1093/nar/gkx573

Sugimura, R., He, X. C., Venkatraman, A., Arai, F., Box, A., Semerad, C., . . . Li, L. (2012). Noncanonical Wnt signaling maintains hematopoietic stem cells in the niche. *Cell, 150*(2), 351-365. doi: 10.1016/j.cell.2012.05.041

Sugiyama, T., Kohara, H., Noda, M., & Nagasawa, T. (2006). Maintenance of the hematopoietic stem cell pool by CXCL12-CXCR4 chemokine signaling in bone marrow stromal cell niches. *Immunity, 25*(6), 977-988. doi: 10.1016/j.immuni.2006.10.016

Thomas, E., Storb, R., Clift, R. A., Fefer, A., Johnson, F. L., Neiman, P. E., . . . Buckner, C. D. (1975). Bone-marrow transplantation (first of two parts). *N Engl J Med, 292*(16), 832-843. doi: 10.1056/NEJM197504172921605

Till, J. E., & Mc, C. E. (1961). A direct measurement of the radiation sensitivity of normal mouse bone marrow cells. *Radiat Res, 14*, 213-222.

Varnum-Finney, B., Brashem-Stein, C., & Bernstein, I. D. (2003). Combined effects of Notch signaling and cytokines induce a multiple log increase in precursors with lymphoid and myeloid reconstituting ability. *Blood, 101*(5), 1784-1789. doi: 10.1182/blood-2002-06-1862

Varnum-Finney, B., Xu, L., Brashem-Stein, C., Nourigat, C., Flowers, D., Bakkour, S., . . . Bernstein, I. D. (2000). Pluripotent, cytokine-dependent, hematopoietic stem cells are immortalized by constitutive Notch1 signaling. *Nat Med, 6*(11), 1278-1281. doi: 10.1038/81390

Vu, L. P., Pickering, B. F., Cheng, Y., Zaccara, S., Nguyen, D., Minuesa, G., . . . Kharas, M. G. (2017a). The N6-methyladenosine (m6A)-forming enzyme METTL3 controls myeloid differentiation of normal hematopoietic and leukemia cells. *Nat Med, 23*, 1369–1376. doi: 10.1038/nm.4416

Vu, L. P., Pickering, B. F., Cheng, Y., Zaccara, S., Nguyen, D., Minuesa, G., . . . Kharas, M. G. (2017b). The N(6)-methyladenosine (m(6)A)-forming enzyme METTL3 controls myeloid differentiation of normal hematopoietic and leukemia cells. *Nat Med, 23*(11), 1369-1376. doi: 10.1038/nm.4416

Wagner, J. E., Barker, J. N., DeFor, T. E., Baker, K. S., Blazar, B. R., Eide, C., . . . Davies, S. M. (2002). Transplantation of unrelated donor umbilical cord blood in 102 patients with malignant and nonmalignant diseases: influence of CD34 cell dose and HLA disparity on treatment-related mortality and survival. *Blood, 100*(5), 1611-1618. doi: 10.1182/blood-2002-01-0294

Walasek, M. A., van Os, R., & de Haan, G. (2012). Hematopoietic stem cell expansion: challenges and opportunities. *Ann N Y Acad Sci, 1266*, 138-150. doi: 10.1111/j.1749-6632.2012.06549.x

Wang, L. D., & Wagers, A. J. (2011). Dynamic niches in the origination and differentiation of haematopoietic stem cells. *Nat Rev Mol Cell Biol, 12*(10), 643-655. doi: 10.1038/nrm3184

Wang, X., Lu, Z., Gomez, A., Hon, G. C., Yue, Y., Han, D., . . . He, C. (2014). N6-methyladenosine-dependent regulation of messenger RNA stability. *Nature, 505*(7481), 117-120. doi: 10.1038/nature12730

Wang, X., Zhao, B. S., Roundtree, I. A., Lu, Z., Han, D., Ma, H., . . . He, C. (2015). N(6)-methyladenosine Modulates Messenger RNA Translation Efficiency. *Cell, 161*(6), 1388-1399. doi: 10.1016/j.cell.2015.05.014

Wang, Y., Li, Y., Toth, J. I., Petroski, M. D., Zhang, Z., & Zhao, J. C. (2014). N6-methyladenosine modification destabilizes developmental regulators in embryonic stem cells. *Nat Cell Biol, 16*(2), 191-198. doi: 10.1038/ncb2902

Wang, Z., Li, G., Tse, W., & Bunting, K. D. (2009). Conditional deletion of STAT5 in adult mouse hematopoietic stem cells causes loss of quiescence and permits efficient nonablative stem cell replacement. *Blood, 113*(20), 4856-4865. doi: 10.1182/blood-2008-09-181107

Warda, A. S., Kretschmer, J., Hackert, P., Lenz, C., Urlaub, H., Hobartner, C., . . . Bohnsack, M. T. (2017). Human METTL16 is a N(6)-methyladenosine (m(6)A) methyltransferase that targets pre-mRNAs and various non-coding RNAs. *EMBO Rep, 18*(11), 2004-2014. doi: 10.15252/embr.201744940

Wei, C. M., & Moss, B. (1975). Methylated nucleotides block 5'-terminus of vaccinia virus messenger RNA. *Proc Natl Acad Sci U S A, 72*(1), 318-322.

Weissman, I. L. (2000). Stem cells: units of development, units of regeneration, and units in evolution. *Cell, 100*(1), 157-168.

Weng, H., Huang, H., Wu, H., Qin, X., Zhao, B. S., Dong, L., . . . Chen, J. (2018). METTL14 Inhibits Hematopoietic Stem/Progenitor Differentiation and Promotes Leukemogenesis via mRNA m(6)A Modification. *Cell Stem Cell, 22*(2), 191-205 e199. doi: 10.1016/j.stem.2017.11.016

Wilson, A., Laurenti, E., Oser, G., van der Wath, R. C., Blanco-Bose, W., Jaworski, M., . . . Trumpp, A. (2008). Hematopoietic stem cells reversibly switch from dormancy to self-renewal during homeostasis and repair. *Cell, 135*(6), 1118-1129. doi: 10.1016/j.cell.2008.10.048

Wojtas, M. N., Pandey, R. R., Mendel, M., Homolka, D., Sachidanandam, R., & Pillai, R. S. (2017). Regulation of m6A Transcripts by the 3'-->5' RNA Helicase YTHDC2 Is Essential for a Successful Meiotic Program in the Mammalian Germline. *Mol Cell, 68*(2), 374-387 e312. doi: 10.1016/j.molcel.2017.09.021

Wu, J., & Izpisua Belmonte, J. C. (2016). Stem Cells: A Renaissance in Human Biology Research. *Cell, 165*(7), 1572-1585. doi: 10.1016/j.cell.2016.05.043

Xiao, W., Adhikari, S., Dahal, U., Chen, Y. S., Hao, Y. J., Sun, B. F., . . . Yang, Y. G. (2016). Nuclear m(6)A Reader YTHDC1 Regulates mRNA Splicing. *Mol Cell, 61*(4), 507-519. doi: 10.1016/j.molcel.2016.01.012

Xie, T., & Li, L. (2007). Stem cells and their niche: an inseparable relationship. *Development, 134*(11), 2001-2006. doi: 10.1242/dev.002022

Xu, C., Wang, X., Liu, K., Roundtree, I. A., Tempel, W., Li, Y., . . . Min, J. (2014). Structural basis for selective binding of m6A RNA by the YTHDC1 YTH domain. *Nat Chem Biol, 10*(11), 927-929. doi: 10.1038/nchembio.1654

Yamazaki, S., Ema, H., Karlsson, G., Yamaguchi, T., Miyoshi, H., Shioda, S., . . . Nakauchi, H. (2011). Nonmyelinating Schwann cells maintain hematopoietic stem cell hibernation in the bone marrow niche. *Cell, 147*(5), 1146-1158. doi: 10.1016/j.cell.2011.09.053

Yoon, K. J., Ringeling, F. R., Vissers, C., Jacob, F., Pokrass, M., Jimenez-Cyrus, D., . . . Song, H. (2017a). Temporal Control of Mammalian Cortical Neurogenesis by m6A Methylation. *Cell, 171*(4), 877-889. doi: 10.1016/j.cell.2017.09.003

Yoon, K. J., Ringeling, F. R., Vissers, C., Jacob, F., Pokrass, M., Jimenez-Cyrus, D., . . . Song, H. (2017b). Temporal Control of Mammalian Cortical Neurogenesis by m(6)A Methylation. *Cell, 171*(4), 877-889 e817. doi: 10.1016/j.cell.2017.09.003

Yue, Y., Liu, J., & He, C. (2015). RNA N6-methyladenosine methylation in post-transcriptional gene expression regulation. *Genes Dev, 29*(13), 1343-1355. doi: 10.1101/gad.262766.115

Zarnegar, B. J., Flynn, R. A., Shen, Y., Do, B. T., Chang, H. Y., & Khavari, P. A. (2016). irCLIP platform for efficient characterization of protein-RNA interactions. *Nat Methods, 13*(6), 489-492. doi: 10.1038/nmeth.3840

Zhang, C., Chen, Y., Sun, B., Wang, L., Yang, Y., Ma, D., . . . Liu, F. (2017a). m6A modulates haematopoietic stem and progenitor cell specification. *Nature, 549*(7671), 273-276. doi: 10.1038/nature23883

Zhang, C., Chen, Y., Sun, B., Wang, L., Yang, Y., Ma, D., . . . Liu, F. (2017b). m(6)A modulates haematopoietic stem and progenitor cell specification. *Nature, 549*(7671), 273-276. doi: 10.1038/nature23883

Zhang, C. C., & Lodish, H. F. (2005). Murine hematopoietic stem cells change their surface phenotype during ex vivo expansion. *Blood, 105*(11), 4314-4320. doi: 10.1182/blood-2004-11-4418

Zhang, J., Niu, C., Ye, L., Huang, H., He, X., Tong, W. G., . . . Li, L. (2003). Identification of the haematopoietic stem cell niche and control of the niche size. *Nature, 425*(6960), 836-841. doi: 10.1038/nature02041

Zhang, S., Zhao, B. S., Zhou, A., Lin, K., Zheng, S., Lu, Z., . . . Huang, S. (2017). m6A Demethylase ALKBH5 Maintains Tumorigenicity of Glioblastoma Stem-like Cells by Sustaining FOXM1 Expression and Cell Proliferation Program. *Cancer Cell, 31*(4), 591-606 e596. doi: 10.1016/j.ccell.2017.02.013

Zhao, B. S., Roundtree, I. A., & He, C. (2017). Post-transcriptional gene regulation by mRNA modifications. *Nat Rev Mol Cell Biol, 18*(1), 31-42. doi: 10.1038/nrm.2016.132

Zhao, B. S., Wang, X., Beadell, A. V., Lu, Z., Shi, H., Kuuspalu, A., . . . He, C. (2017a). m6A-dependent maternal mRNA clearance facilitates zebrafish maternal-to-zygotic transition. *Nature, 542*(7642), 475-478. doi: 10.1038/nature21355

Zhao, B. S., Wang, X., Beadell, A. V., Lu, Z., Shi, H., Kuuspalu, A., . . . He, C. (2017b). m(6)A-dependent maternal mRNA clearance facilitates zebrafish maternal-to-zygotic transition. *Nature, 542*(7642), 475-478. doi: 10.1038/nature21355

Zhao, C., Blum, J., Chen, A., Kwon, H. Y., Jung, S. H., Cook, J. M., . . . Reya, T. (2007). Loss of beta-catenin impairs the renewal of normal and CML stem cells in vivo. *Cancer Cell, 12*(6), 528-541. doi: 10.1016/j.ccr.2007.11.003

Zhao, M., Perry, J. M., Marshall, H., Venkatraman, A., Qian, P., He, X. C., . . . Li, L. (2014). Megakaryocytes maintain homeostatic quiescence and promote post-injury regeneration of hematopoietic stem cells. *Nat Med, 20*(11), 1321-1326. doi: 10.1038/nm.3706

Zhao, M., Ross, J. T., Itkin, T., Perry, J. M., Venkatraman, A., Haug, J. S., . . . Li, L. (2012). FGF signaling facilitates postinjury recovery of mouse hematopoietic system. *Blood, 120*(9), 1831-1842. doi: 10.1182/blood-2011-11-393991

Zheng, G., Dahl, J. A., Niu, Y., Fedorcsak, P., Huang, C. M., Li, C. J., . . . He, C. (2013). ALKBH5 is a mammalian RNA demethylase that impacts RNA metabolism and mouse fertility. *Mol Cell, 49*(1), 18-29. doi: 10.1016/j.molcel.2012.10.015

Zhou, B. O., Yue, R., Murphy, M. M., Peyer, J. G., & Morrison, S. J. (2014). Leptin-receptor-expressing mesenchymal stromal cells represent the main source of bone formed by adult bone marrow. *Cell Stem Cell, 15*(2), 154-168. doi: 10.1016/j.stem.2014.06.008

Zhou, J., Wan, J., Gao, X., Zhang, X., Jaffrey, S. R., & Qian, S. B. (2015). Dynamic m(6)A mRNA methylation directs translational control of heat shock response. *Nature, 526*(7574), 591-594. doi: 10.1038/nature15377